12-2019

The effect of traumatic brain injury on tau pathology by a potential seeding mechanism

George Edwards III

THE EFFECT OF TRAUMATIC BRAIN INJURY ON TAU PATHOLOGY BY A POTENTIAL SEEDING MECHANISM

by

George Edwards III, M.S.

APPROVED:

_____
Claudio Soto, Ph.D.
Advisory Professor

_____
Ines Moreno-Gonzalez, Ph.D.
Co-Advisory Professor

_____
Shane Cunha, Ph.D.

_____
Nicholas Justice, Ph.D.

_____
Anne Sereno, Ph.D.

_____
Jack Waymire, Ph.D.

APPROVED:

_____

Dean, The University of Texas MD Anderson Cancer Center UTHealth Graduate School of Biomedical Sciences

THE EFFECT OF TRAUMATIC BRAIN INJURY ON TAU PATHOLOGY BY A POTENTIAL SEEDING MECHANISM

A

DISSERTATION

Presented to the Faculty of

The University of Texas

MD Anderson Cancer UTHealth

Graduate School of Biomedical Sciences

in Partial Fulfillment

of the Requirements

for the Degree of

DOCTOR OF PHILOSOPHY

By

George Edwards III, M.S.

Houston, Texas

December, 2019

Dedication

First, to my Lord and Savior Jesus Christ for the continuous blessings to be where I am in my life and strength to overcome the challenges involved along this journey.

To my wonderful fiancé, Dr. Abby Barnwell, D.C. Thank you for your love, support, and patience with me. Also, to the Barnwell family, especially my future father-in-law, Dr. Phillip Barnwell, D.C. who recently passed away unexpectedly. Thank you for your great support and interest in my work. I will miss you very much.

To my father, George Edwards Jr., and my grandparents, my late grandmother Loretta Edwards and grandfather George Edwards, Sr. The resilience and hard work I inherited came from all of you. I am thankful for your continuous support.

To all my family and great friends who have always believed in me and supported me.

Finally, to myself. I am proud of my experience, my work, and never giving up.

Acknowledgements

I would like to thank my mentors, Dr. Claudio Soto and Dr. Ines Moreno-Gonzalez. Thank you for supporting and believing in me throughout this process. I will always cherish my time in the laboratory and thank you for sharing your knowledge with me allowing me to grow towards becoming a better scientist. I am proud to work with both of you.

I would like to thank my additional committee members, Dr. Shane Cunha, Dr. Nicholas Justice, Dr. Anne Sereno, and Dr. Jack Waymire. Thank you all for your supervision and for being helpful and as well as for your consistent support.

I would like to thank the Soto laboratory – past and present - for all of the experiences and support. I am very thankful for the opportunity to know each of you throughout the years.

I would like to acknowledge my friends and colleagues as well as the Neuroscience program at The University of Texas MD Anderson Cancer UTHealth Graduate School of Biomedical Sciences. Thank you for your distribution of knowledge, caring critiques, and overall support.

Abstract

THE EFFECT OF TRAUMATIC BRAIN INJURY ON TAU PATHOLOGY BY A POTENTIAL SEEDING MECHANISM

George Edwards III, M.S.

Advisory professors: Claudio Soto, Ph.D. (mentor)

Ines Moreno-Gonzalez, Ph.D. (co-mentor)

The misfolding, aggregation and accumulation of specific proteins is the overarching concept in protein misfolding disorders (PMDs). The microtubule associated protein tau is known to form insoluble filaments known as neurofibrillary tangles (NFTs) composed of hyperphosphorylated tau (pTau) found in a subset of PMDs called tauopathies, such as Alzheimer's disease (AD) and chronic traumatic encephalopathy (CTE), among others. Misfolded tau engenders a structurally alternative intermediate conformation that is prone to aggregate having amyloidogenic properties. Formation of amyloids, such as tau aggregates, is proposed to follow a nucleation-polymerization model where misfolded, soluble oligomeric seeds can trigger native proteins to misfold and aggregate. The processes responsible for the initial formation of seeding competent protein aggregates is not known. One hypothesis is that an insult to the brain could be a trigger for developing aggregate pathology noted in PMDs. Traumatic Brain Injury (TBI) is a pervasive event with an estimated 10 million people worldwide being affected and is defined as an insult to the brain caused by an external force, which may result in impaired neuronal and/or physical functioning. Indeed, TBI is a strong risk factor for PMDs, and following TBI,

there is a detection of pathological tau early in human cases. TBI may be a trigger for the formation of tau seeds that can spread pathology throughout the brain. Thus, our central hypothesis is that TBI induces the early formation of tau misfolded seeds as well as exacerbates tau pathology and spreading throughout the brain by a nucleation-polymerization process, which will then lead to pathological changes relative to disease. Our overarching goal of this work is to elucidate the effect of TBI on the induction, acceleration, and spreading of tau pathology and clinical signs. To assess this, we induced tau transgenic mice with moderate-severe TBI or repetitive mild TBI (rmTBI) and examined tau pathology and spreading. Moreover, the earliest detected tau seeds induced following rmTBI were tested for seeding capability by *in vivo* bioassay. This proposal provides novel molecular mechanisms for these deleterious diseases, such as AD and CTE, and their link to TBI.

Table of Contents

List of Figures

List of Tables

Abbreviations

AD - Alzheimer's disease

AGD - argyrophilic grain disease

AMPA - α-amino-3-hydroxy-5-methyl-4-isoxazolepropionic acid

Amy – amygdala

ANOVA - analysis of variance

APOE(ε4) - apolipoprotein E (epsilon 4)

APP - amyloid precursor protein

ATP - adenosine triphosphate

Aβ - amyloid-beta

B - bregma

BBB - blood brain barrier

BS - brain stem

CA - Cornu Ammonis

Cb - cerebellum

CBD - corticobasal degeneration

cc - corpus callosum

CCI - controlled cortical impact

CFP - cyan fluorescent protein

CJD - Creutzfeldt-Jakob disease

Contra - contralateral

CPu - caudoputamen

CSF - cerebrospinal fluid

CTE - chronic traumatic encephalopathy

Ctx / CTX - cortex/amygdala

d - day

DAI - diffuse axonal injury

Di - diencephalon

EC - entorhinal cortex

ELISA - enzyme-linked immunosorbent assay

FC - fold change

fc – flow cytometry

FRET - Förster resonance energy transfer

FTD - frontotemporal dementia

GABA - gamma-Aminobutyric acid

GCIs - glial cytoplasmic inclusions

GCS - Glascow Coma Scale

GFP - green fluorescent protein

GFTs - glial fibrillary tangles

GLUTs - glucose transporters

GSK-3β - glycogen synthase kinase 3β

Hp / HPa - hippocampal area

hr - hour

i.c. – intracerebral

IL - interaural

Ipsi - ipsilateral

ISF - interstitial fluid

KI - knock-in

KO - knock-out

Lipo - Lipofectamine

LOC - loss of consciousness

LTM - long-term memory

LTP - long-term potentiation

m - month

MAPT - microtubule-associated protein tau

min - minutes

mTBI - mild traumatic brain injury

MTL - medial temporal lobe

ND - not detected

NDs - neurodegenerative diseases

NFL - National Football League

NF-L – neurofilament light chain

NFs - neurofilament proteins

NFTs - neurofibrillary tangles

NMDA - N-methyl-D-aspartate

NPs - neuropil threads

o/n – overnight

PD - Parkinson's disease

PHFs - paired helical filaments

PiD - Pick's disease

PMCA - protein misfolding amplification assay

PMDs - protein misfolding disorders

PP - protein phosphatase

PrP^{C} - normal prion protein

PrP^{Sc} - alternative conformation of prion protein

PSP - progressive supranuclear palsy

pTau - hyperphosphorylated tau protein

R - round

rmTBI - repetitive mild traumatic brain injury

RT - room temperature

SEM - standard error of the mean

SN - substantia nigra

sTBI - moderate to severe traumatic brain injury

TBI - traumatic brain injury

Tg - transgenic

ThS - Thioflavin S

ThT - Thioflavin T

UTSW - the University of Texas Southwestern

wk - week

WT - wild-type

YFP - yellow fluorescent protein

CHAPTER 1

Introduction

This chapter contains portions from original, first author review articles:

Edwards G. III, Moreno-Gonzalez I., Soto C. Amyloid-beta and tau pathology following repetitive mild traumatic brain injury. Biochem Biophys Res Commun. 2016; (16)31252-9. doi: 10.1016/j.bbrc.2016.07.123. PMID: 27492070.

Edwards G.A. III, Gamez N., Escobedo G. Jr, Calderon O. and Moreno-Gonzalez I. (2019) Modifiable Risk Factors for Alzheimer's Disease. Front. Aging Neurosci. 11:146. doi: 10.3389/fnagi.2019.00146.

Protein misfolding diseases and tauopathies

The appropriate folding of a protein is imperative for its function. The primary structure of a protein consists of the amino acid sequence. The secondary structure of a protein can be referred to two primarily common structures – alpha helix and beta sheet, which are composed by the patterns of hydrogen bonds formed between amine hydrogen and carbonyl oxygen atoms as the backbone peptide bonds of the protein. Here, the folding of a protein into its proper native 3-D structure can occur, and this is a well-regulated process. The information for protein folding is encoded in the amino acid sequence; in addition, minimization of the hydrophobic amino acid side chains to the soluble atmosphere is an important factor. However, events can occur that can cause a protein to misfold: genetic mutations, transcriptional/translational errors, failure of the folding/chaperone machinery, errors in post-translational modifications or protein trafficking, environmental changes, and induction by a seeding mechanism. Any of these actions can cause the misfolded state of a protein to be favored over the properly folded form. These factors can lead to the denaturing - disruption of the native state - of a protein where this unfolded protein follows lower energy levels and stability having a proclivity to thereby aggregate [1].

If a protein does not fold into its functional structure, this can give rise to the malfunctioning of living systems and hence to disease, which may be caused by a loss-of-function and/or toxic gain-of-function; moreover, the misfolding of a protein seems to play a significant role in such neurodegenerative diseases (NDs) that involve protein aggregates present in affected tissue that can reveal altered or toxic effects. Thus, the misfolding, aggregation, and accumulation of specific proteins is the overarching concept in protein misfolding disorders (PMDs) (Figure 1). There are more than 20 PMDs including: prion diseases, Amyotrophic Lateral Sclerosis,

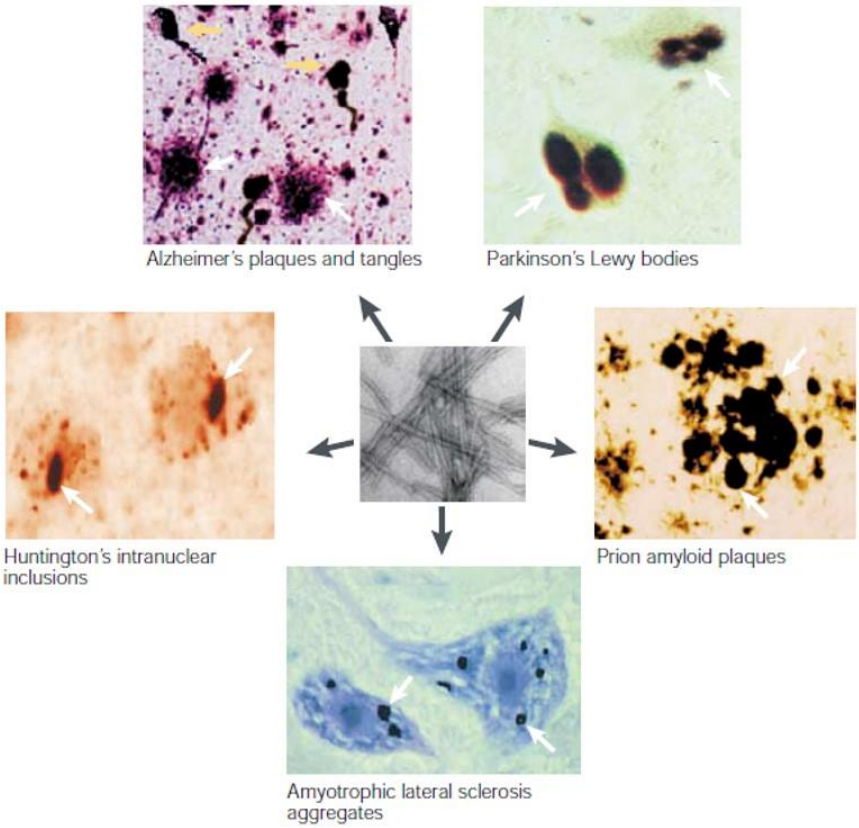

Figure 1. Pathogenic proteins and protein misfolding disorders (PMDs). In general, proteins fold properly into their native conformation; however, the misfolding of a protein results in its aggregation and accumulation as protein deposits in diverse tissues related to various protein misfolding disorders (PMDs). There are more than 20 of these diseases regarded as PMDs including: prion diseases, Amyotrophic Lateral Sclerosis, Huntington's disease, Parkinson's disease (PD), Alzheimer's disease (AD), Type 2 diabetes, and others [1–6]. Soto C. Unfolding the role of protein misfolding in neurodegenerative diseases. Nat Rev Neurosci. 2003 Jan;4(1):49-60. License agreement for reuse of image was obtained from Springer Nature Publishers.

Huntington's disease, Parkinson's disease (PD), Alzheimer's disease (AD), Type 2 diabetes, and others [2–7]. Although there may be disparate clinical abnormalities and disease progression associated with each of these PMDs, there is common ground noted in this group of maladies, such as: a definitive protein adopting an alternative structure, can be age-dependent, form from

Primary Tauopathies - predominantly tau pathology
Progressive supranuclear palsy
Argyrophilic grain disease
Corticobasal degeneration
Picks disease
Frontotemporal dementia and Parkinsonism linked to chromosome 17 (FTDP-17)
Primary age-related tauopathy (PART)
Postencephalitic Parkinsonism
Parkinson's dementia complex (PDC) of Guam
Guadeloupean parkinsonism
Globular glial tauopathies (GGT)
Ageing-related tau astrogliopathy (ARTAG)

Secondary tauopathies - associated with other types of pathology
Alzheimer's disease (AD)
Down's syndrome
Lewy body disorders
Prion disease
Familial British dementia and familial Danish dementia
Chronic traumatic encephalopathy (CTE)
Myotonic dystrophy
Niemann–Pick disease type C
Subacute sclerosing panencephalitis
frontotemporal lobar degeneration with C9orf72 hexanucleotide repeat expansion
Diffuse neurofibrillary tangles with calcification (DNTC)
Neurodegeneration with brain iron accumulation
Mutation affecting the sodium/proton exchanger, SLC9A6,
Cerebrotendinous xanthomatosis with the c.379C > T (p.R127W) mutation in the CYP27A1 gene
TARDBP mutation p.Ile383Val associated with semantic dementia

Table 1. Tauopathies. There are diverse tauopathies that can be classified as primary or secondary tauopathies in terms of pathological protein accumulation. Each of these tauopathies is different by symptoms and neuropathology, yet all of the incorporate the same protein aggregate – tau protein.

inherited or sporadic origin, and can have neurodegenerative capacities [2]. One type of PMD is a group of sporadic or familial neurodegenerative diseases that are designated by filamentous aggregates of hyperphosphorylated tau protein (pTau) in neurons and/or glial cells called tauopathies. Tauopathies consist of more than 20 disorders and can be sub-classified as either primary or secondary tauopathy depending on if tau pathology encompasses the main contribution of neurodegeneration or is an accomplice to another pathology in the disease [8,9] (Table 1). Accordingly, these tauopathies each have their own unique clinical characteristics, yet follow the same general common ground characteristics of PMDs as detailed above. Nonetheless, it is

not clearly understood the exact mechanisms of how a protein in its native state, like tau, can misfold and aggregate and cause disease-related alterations in the brain.

Tau protein – structure and function

As exampled in Figure 2, the microtubule-associated protein tau gene (MAPT) is located on chromosome 17q21 and contains 16 exons; however, the major tau protein in the human brain is encoded by 11 exons. In the human brain, there are six isoforms of tau, which are produced by the alternative splicing of exon 2, 3, and 10 and contain 352 to 441 amino acids. They differ by the number of insertions of 29 amino acids at the N-terminal (exon 2 and 3) – either zero (0N),

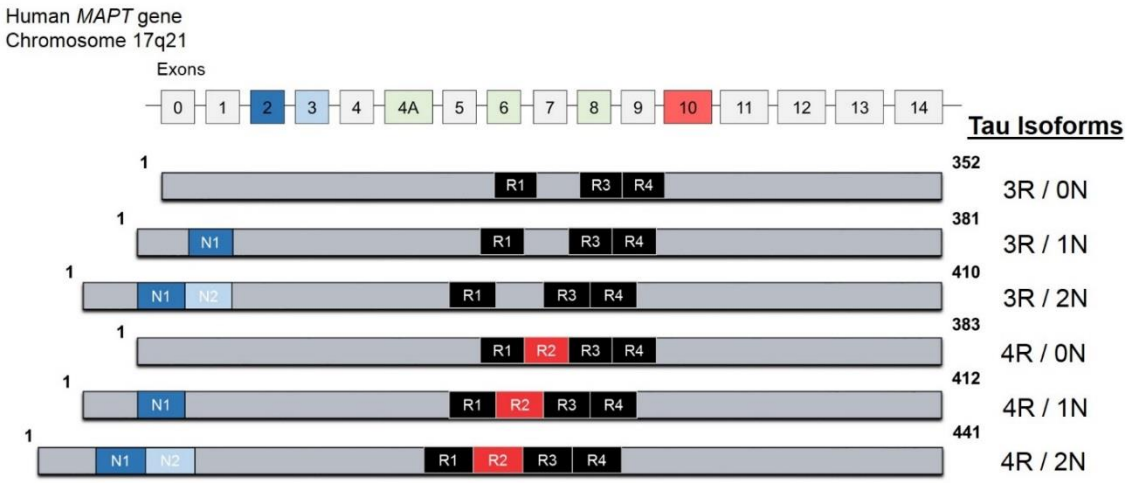

Figure 2. Six microtubule associated protein tau isoforms in the adult human brain. In the brain, exons 2, 3, and 10 are alternatively spliced. Exon 3 (light blue) is only present with exon 2 (dark blue). Exon 10 (red boxes) encodes one of in overall four microtubule binding repeats (R1-R4). Thus, in general, exons 2, 3, and 10 give rise to six isoforms characterized by the absence (0N), one (1N) or two (2N) amino-terminal inserts in arranged with three (3R) or four (4R) microtubule binding repeats.

one (1N), or two (2N) – as well as three (3R) or four repeat-regions (4R) at the carboxy-terminal. Exon 10 corresponds to the second repeat region (R2) and is absent in 3R isoforms. MAPT gene expression is developmentally regulated. Adult human brains consist of all six isoforms, yet fetal brains exhibit only the shortest isoform (3R/0N) in brain. In the adult human brain, 3R and 4R are

fairly similar, yet the N-terminal insertions vary as 0N, 1N, and 2N consist of ~37%, ~54% and ~9% of total tau, respectively. Interestingly, tauopathies can also be categorized by isoforms such as 1) 4R only - progressive supranuclear palsy (PSP), corticobasal degeneration (CBD), argyrophilic grain disease (AGD); 2) 3R only - Pick's disease (PiD); or 3) mixed 3R/4R - AD and chronic traumatic encephalopathy (CTE) [8–14].

Tau protein is a remarkably hydrophilic protein and is thought to lack a fixed or ordered structure in its native state, thereby being intrinsically disordered or natively unfolded, and this dynamic protein in its native state is not thought to have a propensity to aggregate [8,10,13,14]. Studies using circular dichroism spectroscopy delineated tau as a random coil [15], yet tau gravitates to form a paperclip-like conformation, where the N-terminal, R regions, and C-terminal come in close approximation to each other. However, tau can become prone to aggregation when bound to an interacting protein or partner [10,14]. Tau's most canonical function is binding to microtubules to promote cytoskeletal support and flexibility, thereby aiding in axonal transport, as shown in Figure 3; although, it has numerous other functions. Tau proteins interact with tubulin to stabilize microtubules and promote tubulin assembly into microtubules. The 3R/4R repeat-regions, also referred to as the microtubule-binding domain, are positively charged amino acid regions that are important for binding to the negatively charged microtubules. 4R tau, which has the R2 region, displays higher propensity for microtubules and thus can affect microtubule assembly better than 3R tau [8–14]. Moreover, residues located in the microtubule binding region 269-284 and 300-310, which comprise two hexapeptide motifs ^{275}VQIINK^{280} and ^{306}VQIVYK^{311}, as well as some adjacent regions are critical for microtubule binding and for tau aggregation [10,16]. Splicing and missense mutations can affect the isoform ratio or microtubule-tau binding regions allowing disassociation of tau to the microtubule and/or propensity for aggregation, respectively. Thus, tau

has several ways of controlling microtubule stability – isoforms, amino acid binding domain regions, and phosphorylation.

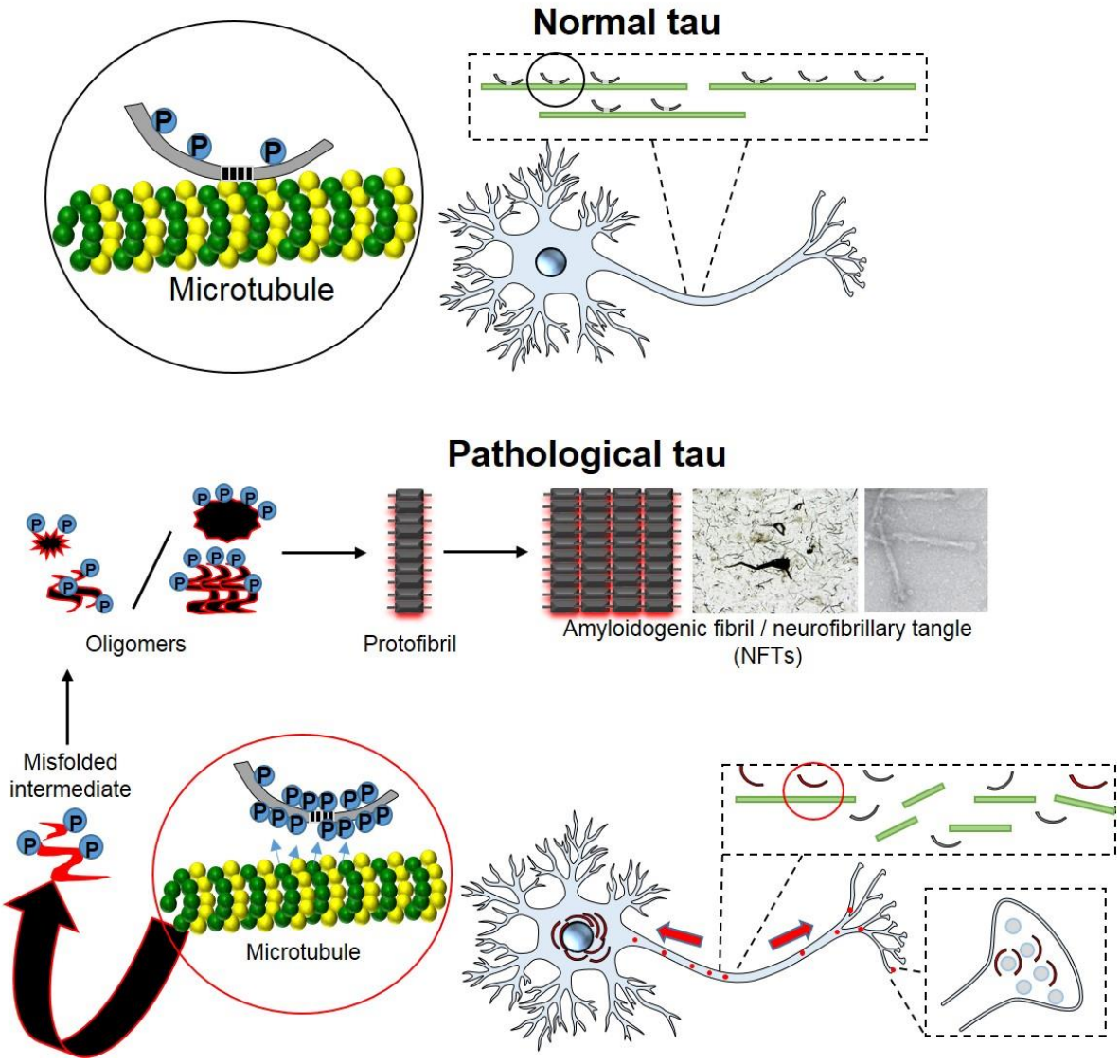

Figure 3. Physiological versus pathological tau. Under physiological conditions, tau's main function is binding to microtubules to aid in cytoskeletal support and axonal transport. When hyperphosphorylation occurs it affects the binding properties of tau to the microtubule, detaching tau, and unbound tau can begin accumulating in the cytosol where it has the chance to form a misfolded conformation. This free tau is also suggested to mislocalize by arranging from the axons to the somatodendtric compartment. Tau is thought to begin self-templating from dimers, trimers, oligomers to a protofibril or filamentous structure (paired helical filaments) and finally to the insoluble amyloid aggregate neurofibrillary tangles (NFTs) distinguished in tauopathies.

Tau is a known phosphoprotein where phosphorylation plays an integral role for its physiological function. The number of phosphorylation sites for tau has been enumerated up to 85 reported residues (80 serine or threonine and 5 tyrosine) with approximately 30 of these sites in normal tau protein [8]. One example, tau in AD-derived paired helical filaments (PHFs) can be phosphorylated at approximately 45 residues [14]. Tau is phosphorylated by numerous kinases including microtubule affinity-regulating kinases; cyclic AMP-dependent protein kinase; Ca^{2+} - or calmodulin-dependent protein kinase II; tyrosine kinases; proline-directed kinases like glycogen synthase kinase 3β (GSK-3β), cyclin-dependent kinase 5, mitogen-activated protein kinase, and JUN N-terminal kinase; among others [17]. As tau phosphorylation and dephosphorylation is a dynamic process, protein phosphatases, such as protein phosphatase 1 (PP1), PP2A/B/C, and PP5, mediate dephosphorylation of tau protein. Notably, PP2A is the most prominent phosphatase, accounting for ~70% of tau phosphatase activity in the human brain, and its activity is significantly reduced at least 20-40% in AD brains [18]. It is not exactly clear if the excess or hyperphosphorylation of tau or individual site-specific abnormal phosphorylation of tau is the driver of tau pathology in diseased brains. On one side, fetal tau is much more highly phosphorylated compared to adult tau – approximately 7 to 2 phosphates per molecule [19]. Likewise, hibernating animals and anesthesia-induced hypothermia exhibit tau hyperphosphorylation without identified aggregation [20,21]. On the other hand, many tauopathies reveal hyperphosphorylated tau (pTau) in brain *post-mortem* [22]. Nevertheless, the role of hyperphosphorylation or even site-specific phosphorylation is still not fully understood; one example of quandaries regarding individual site-specific phosphorylation, Ser^{262} and Ser^{396} phosphorylation sites are phosphorylated in fetal tau, yet are also found hyperphosphorylated in paired-helical filaments in AD brains [23]. Still, it is assumed that increasing phosphorylation of tau

negatively affects microtubule-tau binding and may play a role in tau aggregation and related disease pathology.

Tau is known to undergo numerous modifications and has multiple functions, and these characteristics may be isoform- and cellular distribution-dependent. Other explored post-translational modifications of tau include: glycosylation, glycation, deamidation, isomerization, nitration, methylation, ubiquitylation, sumoylation, and truncation [10,13,24–26]. The compartmentalization of tau is suggested to be important for tau function as well. Axonal tau assists in cytoskeletal support by binding to microtubules and may also influence motor proteins, dynein and kinesin, and axonal elongation and maturation [27]. A small quantity of tau has been detected in dendrites and dendritic spines, which may have an effect on synaptic plasticity, although this remains a matter of debate [8,13]. Tau has also been hypothesized to be distributed in the nuclei of neurons and non-neuronal cells, which may protect genomic DNA, cytoplasmic RNA, and nuclear RNA under cellular duress [28,29]. Furthermore, other novel functions of tau have been determined by the utilization of transgenic (Tg) mouse models, like the tau-knockout mice, including a role in development, neuronal activity, neurogenesis, iron export, and long-term depression [10].

There are numerous molecular mechanisms that could propel normal tau protein into misfolding and aggregating, such as: mutations, overexpression, post-translational modifications, binding regulators, aging and environmental factors, dysregulation of kinases and phosphatases, and others [10,13,24–26]. As previously mentioned, there are at least ≤80 splicing and missense mutations of tau that result in a loss- and/or gain-of tau function as confirmed in tauopathies in patients, Tg animal models harboring genetic mutations, and/or *in vitro* cellular assays. Presence of various post-translational modifications, as in hyperphosphorylation, are posited to be an early and critical event in tau misfolding and aggregation. *In vitro*, tau aggregation can be accelerated

by the presence of cofactors including polyanionic compounds, such as sulfated glycosaminoglycans like heparin, to induce aggregation of tau [24,25,30]. Nevertheless, some mechanism described above occurs that causes tau protein to be hyperphosphorylated, which will then neutralize the positive charge on tau, and releasing tau from the microtubule [8,10,12–14,25]. Without microtubule-bound tau mechanically stabilizing axonal microtubules there can be issues with supporting the long, extended structure of the axon, as well as the missing interaction of tau with motor proteins can impair axonal transport and ultimately resulting in synaptic impairment and axonal retraction [8]. Congruently, unbound tau begins to pool in the cytosol, thereby increasing the critical concentration of tau. These events can facilitate the generation of a misfolded, soluble intermediate that instigates the aggregation process (Figure 3).

The nucleation-polymerization model and tau protein

It is hypothesized that amyloidogenic proteins, like tau, follow a nucleation-polymerization model [28-32]. This model posits the stages of aggregation process of amyloid formation – starting with a soluble protein transitioning ultimately to a fibrillary structure (Figure 4). There is a sigmoidal time course corresponding to aggregation over time where the rate-limiting step is the formation of oligomeric nuclei or seeds for aggregation in the nucleation phase. This is thought to be normally a very slow process; however, once the seed is formed, polymerization occurs in a rapid manner by self-templating in the polymerization or exponential phase, accumulating monomeric subunits to free ends of the oligomers thereby developing a fibril structure. *In vitro*, these fibrils could be fragmented thereby generating auxiliary seeds that could thus restart the process. With the addition of external seeds in the nucleation phase, the nucleation phase can be circumvented thus accelerating the overall assembly as demonstrated by an attenuation of time for the nucleation phase and concomitant advancement into the polymerization phase. The nucleation-polymerization model has also been described in other ordered processes

such as: protein crystallization, viral coat assembly, microtubule formation, flagellum formation, and sickle-cell fibril formation [32,33]. The reason and mechanism for the formation of a misfolded nucleus or seed remains to be elucidated; however, suggestions for this engendered soluble intermediate include: hydrophobicity profile of amino acids, the need for stability, hydrogen

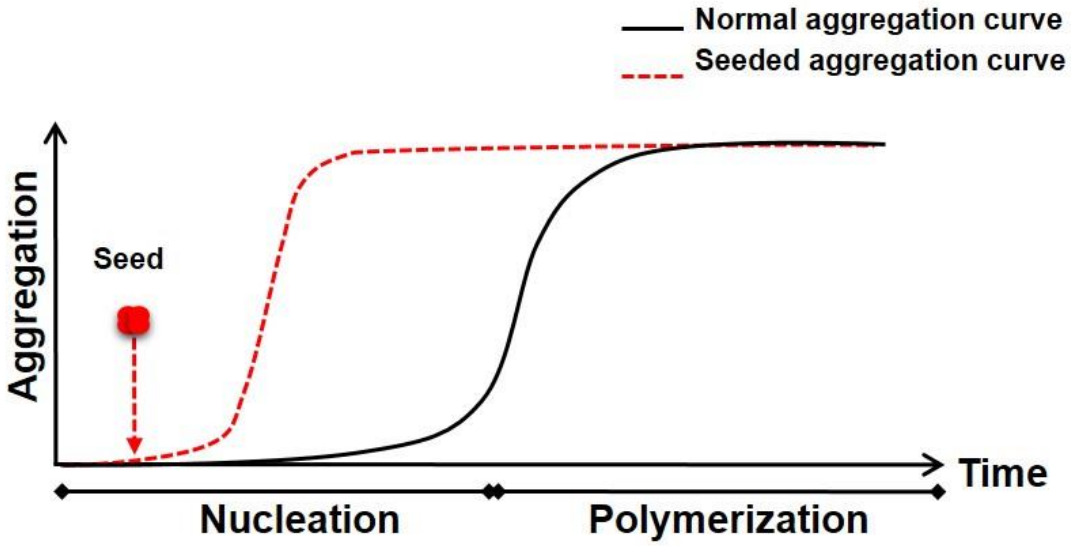

Figure 4. The nucleation/polymerization model for amyloids. Tau is believed to follow a model of amyloid formation called the nucleation-polymerization model. The sigmoidal time course reaction for the model, which begins with the rate-limiting step that is the nucleation or lag phase. This nucleation phase is responsible for the initial formation of aggregates that starts with this misfolded intermediate. This is normally a very slow process. This is then followed by a rapid growth phase or polymerization phase. Here, the misfolded protein is developed into a fibril amyloid structure and can begin self-templating accumulating more monomers to create larger aggregates. With the presence of a preformed seed, we attenuate this nucleation phase generating this misfolded intermediate faster as well as reaching the polymerization phase at a quicker rate, thereby presenting the seeding-nucleation model

bonding, high local critical concentration of the endogenous monomers, the "aggregation environment", among others [2,14,31,32].

In this process, the protein undergoes secondary conformational changes generally comprising of oligomers to protofibrils to fibrils as revealed in Figure 3. Oligomers are seen as intermediates along the fibrilogenesis pathway and are soluble, small assembled misfolded proteins (from dimers to large multimers) that are difficult to define due to the quickness of aggregation and heterogeneity in preparation, and a paucity of delicate molecular techniques to determine the protein structure [4,10]. Current research suggests that oligomeric conformations of amyloids are thought to be the most toxic species compared to preceding research [4,10,14,24,25]. Protofibrils are formed by oligomers assembled into elongated linear or rod-like structures that may intertwine; these are referred to as PHFs or neuropil threads (NPs) regarding tau protein [2,4,14,30]. Finally, a highly ordered fibrillary structure or amyloid is formed being ~10 nm wide with long, generally unbranched ribbon-like structures as demonstrated by electron microscopy [1,2]. These amyloidogenic fibrils are insoluble and resistant to proteolytic degradation, organized in a cross β-sheet conformation, bind to dyes such as Congo red and Thioflavin, and may be a key factor in PMDs. These are associated to intracellular NFTs that are formed from pTau and are described as closely packed, highly ordered structures that contain multiple twisting protofibrils with interacting side chains and characterized by classical Gallyas silver staining in tauopathies.

As mentioned previously, in the past, NFTs were assumed to be the predominantly neurotoxic species as research speculated tangle regional burden in diseased-brain correlated with cognitive deficits and neurodegeneration [35]. Conversely, current views of NFT formation from tau assembly suggests actually a protective cellular response in the brain. Several transgenic mouse models for wild-type (WT) or mutant human tau exhibit compromised synaptic impairment and loss, and cognitive dysfunction prior to tangle formation, while tangle-bearing neurons and neuronal loss show no correlation[10,11]. More so, NFT-laden neurons in cornu ammonis 1 (CA1) hippocampal area in AD could survive for about 20 years, and it has been proposed these neurons

may not die [36]. On the other hand, NFTs could still have a deleterious effect by accruing other necessary cellular components and even taking up space in the cell, thereby hindering transport mechanisms as viewed by the somatodendritic location of NFTs. Research is still on-going to determine the structural components and molecular properties of tau soluble oligomers as the neurotoxic culprit in disease. Concurrent with the nucleation-polymerization model, experimental evidence has demonstrated that tau protein can be considered to have "prion-like" characteristics [2,4,7,37–40]. In humans, prion diseases (transmissible spongiform encephalopathies) are rare, fatal neurodegenerative disorders that include Creutzfeldt-Jakob disease (CJD), fatal familial insomnia, Gerstmann-Sträussler-Scheinker Syndrome, and Kuru. In prion diseases, the normal prion protein (PrP^{C}) acquires an alternative conformation known as PrP^{Sc}, which can template the misfolding of endogenous PrP^{C}, leading to its aggregation and accumulation in the brain, and the ability of PrP^{Sc} to transmit the disease in an infectious manner [2,4,7,37–40]. Prions are suggested to spread from cell-to-cell, region to region, and between organisms [4,7,37-40]. Mounting evidence posits that many amyloidogenic proteins, such as tau, emulate these prion-like molecular mechanisms for the initiation and spreading of aggregates in disease cases.

Tau spreading

The localization of tau within the neuron in pathological settings could play a role in spreading and disease and is continually being investigated. Tau protein is thought to be primarily axonal, yet an early pathological hallmark of tauopathies, like AD, suggested is the abnormal sorting of tau into the somatodendritic compartment of neurons where hyperphosphorylated tau can aggregate, thereby preceding neurodegeneration [10,41,42]. Frandemiche et al. has shown a widespread distribution of tau in the dendrites, which responded to synaptic input and translocated to postsynaptic compartments in primary cultured cortical neurons [42]. Endogenous tau was also determined to missort due to introduction of amyloid-beta (Aβ) oligomers [42]. Moreover, in a tau

Tg mouse model, early tau-related deficits developed not from the loss of synapses or neurons, but rather from synaptic abnormalities caused by the accumulation of pTau within intact dendritic spines. The overall effects of this missorting remain unknown.

Several reports indicate tau's capability to propagate aggregation transcellularly [7,10,26,38,40]. The exact mechanism or combination of mechanisms remain to be elucidated, but it has been speculated that tau spreading could occur by soluble tau traversing the cellular membrane, extracellular release by dead neurons or synaptic excitation, endocytosis and exocytosis, pinocytosis, nanotubes, passage through diffusion barriers, and others [7,10,26,38,40]. Tau spreading can occur transynaptically as emerging evidence supports the account of pathological spreading by the neural connectome [2,4,7,10,13,14]. Indeed, exogenous inoculation of seeding-competent tau (i.e. synthetic tau aggregates or brain homogenates from human tauopathies or Tg tau mice) demonstrates migration of pathological tau from the injection site to synaptically connected brain regions in humanized tau Tg mice and even in WT mice in a time-dependent manner [43–49]. Studies utilizing microfluidic chambers and cellular assays demonstrated the cellular and synaptic propagation of pathological tau, as well [45,50–53]. Advancements in *in vivo* imaging of structural and pathological features has divulged a general involvement of the connectome in AD and other neurodegenerative processes [54–56]. Tg animals are useful to assess endogenous tau spreading [57–59]. rTg2510 mice express the pathogenic human tau transgene restricted to projection neurons of the entorhinal cortex demonstrating burgeoning tau spreading, while incorporating normal mouse tau into misfolding and aggregating, along functional brain connections over time [57,58]. Another example of synaptic tau spreading is that designated by the pathological tau staging in disease, such as AD and CTE. As shown in Figure 5, Braak and Braak staging describes the pathological phases of tau aggregation in AD as following a stereotypical and temporal pattern of deposition emulating areas neuronally connected. I-II) NFTs spawn in the entorhinal cortex and locus

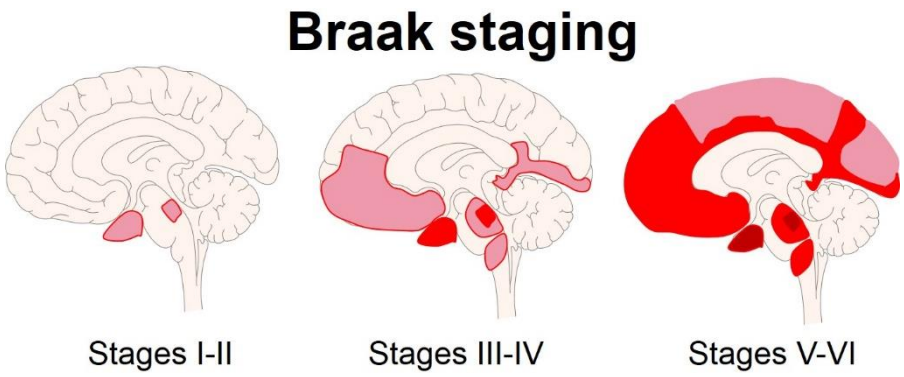

Figure 5. Braak staging – the spatiotemporal progression of tau pathology in Alzheimer's disease (AD). The characterization of tau pathology in AD performed by Braak and Braak is one paragon of the "prion-like" capabilities of tau protein as revealed by spreading from region-to-region in the brain. The spatial propagation of tau assemblies is thought to follow the brain's neural connectome. Hyperphosphorylated tau and tangles in AD cases seems to follow a distinct, well-organized pattern for spreading *in vivo:* I-II) NFTs spawn in the entorhinal cortex and perhaps locus coeruleus; III-IV) previous areas have more robust tau deposition, and NFTs are located in the hippocampus, fusiform gyrus, and temporal cortex; V-VI) NFTs are abundant and spread throughout the cortex [60-62.]

coeruleus; III-IV) previous areas have more robust tau deposition, and NFTs are located in the hippocampus, fusiform gyrus, and temporal cortex; V-VI) NFTs are abundant and spread throughout the cortex [60,61]. However, contrary to prion disease, there is very little and debatable epidemiological evidence for an infectious etiology for non-prion neurodegenerative diseases. In these diseases, it is likely that the prion-like spreading of protein misfolding and aggregation operates more in the cellular-to-cellular and area-to area transmission of the pathology within the same individual than in the inter-individual transmission as in prion diseases [62]. Overall, there is strong evidence that pathological tau can translocate and synaptically spread throughout the brain by a prion-like manner.

Traumatic brain injury (TBI) and Relation to AD

Most PMDs like tauopathies are primarily of sporadic origin with no established causation; however, there are ample risk factors that could play a role in the etiology and/or progression of disease. Recent research has posited that traumatic brain injury (TBI) can be considered an environmental factor that leads to the onset of AD or dementia. TBI is the direct impact from an external force that may alter consciousness and have an effect on mental and behavioral capacities. The World Health Organization estimates that 10 million people in the world are affected by TBI per year. It is the leading cause of death or disability in children, young adults, and in industrialized cities, and it can even reduce life expectancy by 7 years [63–65]. The severity of TBI is quantified by Glascow Coma Scale (GCS) and is distinguished in three relative categories: severe, moderate, and mild. Severe TBI represents head injuries that result in permanent or an extended period of unconsciousness, amnesia, or death following a head injury with a GCS of 3-8. Moderate TBI involves of a period of unconsciousness or amnesia from 30 minutes $\geq$ 24 hours with a GCS of 9-12. Mild TBI (mTBI) is recognized as head injuries that cause a brief state of altered consciousness resulting $\leq$ 30 minutes of unconsciousness, though most mTBIs do not result in a loss of consciousness [66]. Despite this interpretation, one major problem for researchers and clinicians regarding TBI is the high heterogeneity among injuries. Mild TBI represent a majority of reported cases [63]. A moderate to severe TBI (sTBI) can be described by a car wreck, act of violence, or fall, which will more likely produce systemic complications following the insult and can create long-term adverse effects in the brain or even death. The harsher a TBI, as that of sTBI, that occurred produces a greater risk of developing AD [64,67–69]. Plassman et al. reported World War II veterans having a moderate TBI (hazard ratio: 2.32) or severe TBI (hazard ratio: 4.51) event had an increased risk of developing AD [70]. After a TBI event, dementia diagnosis was found to be strongest within the first year (4-6 times) but maintained significance up to 30 years as well as when compared to a cohort sibling pairs with

opposing TBI status; moreover, the greater the TBI experience (severity or number of TBIs) demonstrated the higher the risk [71]. Researchers in a large cohort study in Denmark reported the overall risk of dementia in individuals with a history of TBI was 24% higher than those without a history of TBI. A severe TBI increased the risk by 35%, and a single mild TBI or concussion augmented the risk by 17%. The risk of dementia was increased with the number of TBI events - 33% higher for 2 or 3 TBIs, 61% higher for 4 TBIs, and 183% higher for 5 or more TBIs [72]. Johnson and colleagues found elevated Aβ and NFTs levels by immunohistochemistry in approximately 1/3 *post-mortem* individuals that had a surviving sTBI after 1 year (between 1-47 years) compared to controls, thus demonstrating the deleterious long-term effects of a single fatal TBI [73]. There are multiple factors involved in regards to an individuals' susceptibility to AD following a TBI including age, gender, and genetics. For example, individuals carrying the genetic polymorphism of apolipoprotein E epsilon 4 (APOE-ε4) have been described to have a 10-fold increase of AD disposition after a TBI [65,74].

Molecular Mechanisms of TBI

As demonstrated in Figure 6, primarily, TBI begins with an instant, irreversible initial blow or impact causing direct damage to surrounding neuronal and astroglial cells and vasculature. This primary insult can be in two modalities – either a focal or diffuse injury. A focal injury or blunt trauma is a direct, physical impact to an area that can be followed by a linear shift to the head, and it is associated with contusions and/or subdural hemorrhaging [75–78]. Diffuse axonal injury (DAI) is an injury of literally shearing or tearing the axons caused by rapid acceleration and deceleration forces, mostly thought from rotational forces [75–78]. This incipient impact can trigger a rapid necrosis due to the mechanical damage as well as systemic alterations in the brain such as: edema, increased intracranial pressure, and ischemia [75–78]. An initiation of secondary mechanisms occurs in the form of multiple molecular and cellular deviations perturbing

the overall environment of the central nervous system including: neuronal excitotoxicity, Ca^{2+} overload, mitochondrial dysfunction, oxidative stress due to formation of free radicals, inflammation, and abnormal protein aggregation. These cellular and biochemical cascade alterations lead to synaptic dysfunction, axonal degeneration, and neuronal death ultimately instigating cognitive and behavioral impairments [75–78]. However, it is not clear where the onset of diseases, like AD, would occur in this process, yet most of these aforementioned molecular pathways are very similar in both TBI and AD.

TBI and tau pathology

Tau pathology has been strongly implicated with repetitive mild TBI (rmTBI), especially with its connection to CTE, yet tau pathology following sTBI may not be as rampant – but does occur. This evidence may be due to the nature of the TBI and other variable factors [63,77,79–81]. Hyperphosphorylated tau and NFTs are more correlated with rmTBI than sTBI, but there are accounts of tau inclusions after sTBI being present at higher than control levels subsequent to a surviving fatal TBI over long-term assessment [73]. One study used the conformation specific tau antibody Alz50 and found neurofibrillary pathology in 8 out 27 *post-mortem* sTBI brains – mostly in the elderly, but in one case of a 16 year old male [82]. Johnson et al. discovered widespread NFTs were present in up to a third of patients following survival of a year or more from a single TBI [73]. Tau levels in cerebrospinal fluid (CSF) from fatal TBI patients expressed over a 1,000-fold increase compared to various neurological-diseased and non-diseased controls, and a cleaved and reduced sized form of tau protein was detected in these brain injured patients [83]. Formation of tau aggregates after TBI is not implausible. Functionally, as noted tau protein binds to microtubules for cytoskeletal support; when there is physical disruption or other secondary mechanisms affecting microtubule dynamics, tau can detach from the microtubule and begin the misfolding and aggregation process [63]. Moreover, other on-going activated cellular mechanisms associated

to TBI and disease can trigger tau aggregation including: Ca^{2+}-induced activation of calpains and calcineurin which activates kinases, such as GSK-3β, triggering hyperphosphorylation of tau; Aβ and inflammation-induced tau aggregation; generation of cleaved tau; alterations of multiple protein kinases and phosphatases implicated both in TBI and AD; among others [78].

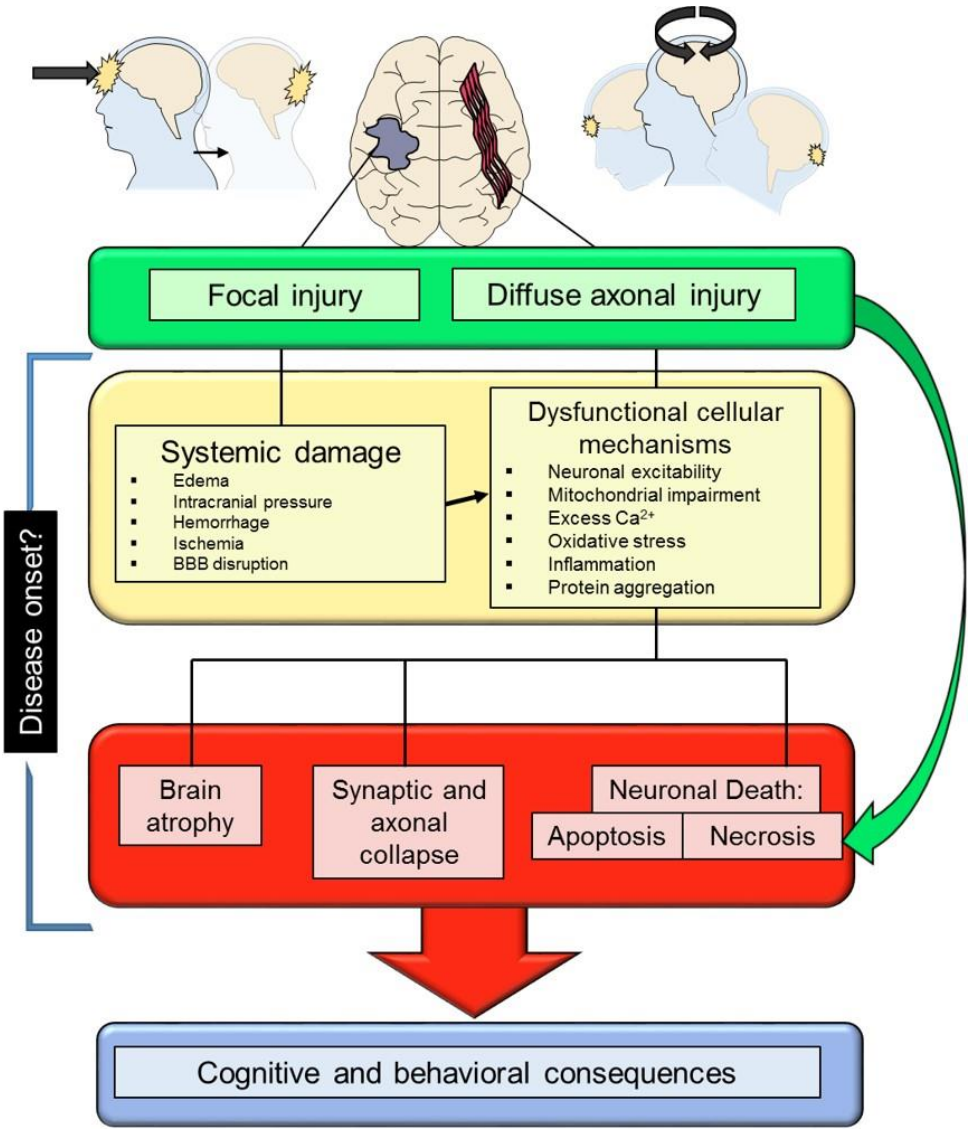

Figure 6. Neural pathways triggered following TBI. After initial primary injury, focal and/or diffuse axonal injury, there can be an elicitation of secondary neural mechanisms including hyperexcitability, Ca^{2+} release and mitochondrial dysfunction, oxidative stress, inflammation, and protein aggregation. Ultimately, this leads to neuronal degradation accompanied by cognitive and behavioral changes. It is not known when or how neurodegenerative disease onset and progression could originate following TBI.

Mild TBI and chronic traumatic encephalopathy

Mild TBI (mTBI) is acknowledged as head insults that cause a brief state of altered consciousness resulting ≤ 30 min of unconsciousness, yet most mTBIs do not result in loss of consciousness. The consequences of rmTBI is an important topic in research due to the fact that war veterans and contact sports athletes (i.e. American football, boxing, hockey, soccer, etc.) with TBI experiences are linked with a recently defined disease, CTE, formerly termed dementia pugilistica. Though the particular type of lesions resulting from mTBI are highly variable, various factors may play an important role in the consequences of the impact, including rotational acceleration and deceleration forces, fluidic pulses from the lateral ventricles generating shearing forces, and blow location, among others [63,77,81,84]. CTE-afflicted patients display an overlapping and broad range of abnormal behaviors emerging mid-life that ultimately result in psychological issues that lead to violence and/or suicide. Following a primary TBI insult, a multitude of secondary mechanisms take effect causing cytopathogenesis and neurological changes within the brain, as indicated by an association with neurodegenerative diseases, cognitive impairment, seizures, sleep disorders, neuroendocrine disorders, and other complications [63,64]. Interestingly, autopsy brain samples from CTE-diagnosed athletes and military veterans with some form of TBI (from teen ages to 80's) display massive accumulation of misfolded protein aggregates, mainly composed of tau and some cases Aβ [63,77,81,84–88]. CTE is a slow-progressing disease and even if the trauma activity is halted the disease still proceeds long term, thereby suggesting that the multiple molecular pathways elicited by rmTBI have long-lasting effects. Although mTBI is linked to the development of neurodegenerative diseases, additional factors that may contribute to the development of CTE after rmTBI include: 1) age, a young brain is more plastic for recovery than an old brain; 2) extent, nature and timing of the trauma; 3) genetics, i.e. ApoE gene; and 4) other health-related factors [63].

Currently, a conclusive CTE diagnosis cannot be made until *post-mortem*. CTE is generally distinguishable from other tauopathies, even AD, because it consists of a unique distribution of pathological tau throughout the brain. Furthermore, tau accumulation is the predominant feature of CTE associated to rmTBI, while Aβ deposits are not very conspicuous, unless in more severe forms of TBI or peculiar cases. NFTs, neuropil threads, and astrocytic tangles form in an irregular distribution and heavy density in the frontal and temporal cortices. They have a proclivity to arrange near small blood vessels, ventricles, and sub-pial tissues and are chiefly located at cortical layers II and III [81,84,87,89]. Similar to Braak staging of tau pathology in AD, staging of tau pathology in CTE has been described: I) NFTs are located in the depths of frontal cortical sulci and locus coeruleus along with gliosis and axonal loss in white matter tracts; II) NFTs deposit in the cortex with minimal detection in the amygdala (Amy), hippocampal area (HPa), and substantia nigra (SN); III) NFTs spread throughout Amy, HPa, and SN; IV) NFTs detected widespread through the cortex and temporal lobe [89]. Despite these pathological and neuroanatomical differences in CTE and AD, the tau isoforms (3R and 4R) that are hyperphosphorylated remain identical between CTE and AD [63]. It is still unclear the mechanism and signaling pathways implicated in NFT formation in CTE, and what the role that this deposition plays in CTE-specific behavior.

Concussions and/or mTBI are some of the most common forms of neurological disabilities, estimating around 90% of all brain injuries recorded [63,84]. The Center for Disease Control and Prevention reported 300,000 mTBI cases per year in contact sports, and about 122,000 children (ages 10-19) went to the ER annually for nonfatal brain injuries [63,84,90]. Studies involving American football players revealed that the absorbed head impacts per season rose in an exponential fashion: around 80 hits (ages 7-8); >240 hits (ages 9-12); >1000 hits (high school); and 420-2492 (college) [63,90,91]. The National Football League (NFL) reported an average

concussion incidence of 131.2 ± 26.8 concussions per year - a rate of 0.41 concussions per game [92]. This demonstrates that an individual sport player suffers multiple damaging head blows and/or concussions that may produce accumulative damage over the years. However, the number and strength of impacts (i.e. sub-concussive versus concussive) required to lead to AD or CTE associated pathology remains to be elucidated. Though epidemiological studies are contentious, one major finding in human rmTBI cases is that the onset and severity of CTE appears to correlate with the length of time engaged in contact sports or military service and number of traumatic injuries that occur [63,65,84,92–94]. A previous study stated that 17% of retired boxers developed CTE, yet prevalence of CTE might be underestimated possibly due to paucity of reporting or cognizance of even acquiring mTBI [63,65,84,92]. Retired NFL players having three or more concussions were found to have a 5-fold increase of developing mild cognitive impairment - a stage that can evolve into AD or other forms of dementia [93]. In addition, 68 out of 85 *post-mortem* individuals with a history of rmTBIs developed CTE pathology [84]; additional studies revealed 98% CTE *post-mortem* diagnosis in professional level American football players and even reported mild pathology in 3/14 cases at the high school level [79]. Although the brain has been hypothesized to have the ability to recover following rmTBI, brain scans performed on high school American football players showed that the current in-season players versus those in off-season demonstrated comparable brain damage [95].

Hypothesis

The formation and accumulation of misfolded aggregates in various PMDs follows a seeding/nucleation model [28-32], and these misfolded proteins related to various PMDs are assumed to have prion-like properties [2,4,7,14,24,25,37–40]. Many of these maladies originate sporadically with no clear manner of etiology. The prion-like spreading may be the molecular explanation for the long known - but puzzling observation - that the pathological abnormalities in neurodegenerative diseases progress in a stereotypical and predictable manner across anatomical connections, usually starting from a circumscribed area and spreading all over the brain. In this scenario, the key question is what factors or processes trigger the formation of the first misfolded seeds that then will propagate the pathology throughout the brain and progress to disease. One intriguing possibility is that TBI could act to trigger the formation of the first stable misfolded tau oligomeric seeds that then will spread the pathology in the brain by the prion principle and produce a more severe and faster onset of pathological alterations. Thus, our central hypothesis is that TBI induces the early formation of tau misfolded seeds as well as exacerbates tau pathology and spreading throughout the brain by a nucleation-polymerization process, which will then lead to neurodegenerative changes relative to disease. Our overarching goal of this work is to elucidate the effect of TBI on the acceleration and spreading of tau pathology and behavior. Therefore, we will study the effect of TBI on tau pathology by the following aims:

1) Determine the effect of sTBI on the formation and spreading of tau pathology *in vivo*.

2) Determine the generation and spreading of tau pathology and behavior following rmTBI *in vivo*.

3) Investigate the seeding capability of rmTBI-induced seeds by *in vivo* bioassay.

CHAPTER 2

Determine the effect of sTBI on the formation and spreading of tau pathology *in vivo*.

This chapter is based upon:

Edwards III G.A., Zhao J., Dash P.K., Soto C., Moreno-Gonzalez I. Traumatic brain injury induces tau aggregation and spreading. J Neurotrauma. 2019 August 28. doi: 10.1089/neu.2018.6348. [Epub ahead of print]

Rationale

Hyperphosphorylated tau aggregates generate NFTs that are considered the pathological hallmark of tauopathies including AD, CTE, and frontotemporal dementia (FTD), among others. Most tauopathies have a sporadic origin and can be associated to multiple risk factors. Traumatic brain injury has been suggested as a risk factor for tauopathies by triggering disease onset and facilitating its progression. In fact, elevated NFTs levels have been found in approximately 1/3 *post-mortem* individuals that had a surviving moderate to severe TBI demonstrating the relationship between tau aggregation and a single TBI [73]. In addition, the diagnosis of dementia was significantly increased up to 30 years following TBI with the strongest association with TBI severity [71].

The primary insult of a TBI can trigger systemic alterations in the brain as well as initiate secondary mechanisms in the form of multiple molecular and cellular deviations perturbing the overall environment of the central nervous system [63,65,76–78]. More so, the greater the severity of TBI increases the risk of AD [64–66,76]. The risk of CTE is also suggested to be increased when linked to the number of TBI events and the length of time contact sports athletes and military personnel are active [79,96]. In these tauopathies, tau follows an explicit and predictable spatiotemporal pattern of deposition as described by the neuropathological staging of tau accumulation in AD and CTE, among others. Recently, tau aggregates have been attributed with prion-like properties, including *in vitro* and *in vivo* seeding and spreading capability [97–99]. It has been suggested that spreading can be due to tau propagating by the functional connectome in the brain [49,100,101]. The formation of tau misfolded aggregates and progression to disease could be a result of TBI events. In this study, we evaluated whether moderate to severe TBI can trigger the initial formation of pathological tau that would induce the development of the pathology throughout the brain. To this end, we subjected tau transgenic mice to TBI and assessed tau

phosphorylation and aggregation pattern to create a spatial heat map of tau deposition and spreading in the brain. Our results suggest that brain injured tau transgenic mice have an accelerated tau pathology in different brain regions that increases over time compared to sham mice. The appearance of pathological tau occurs in regions distant to the injury area which are synaptically connected, suggesting dissemination of tau aggregates. Overall, this work posits TBI as a risk factor for tauopathies through the induction of tau hyperphosphorylation and aggregation.

Results

TBI induces rapid acceleration of tau hyperphosphorylation

In an effort to determine the effect of TBI in the induction of tau aggregates, 3 month old P301S transgenic mice were subjected to TBI by controlled cortical impact (CCI) and sacrificed 1 day, 1 week, 2 months, or 6 months post-injury. A set of P301S transgenic mice was sham-induced (skin opened under anesthesia) and used as a control. To assess the effect of CCI injury and associative degree of tau pathology on behavior, acute neurological assessment was performed following CCI. Animals exposed to TBI had impairments in simple, non-postural somatosensory functions and complex, postural somatosensory functions ($p<0.001$) indicating the immediate impact of CCI injury on the central nervous system (Figure 7A). Hematoma and edema were seen transiently after TBI in brain at 1 day and 1 week post-operation. Later time-points revealed a collapsed deformation (Figure 7B). Brains were analyzed by immunohistochemistry to determine the presence of pTau using AT8 antibody. We assessed burden quantification of the immunoreactive AT8-positive area and generated an overall heat map of tau deposition in brain in both TBI-induced mice and sham animals from early to late stage time-points. The presence of AT8-positive tau aggregates was analyzed both in the ipsilateral and contralateral hemispheres and in four brain areas (rostral to the impact, in the rostral impacted area, in the caudal impacted area, and caudal to the impact).

Just 1 day after the TBI induction, we detected pathological tau in P301S TBI mice in comparison to age-matched sham mice in primarily the overall and ipsilateral (Ipsi) area of the impacted side (Figure 8A-B). We observed a significant difference of AT8 burden (percentage of AT8-immunoreactive area per total area analyzed) in the cortex and amygdala (Ctx), hippocampal area (Hp), and brainstem (BS) (Ipsi Ctx $p<0.001$; overall Ctx $p<0.01$, overall Hp, Ipsi Hp, and BS

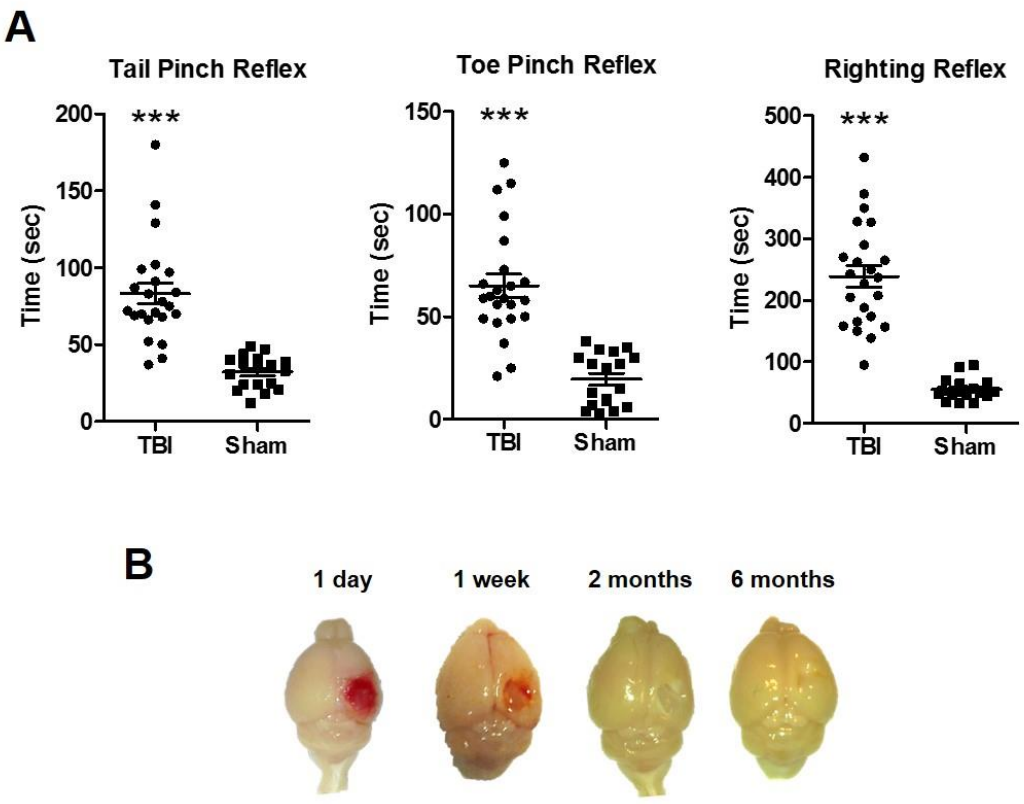

Figure 7. Traumatic brain injury (TBI)-associated impaired function and brain damage. (A) Mice were tested for somatosensory functions immediately after controlled cortical impact (CCI) or sham surgery by Mann-Whitney test (***$p < 0.001$). (B) Representative images of brain damage after CCI over the right parietal cortex in mice after one day, one week, two months, and six months post-operation are shown. Hematoma and edema are indicated transiently after impact, thereby forming a collapsed 1mm deformation in brain at later stages.

$p<0.05$) (Figure 8B). With this data, we created the spatial heat map of tau deposition in the brain of TBI versus sham mice (Figure 8C). P301S mice subjected to TBI developed AT8-immunoreactive tau highest in the amygdala, in particular lateral and medial amygdaloid nucleus; neocortical areas such as entorhinal, piriform, and perirhinal cortices; as well as brainstem structures, such as pons and medulla. The deposition exhibited a range from a caudal to rostral mosaic and ventral to dorsal approach within and near the area of impact as well as below the impact, mainly affecting the hippocampal formation. To determine the aggregation stage of the

phosphorylated tau, we performed an ELISA test to detect the amount of insoluble tau. Brain homogenates from a different set of animals were ultra-centrifuged to obtain the formic acid-soluble fraction. TBI-induced animals have higher levels of insoluble tau in the ipsilateral hemisphere than the non-impacted area (Figure 8D). In addition, the level of insoluble tau is increased in the TBI group compared to sham mice (Figure 8E). To evaluate the AT8 burden levels over time, we analyzed tau deposition in TBI and sham mice after 1 week. Immunohistochemical staining using AT8 antibody (Figure 9A) was quantified in both groups. TBI mice displayed a significantly exacerbated tau pathology compared to sham mice 1 week post-injury in the following brain regions (Ipsi, Contra, and overall Ctx $p<0.01$; overall Hp and BS $p<0.05$) (Figure 9B).

Figure 8. Tau aggregation is induced one day after traumatic brain injury (TBI). Tau hyperphosphorylation was assessed in brain homogenates and coronal tissue sections in three-month-old P301S TBI and sham induced mice one day after the event. (A) Representative bright field microscopy images of AT8 immunoreactivity in TBI and sham mice brain sections. (B) The AT8 burden quantification was obtained by analyzing the percentage of the area reactive with AT8 antibody in relation to the total area analyzed in the cortex/amygdala, hippocampal area, and brainstem. Statistical analysis was performed by Student t test or Mann-Whitney test for the ipsilateral (Ipsi) and contralateral (Contra) areas of impact as well as overall brain region. Ipsilateral and contralateral hippocampus quantifications were analyzed by Mann-Whitney test. (C) Semi-quantitative evaluation (lowest [0] to highest [5]) of tau deposition is captured in the heat map at different distance from the impacted area. The star denotes the estimated placement of impact. (D,E) Insoluble tau levels were evaluated by serial extraction and enzyme-linked immunosorbent assay performed in the formic acid fraction of the brains. Graphs in panels B, D, and E show the mean – standard error of the mean of the n = 5 animals analyzed per group. Scale bar: 100 μm. *$p < 0.05$, **$p < 0.01$, ***$p < 0.001$.

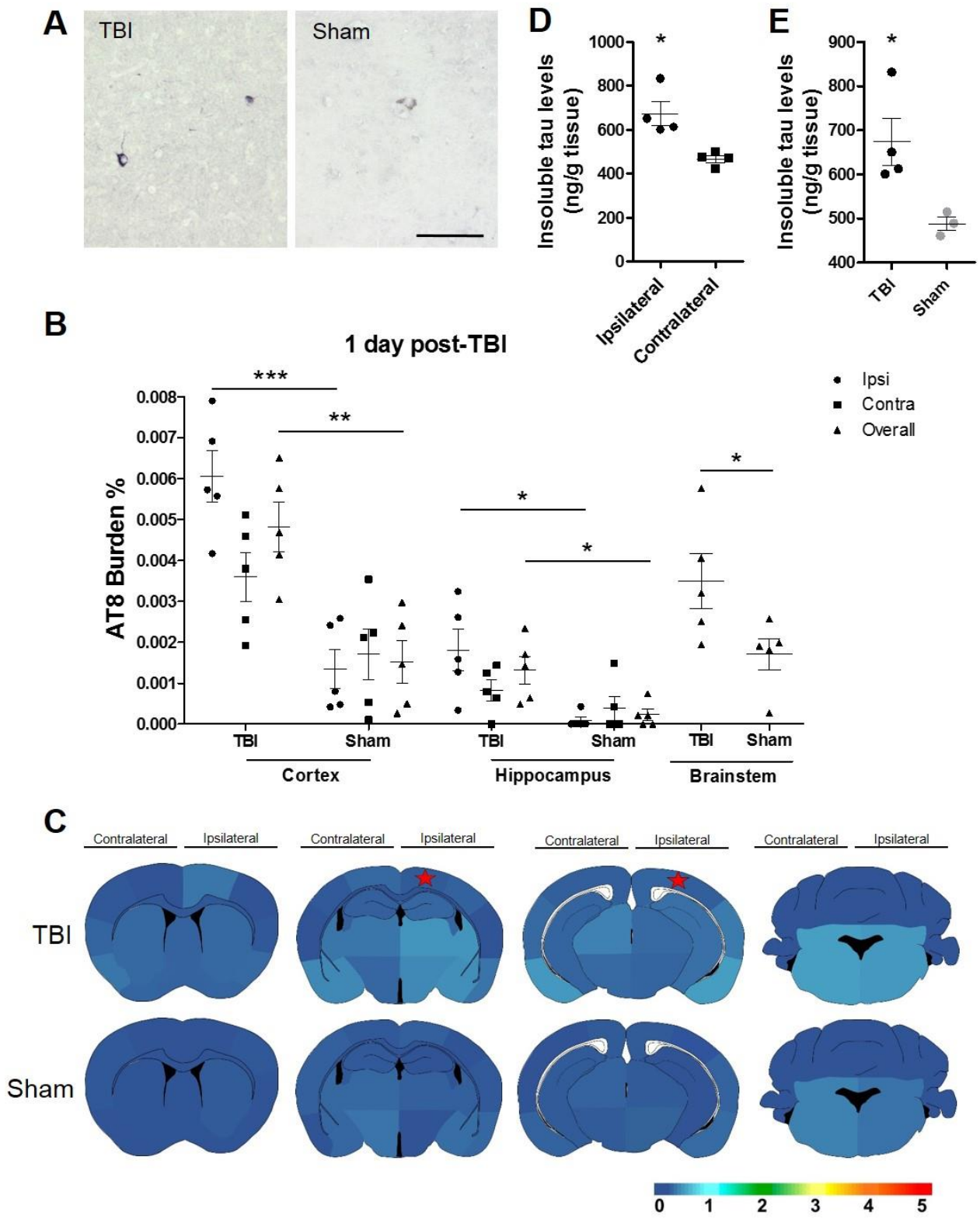
A
TBI
Sham
D
Insoluble tau levels (ng/g tissue)
1000
800
600
400
200
0
*
Ipsilateral
Contralateral
E
Insoluble tau levels (ng/g tissue)
900
800
700
600
500
400
*
TBI
Sham
B
1 day post-TBI
Ipsi
Contra
Overall
AT8 Burden %
0.008
0.007
0.006
0.005
0.004
0.003
0.002
0.001
0.000
***
**
*
*
*
TBI
Sham
TBI
Sham
TBI
Sham
Cortex
Hippocampus
Brainstem
C
Contralateral
Ipsilateral
TBI
Sham
0
1
2
3
4
5

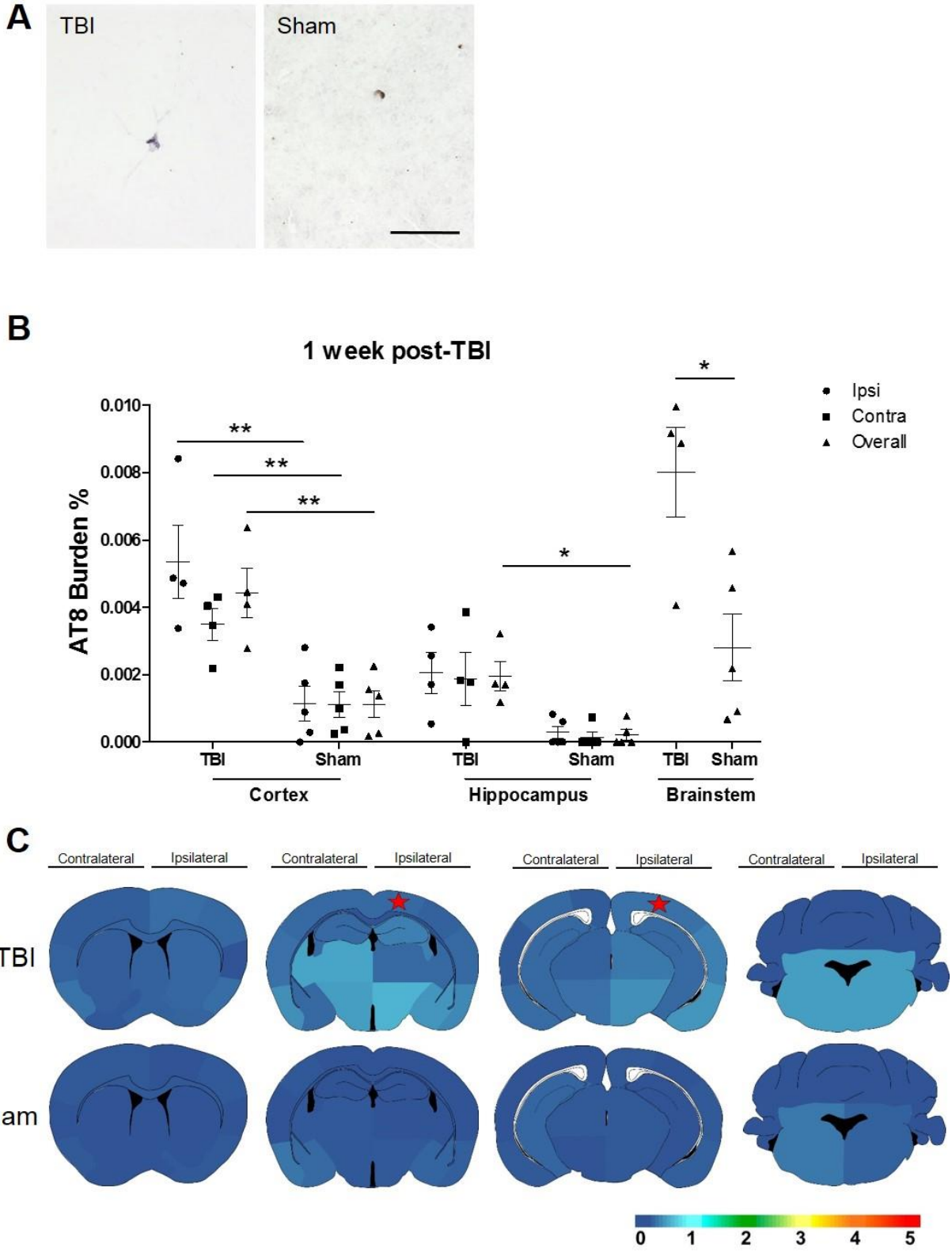
A
TBI
Sham
B
1 week post-TBI
AT8 Burden %
0.010
0.008
0.006
0.004
0.002
0.000
**
**
**
*
*
Ipsi
Contra
Overall
TBI
Sham
TBI
Sham
TBI
Sham
Cortex
Hippocampus
Brainstem
C
Contralateral
Ipsilateral
Contralateral
Ipsilateral
Contralateral
Ipsilateral
Contralateral
Ipsilateral
TBI
Sham
0
1
2
3
4
5

Figure 9. Spatial pattern and burden of pathological tau one week after traumatic brain injury (TBI). The P301S mice having either a TBI or sham surgery were assessed for tau aggregate formation and spreading by AT8 immunostaining. **(A)** Representative images of the TBI and sham animals using AT8 antibody are displayed. **(B)** The AT8 burden was evaluated in the cortex, hippocampal area, and brainstem in overall, ipsilateral (Ipsi), and contralateral (Contra) side of impact. Ipsilateral and contralateral hippocampus were evaluated by Mann-Whitney test, while all other data underwent Student t test. **(C)** Four coronal areas per animal were assessed to recreate a heat map to navigate tau spreading after TBI. Heat map scale: lowest (0) to highest (5) score. The star denotes the estimated placement of impact. Scale bar: 100 μm. *$p < 0.05$, **$p < 0.01$. Data is expressed as means ± SEM.

The spatial heat maps revealed more sporadic tau formation in the TBI mice in comparison to their respective sham counterparts (Figure 9C). We observed that after 1 week, TBI mice projected a spatial tau pattern reminiscent of the 1 day TBI mice, but extending to the contralateral side of impact of the cortical and hippocampal areas, albeit at modest yet progressing levels, and increased compared to age-matched sham mice. 1-2 months after CCI induction, TBI mice demonstrated higher AT8 burden in the overall Ctx and BS ($p<0.01$) and Ipsi Hp ($p<0.05$) as observed in the representative pictures and the burden quantification (Figure 10A-B). Both groups represented advancing tau pathology at 4-5 months of age; however, TBI-induced animals demonstrated higher average burden scores in comparison to sham mice as observed in the heat map of global tau distribution (Figure 10C).

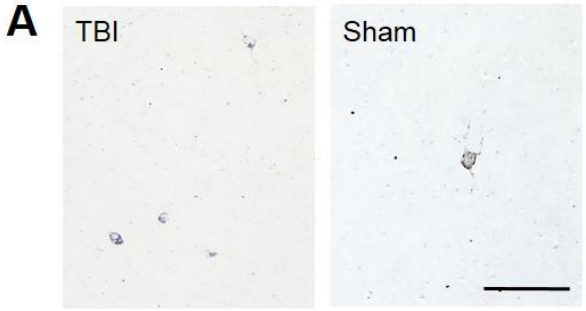
A
TBI
Sham

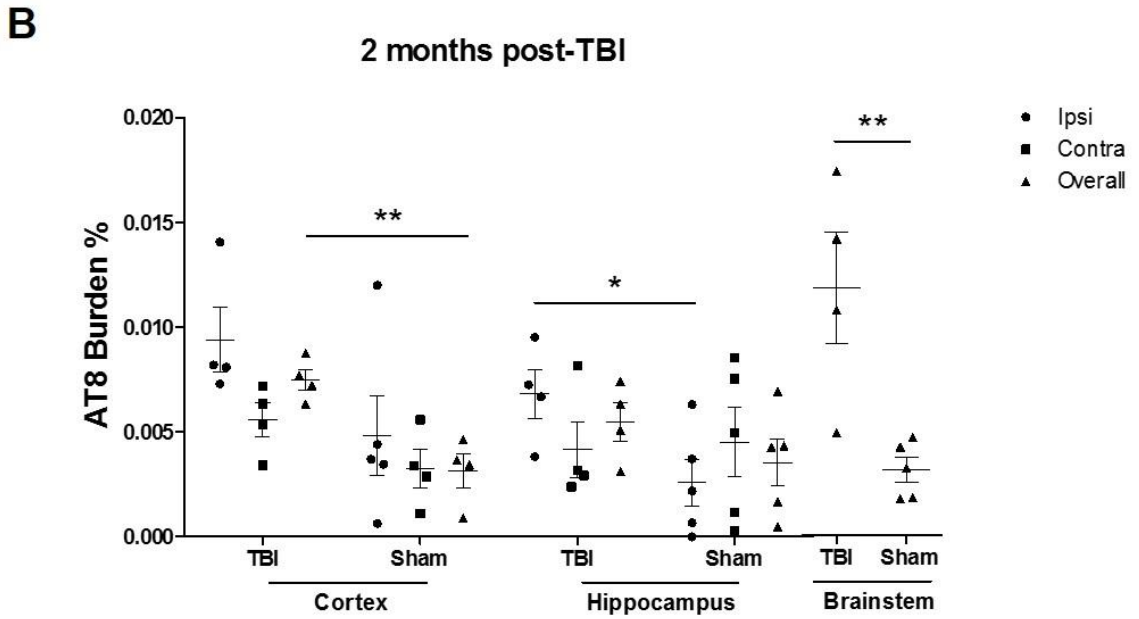
B
2 months post-TBI
AT8 Burden %
0.020
0.015
0.010
0.005
0.000
**
*
**
Ipsi
Contra
Overall
TBI
Sham
TBI
Sham
TBI
Sham
Cortex
Hippocampus
Brainstem

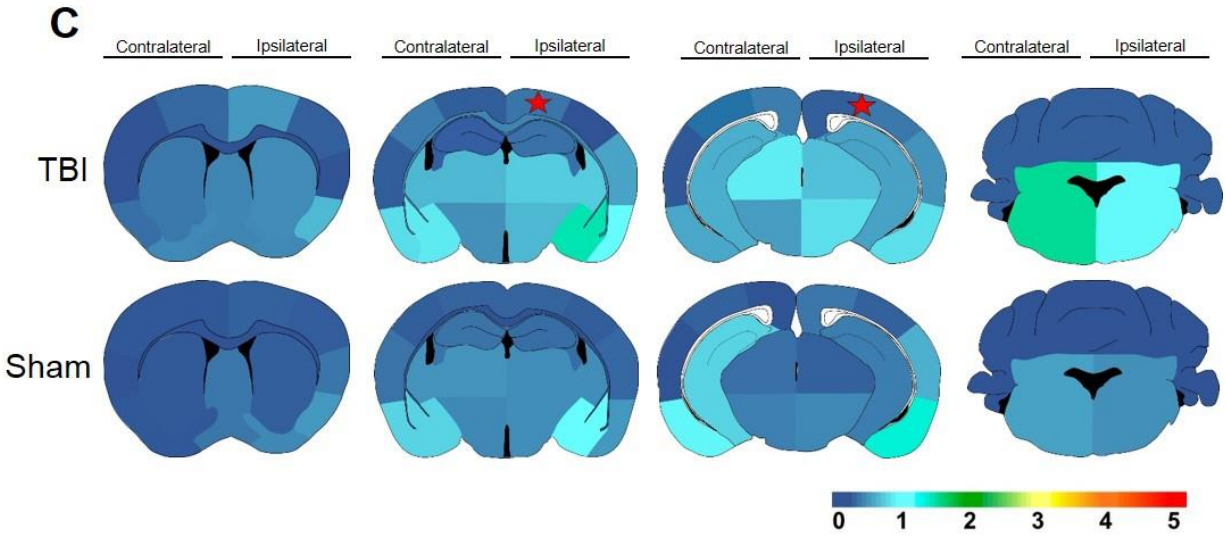
C
Contralateral
Ipsilateral
Contralateral
Ipsilateral
Contralateral
Ipsilateral
Contralateral
Ipsilateral
TBI
Sham
0
1
2
3
4
5

Figure 10. Tau aggregation is significantly increased two months after traumatic brain injury (TBI) injury. (A) Illustrative microphotography of AT8 immunopositive staining visually displayed growing pathologic tau aggregation. (B) The AT8 burden quantification in the overall, ipsilateral (Ipsi), and contralateral (Contra) impacted area in the three main brain regions analyzed. Ipsilateral cortex and Contra hippocampus were evaluated by Mann Whitney test, while all other statistical analysis was performed by Student t test. (C) The spatial heat map revealed increasing tau burden and presence of pathogenic tau aggregates in multiple areas in TBI-induced mice having more aggressive pathology compared with sham mice. Scale bar: 100 μm. Heat map scale: lowest (0) to highest (5) score. The star denotes the estimated placement of impact. *$p < 0.05$, **$p < 0.01$.

TBI induces long-term cognitive impairment and accelerated tau pathology.

To evaluate the long-term effect of a single moderate to severe TBI event, we induced CCI in Tg and WT animals and analyzed them 6 months post-injury. Transgenic sham animals were also evaluated. Animals 5.5 months following either CCI or sham surgery were analyzed in Barnes maze to evaluate spatial learning and memory. During the learning period, TBI-induced WT and Tg sham mice demonstrated their ability to learn a new task by a quicker latency to the escape hole over time, however Tg TBI-induced mice took longer compared to the control animals to learn the task ($p <0.05$, $p<0.001$) (Figure 11A). 7 days later, long-term memory was examined, and Tg TBI-induced animals revealed significant impaired memory abilities in comparison to controls ($p< 0.01$) (Figure 11B). Thus, Tg TBI mice posited impaired learning and memory several months after the CCI induction. Then, we evaluated tau burden and created a heat map of tau deposition 6 months post-TBI. Tau pathology was more dramatic in the TBI-induced mice in comparison to age-matched sham controls as observed in representative immunohistochemical images. As observed in Figure 12A, NFTs-like structures were seen profusely throughout the

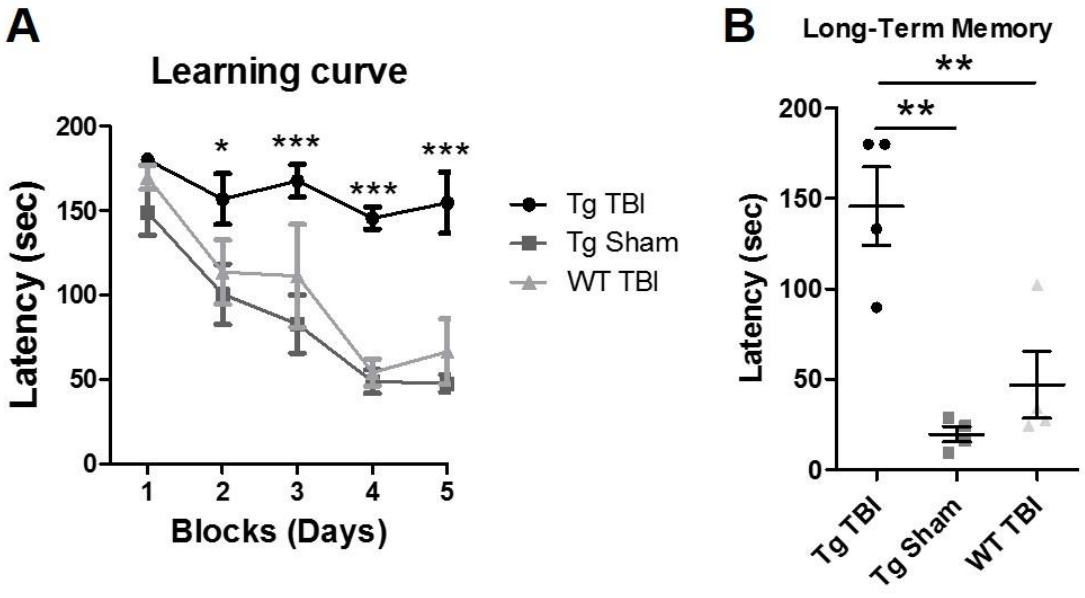

Figure 11. Traumatic brain injury (TBI) promotes behavior impairment in transgenic tau mice in the chronic stage of injury. Barnes maze test was performed on P301S TBI, P301S sham, and wild-type (WT) littermate TBI mice six months after controlled cortical impact injury. The P301S TBI mice exhibited attenuated learning and memory capabilities observed by the learning curve **(A)** and long term memory assessment **(B)** *$p < 0.05$, **$p < 0.01$, ***$p < 0.001$. Data is expressed as means ± SEM.

entorhinal cortex and hippocampus both in the superficial molecular and deep polymorphic layers with intense staining in the pyramidal cells in CA1. Tg TBI mice display a robust tau burden in the isocortex and throughout the hippocampal formation. AT8 burden quantifications revealed significant differences between TBI and sham mice in cortical and hippocampal areas (Ipsi, Contra, and overall Ctx; Ipsi, Contra, and overall Hp $p<0.05$) (Figure 12B). The tau heat map shows the intrinsic tau spreading mosaic of the Tg model of the sham group that seems to be maintained in the TBI-induced mice albeit with augmented dispersion and increased tau levels (Figure 12C). Areas that exhibited the greatest tau burden scores at this late stage time-point were

the amygdaloid nucleus and piriform/entorhinal cortex as well as caudally in the brainstem (pons-medulla).

Figure 12. Robust tau pathology six months after traumatic brain injury (TBI). (A) Example AT8 microscope images illustrate substantial tau pathology in TBI mice six months after injury compared with age-matched sham mice. **(B)** The AT8 burden quantification shows a significant overall increase of tau deposition in TBI mice compared with sham mice in the ipsilateral (Ipsi), contralateral (Contra), and overall cortex and hippocampal area. Statistics for brainstem were calculated by Mann-Whitney test, while all other were performed by Student t test. **(C)** The AT8 burden scores exhibited in a spatial heat map of four rostrocaudal areas in TBI versus sham mice. Heat map scale: lowest (0) to highest (5) score. Star denotes the estimated placement of impact. Scale bar: 100 μm. *$p < 0.05$. Data is expressed as means ± SEM.

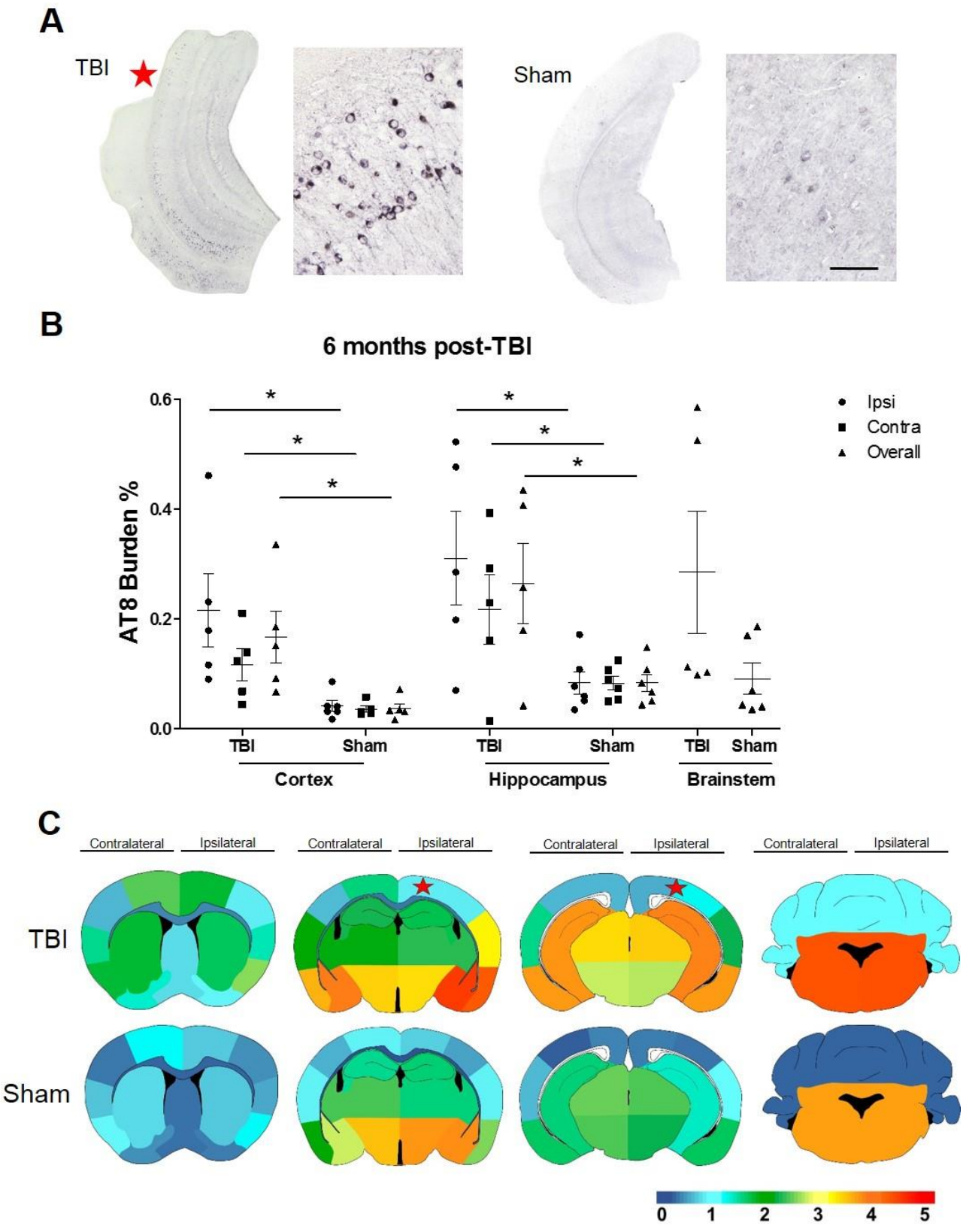
A
TBI
Sham
B
6 months post-TBI
AT8 Burden %
0.6
0.4
0.2
0.0
Ipsi
Contra
Overall
TBI
Sham
Cortex
Hippocampus
Brainstem
C
Contralateral
Ipsilateral
TBI
Sham
0
1
2
3
4
5

TBI-induced mice demonstrate tau deposition altered tropism

To investigate whether the increase of tau burden produced by TBI is just due to an increase in the endogenous tau production or the induction of tau aggregation in areas where tau usually do not deposit, we analyzed at different time-points the brain areas where the P301S mice typically do not have tau deposition. Images taken 1 day post-TBI using the AT8 antibody indicate the existence of tau hyperphosphorylation in the CA1 region of the Ipsi Hp, infrequent at this age in non-induced P301S mice (Figure 13, left panel). The altered tropism of tau aggregation following TBI is also observed 1 week post-TBI in the cortical area, close to the retrosplenial cortex (Figure 13, middle panel), as well as in the cerebellum 6 months after TBI (Figure 13, right panel). It is noteworthy that, along with the total aggregated tau burden assessment done in Tg TBI and Tg sham mice, no AT8 immunopositive tau was detected in WT TBI-induced animals even 6 months post-injury (data not shown). Table 2 summarizes the fold-change for aggregated tau burden in brain between TBI- and sham-induced mice after 1 day, 1 week, 1-2 months, and 6 months following the surgery. This table of tau distribution encompasses the Ctx, Hp, and BS in relation to the impacted area (overall, Ipsi, and Contra). In general, there is a significant fold-change response in the Ctx, Hp, and BS of the TBI mice compared to sham mice at the various assessed time-points with a majority of the regions displaying significant increase overall and on the Ipsi side of impact. The largest fold-change (21.14) is seen following 1 day after CCI impact in the ipsilateral Hp, followed by the more caudally impacted area in the Hp (10.14 fold-change). After 1 week, the largest fold change difference that occurred following CCI was on the contralateral side of impact for the Hp followed by the Ctx compared to their respective sham group. Thus, tau aggregate formation exacerbates 1 day after TBI and spreads throughout the brain significantly, even to the contralateral side of impact, 1 week after. Although differences in tau burden fold-change decrease at 1 and 6 months post-TBI, these alterations are kept at 3-8 fold-

increase in the Hp and Ctx over time. On the other hand, one area with the highest endogenous tau deposition in this animal model, the BS, is the least affected by TBI (between 2 to 3 fold increase).

Figure 13. Altered tropism of tau deposition after traumatic brain injury (TBI). Representative figures of pathological tau deposition as evaluated by AT8 immunohistochemistry in hippocampus, cortex, and cerebellar lobes in mice six months after TBI. Age-matched P301S sham animals revealed very low detectability using AT8 at the different times analyzed. Scale bar: 300 μm; insets: 100 μm. CA1, cornu ammonis 1 area; cc, corpus callosum; DG, dentate gyrus; Ctx, cortex; Hp, hippocampus; ml, molecular layer, gl, granular layer; wm, white matter**.**

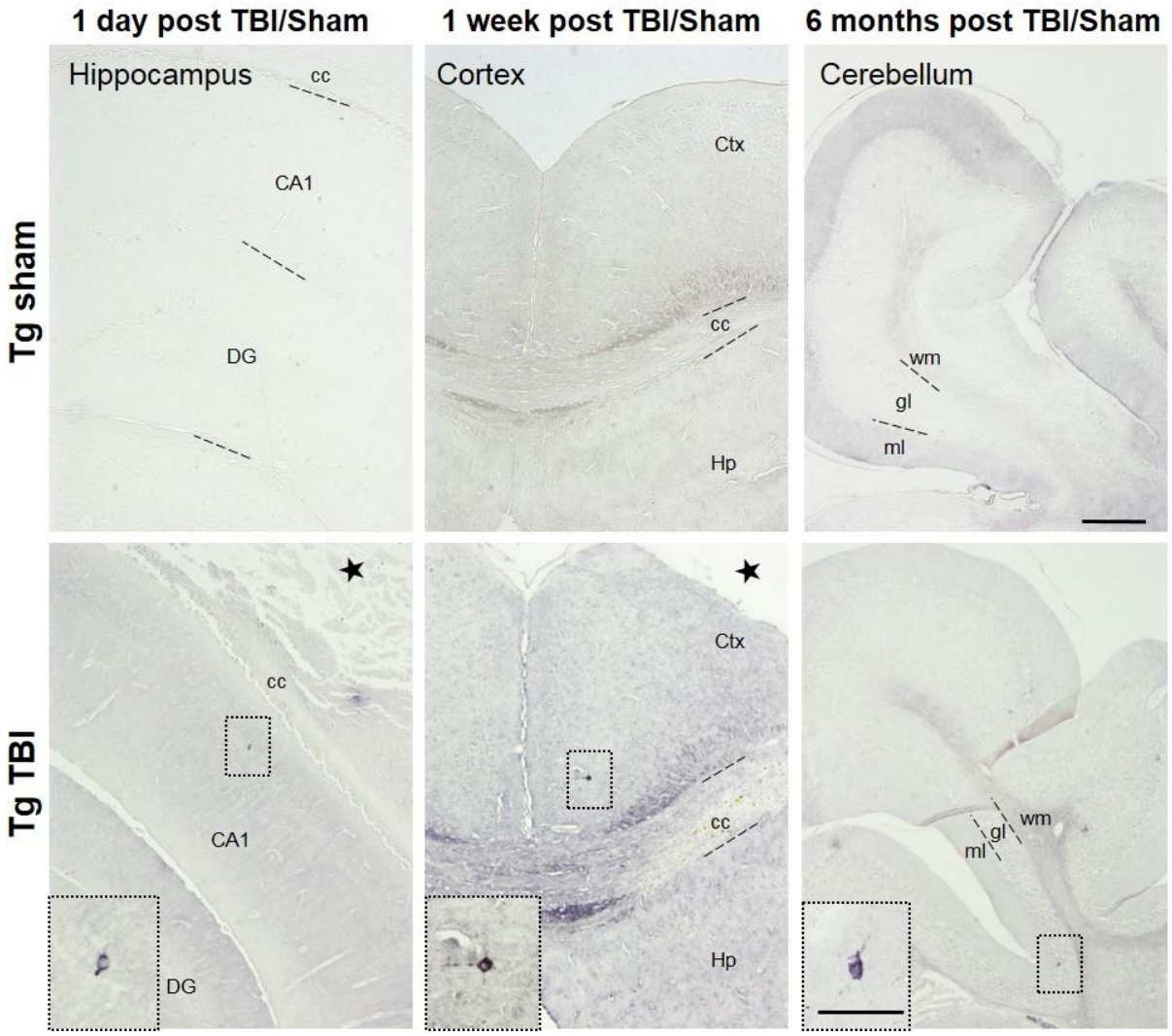

Time post-TBI	Area	Rostral			Impacted rostral			Impacted caudal			Caudal	Average		
		Contra	Ipsi	Overall	Contra	Ipsi	Overall	Contra	Ipsi	Overall	Overall	Contra	Ipsi	Overall
1 day	HPa				N/A	N/A	8.54* 0.00010 to 0.0019 -0.00021 to 0.00044	2.91 8.2e-005 to 0.0030 -0.00047 to 0.0015	10.14* 5.7e-005 to 0.0034 -0.00030 to 0.00065	4.67* 0.00028 to 0.0030 -0.00012 to 0.00082		2.15 0.00012 to 0.0015 -0.00042 to 0.0012	21.14* 0.00040 to 0.0032 -0.00015 to 0.00032	5.63* 0.00037 to 0.0023 -0.00014 to 0.00061
	Cortex	2.32 0.00055 to 0.0029 -0.00053 to 0.0020	4.46* 0.00094 to 0.0062 0.00019 to 0.0014	3.43* 0.00087 to 0.0044 -2.3e-005 to 0.0016	2.98 0.00028 to 0.0047 2.8e-005 to 0.0017	3.11 -0.0014 to 0.0080 -0.00072 to 0.0029	3.04 0.00024 to 0.0056 -4.9e-005 to 0.0020	1.86 0.0027 to 0.010 -0.0019 to 0.0089	5.24* 0.0016 to 0.021 -0.00094 to 0.0052	3.14 0.0024 to 0.015 -0.0014 to 0.0070		2.11 0.0019 to 0.0053 -2.5e-005 to 0.0034	4.52* 0.0043 to 0.0078 9.7e-006 to 0.0027	3.17* 0.0031 to 0.0065 6.2e-005 to 0.0030
	BS										2.04* 0.0016 to 0.0054 0.00065 to 0.0028			2.04* 0.0016 to 0.0054 0.00065 to 0.0028
1 week	HPa				N/A	6.77 -0.0013 to 0.0058 -0.00059 to 0.0012	11.91* 0.00043 to 0.0035 -0.00029 to 0.00062	6.89 -0.0029 to 0.0070 -0.00052 to 0.0011	7.71 -0.0016 to 0.0053 -0.00043 to 0.00092	7.26 -0.00027 to 0.0042 -0.00019 to 0.00073		12.67 -0.00064 to 0.0044 -0.00026 to 0.00056	7.16 0.00010 to 0.0040 -0.00021 to 0.00078	9.03* 0.00058 to 0.0033 -0.00021 to 0.00064
	Cortex	2.98 -0.00081 to 0.0032 -0.00031 to 0.00066	6.82 0.00046 to 0.0037 -0.00012 to 0.0020	2.25* 0.0011 to 0.0022 2.4e-005 to 0.0011	4.25* 0.0020 to 0.0079 0.00011 to 0.0022	5.58* 0.0045 to 0.0061 -0.00069 to 0.0026	4.85* 0.0035 to 0.0067 -0.00023 to 0.0023	2.22 0.00042 to 0.0083 -0.00041 to 0.0043	5.49* -0.00059 to 0.018 -0.00031 to 0.0035	3.68* 0.00042 to 0.013 -0.00016 to 0.0037		3.18* 0.0020 to 0.0050 4.4e-005 to 0.0022	4.65* 0.0019 to 0.0088 -0.00027 to 0.0026	3.93* 0.0021 to 0.0068 2.4e-005 to 0.0022
	BS										2.86* 0.0038 to 0.012 4.5e-005 to 0.0056			2.86* 0.0038 to 0.012 4.5e-005 to 0.0056
1-2 months	HPa				N/A	2.28 -0.0027 to 0.020 -0.00021 to 0.0078	1.23 -0.0011 to 0.014 0.00078 to 0.0094	1.7 0.00082 to 0.0082 -0.0016 to 0.0070	3.69 -0.0023 to 0.012 -0.0019 to 0.0046	6.72* 0.0028 to 0.0067 -0.00061 to 0.0020		0.93 -0.00010 to 0.0084 -9.4e-005 to 0.0091	2.65* 0.0031 to 0.011 -0.00057 to 0.0057	1.55 0.0025 to 0.0084 0.00040 to 0.0067
	Cortex	1.05 0.00056 to 0.0034 -0.00013 to 0.0039	1.05 0.00030 to 0.0067 -0.0011 to 0.0078	1.05 0.0012 to 0.0043 -0.00035 to 0.0056	6.82 -0.0031 to 0.018 0.00052 to 0.0016	3.71* 0.0022 to 0.024 -0.0022 to 0.0093	7.71* 0.0040 to 0.017 -0.00043 to 0.0031	1.03 -0.0037 to 0.018 -0.0019 to 0.016	1.51 0.00068 to 0.022 0.0014 to 0.014	1.48 -0.00055 to 0.019 -0.0040 to 0.028		1.72 0.0030 to 0.0082 0.00032 to 0.0062	1.94 0.0044 to 0.014 -0.00043 to 0.010	2.38* 0.0059 to 0.0091 0.00060 to 0.0057
	BS										3.76* 0.0033 to 0.020 0.0015 to 0.0048			3.76* 0.0033 to 0.020 0.0015 to 0.0048
6 months	HPa				2.29* 0.068 to 0.30 0.021 to 0.14	3.04* 0.23 to 0.33 0.029 to 0.16	2.44* 0.075 to 0.34 0.029 to 0.14	4.39 -0.014 to 0.52 0.021 to 0.093	9.29* 0.039 to 0.75 0.016 to 0.068	6.53* 0.027 to 0.62 0.020 to 0.079		2.62* 0.041 to 0.40 0.052 to 0.11	3.69* 0.076 to 0.55 0.032 to 0.14	3.16* 0.062 to 0.47 0.043 to 0.12
	Cortex	4.07 -0.0038 to 0.15 0.0067 to 0.028	4.02 -0.01712 to 0.1773 .009921 to 0.02997	4.04 -0.0098 to 0.16 0.0096 to 0.028	3.42* 0.048 to 0.24 0.028 to 0.055	4.65* 0.11 to 0.52 0.012 to 0.12	4.18* 0.080 to 0.37 0.021 to 0.088	3.54* 0.025 to 0.25 0.011 to 0.067	6.61* -0.020 to 0.53 0.019 to 0.058	5.06* 0.0063 to 0.39 0.015 to 0.063		3.58* 0.037 to 0.20 0.018 to 0.048	5.15* 0.032 to 0.40 0.017 to 0.066	4.46* 0.036 to 0.30 0.018 to 0.057
	BS										3.12 -0.023 to 0.59 0.019 to 0.16			3.12 -0.023 to 0.59 0.019 to 0.16

Fold increase	<5 fold	5-10 fold	>10 fold

Table 2. Traumatic brain injury (TBI)-induced tau aggregates fold-change summary. The AT8 burden fold-change is represented in the overall, ipsilateral (Ipsi) and contralateral (Contra) side of impact in the hippocampal area (HPa), cortex/amygdala, and brainstem (BS) in relation to the respective brain areas rostrocaudally to the impacted side in TBI versus sham induced mice. The colored scale exhibits the lowest to highest fold change compared with sham brains. The fold change values displayed in red were analyzed by Mann-Whitney test while all other data analysis was performed by Student t test. The values below the fold change display the lower to upper 95% confidence interval of the mean of the TBI (top) and sham (bottom) groups. *$p < 0.05$.

Discussion

TBI has been reported to be an important risk factor for several tauopathies [71-75,81]. Experimental models and human cases have shown formation of tau aggregates following a moderate to severe TBI; however, the exact linkage to deposition of pathological tau and disease remains to be elucidated [63,102]. In this study, young P301S mice subjected to TBI were analyzed at short and long time-points after the impact, and brains were assessed for tau aggregation and spreading. We have determined that TBI induction is able to increase tau burden as early as 1 day post-TBI in the cortex/amygdala, hippocampal area, and brain stem with robust deposition on the ipsilateral side of the impact. 1 week after TBI, induced mice exhibited a robust deposition on the contralateral side of the brain compared to sham animals. Increased levels of tau following TBI can translate to aggravated behavior and clinical symptoms, as observed 6 months after injury. Overall, we have demonstrated that TBI intensifies tau pathology compared to sham transgenic mice in different brain regions, especially those close to the impacted area, showing a peak a few days later. Levels of aggregated tau have been found augmented in 6 month-old P301L mice 1 day after induction of CCI, thus supporting our results [103]. Other moderate-severe TBI models, such as fluid percussion injury [104], Feeney's weight drop [105], and blast injury [106] have reported

pTau augmentation in mouse and rat models. In addition, induction of CCI in AD mouse models overexpressing amyloid beta, such as 3xTgAD and Tg2576, have also demonstrated increased pTau [107,108]. However, none of the previous studies have shown the temporal distribution of pTau and tau aggregates after the initial insult and the spatial spreading of the misfolded tau from the original impacted area.

The results obtained in our study support the idea that TBI is a risk factor for tauopathies and provides novel insight into the induction of pTau pathology following TBI. However, our study has some limitations. The PS19 (P301S mutation) model overexpresses 5-fold the human mutant tau protein under the prion promoter, which may differentially alter expression of MAPT in different brain regions leading to ectopic endogenous expression. In addition, the human version of tau in this animal is 4R1N, which may influence the propensity of tau to aggregate after TBI, the type of aggregates that are formed, or even their tropism. Nevertheless, the PS19 model has been proposed as a good alternative to study acceleration of the disease and tau transmission [109,110]. The use of humanized tau models expressing wild-type human tau may help to overcome these limitations. The use of animals conserving the human 3R/4R ratio will also be beneficial to determine the effect of TBI, specifically for AD.

TBI-induced mice had elevated levels of pTau compared to sham mice in the ventral isocortex, in particular amygdaloid nucleus, piriform and entorhinal cortices, indicating an innate tau progression associated to the regular tau pattern deposition in the P301S mouse model [110]. These areas are also the first ones affected by tau pathology in early stages of Alzheimer's disease [6-9,23,24,56–58]. When comparing the ipsilateral and contralateral sides of impact, it revealed higher tau burden on the impacted hemisphere, indicating the direct association between the TBI and increased aggregation of tau. Tau deposition was seen in the ipsilateral hippocampus, just below the directly impacted area, as well as less common areas that would not normally have tau

deposition in the naïve transgenic mouse such as the cingulate gyrus, auditory and vision cortices, corpus callosum, and cerebellum. In fact, cerebellar tau aggregation has been noted in the P301S mouse model but usually occurs at a later age than assessed here, similar to the tau pathology observed in AD patients [111,112]. Therefore, TBI not only increases tau deposition nearby the impacted area, but also induces tau aggregation in distant areas that are not usually affected in animals not subjected to TBI. The uncommon, altered tropism of tau phosphorylation observed in TBI-induced animals could be due to different mechanisms such as contrecoup, where the ventral portion of the brain could collide on the posterior skull or by acceleration and deceleration forces. Consequently, the contrecoup could be playing a role in tau aggregation as the ventral cortex continuously displayed elevated tau burden following TBI due to the secondary brain injury inside the skull. Our results posit that TBI can elicit the formation of early tau aggregates exacerbating the ipsilateral side of impact while pathological tau propagates to other brain areas increasing its burden along neuronal connections causing widespread distribution of tau pathology over time.

Another possibility for the increase of tau aggregation in areas distant from the impacted region is the spreading of pathologic tau through neuronal connections. It is already accepted that tau aggregates can propagate through functionally connected brain regions after the exogenous addition of seeding-competent material, whether disease-associated brain homogenate or recombinant tau aggregates [43–49]. In addition, the rTg4510 mouse model, which expresses human mutant P301L tau in the entorhinal cortex, is able to develop full brain tau pathology due to the spreading of tau pathology from the initial expression brain region to the hippocampus, neocortex, and amygdala over time, indicating the propagation of misfolded tau through interconnected regions as a mechanism for disease progression [57,58]. Our results indicate that tau propagation seems to occur by neuronally connected areas following TBI in a stereotypical and temporal

pattern, and less likely by spatial proximity, since we do not see an increase in tau aggregation in the damaged area over time – mostly in nearby proximity. As observed in the heat maps, the brain regions most affected are those with direct projections to or from the impacted area including the entorhinal cortex, hippocampal area, amygdala, brainstem, piriform and rhinal cortices, hypothalamus, and septal nucleus. It is worth to mention that this study does not validate spreading of tau pathology by a prion-like manner following TBI. Seeding capability of the aggregates formed after TBI has not been tested by techniques such as protein misfolding amplification assay (PMCA) or bioassays; therefore, TBI-induced misfolded tau may or may not be seeding-competent [113]. The spreading observed here may be due to regular transport through the synapses or induction of tau hyperphosphorylation in different regions due to a contrecoup or associated inflammation maintained over time.

The alternative spatial aggregation pattern could also be determined by the formation of new tau conformations after TBI. Tau can aggregate acquiring different conformations, also termed "strains" [113–115]. Inoculation of brain homogenate from different tauopathies into mice induced comparable tau inclusions to that of the exogenous brain extract, thereby stably maintaining the specific strain assembly or conformation reminiscent of the initial pathology [3,24,36,40-42,113]. 18 tau strains have been characterized and when inoculated in P301S mice, they trigger strain-specific intracellular pathology in specific brain regions, spreading, and toxicity [115]. It is yet to be determined if TBI is responsible for generating different tau strains than those regularly expressed in the mouse model, and whether this phenomenon might be responsible for spreading the pathology to brain regions that are not commonly affected. In fact, AT8 antibody was utilized for assessing tau pathology after TBI, and it is able to recognize both pre-tangle and tangle pathology in brain. Therefore utilization of conformational specific antibodies of tau could be used to determine the exact pathological tau species and their location in brain after TBI. In

addition, the increase in tau hyperphosphorylation may have a potential pathophysiological role in the progression of the disease or be simply a consequence of other effects that TBI could be causing, such as a modification in the kinase/phosphatase expression and activity by which elevation of pTau could be initiated as a response to a general damage in the brain [78]. An ancillary factor in regards to the sequential pattern of tau deposition is a different brain regional vulnerability, and the existence of a variety of neuronal types that can get affected differently to tau pathology progression. The areas chiefly affected by tangles in AD, according to Braak staging, are those involved in higher-order cognitive functions, areas vulnerable in aging, as well as those that take the longest time for reaching maturity during development [8,9,11,60,61]. TBI could also generate a hostile brain microenvironment facilitating tau aggregation and propagation. Following a TBI event, this response can therefore be intensified, stimulating early disease-affiliated tau aggregates leading to disease onset and irreversible progression.

Overall, our results propose an increasing progression of tau aggregation after one single moderate to severe TBI, indicating that TBI accelerates tau hyperphosphorylation and aggregation in a time- and spatial-dependent manner. The formation of tau misfolded aggregates after the initial TBI may further template the aggregation of additional pathogenic units, participating in the formation of primordial protein misfolded seeds that will template pathological features leading to AD, CTE or other tauopathies. It remains to be identified the conformation and molecular properties of pathological tau induced by TBI events and what features these *de novo* generated aggregates have compared to tau deposition found in sporadic tauopathies.

CHAPTER 3

Determine the generation and spreading of tau pathology and behavior following repetitive mild TBI *in vivo*.

Rationale

The 90% of cases reported with TBI are those of a mild nature, especially strong prevalence in contact sports athletes and military personnel. Concussion or mTBI is a pathophysiological process affecting the brain induced by direct or indirect biomechanical forces that may include abnormal linear and rotational accelerations. With an estimated of 170 million adults and 38 million adolescents participating in physical activities, including sports, there is a high probability of a mTBI/concussion with approximately 1.6 to 3.8 million concussions occurring annually [116]. Moreover, this number is grossly underestimated with individuals either not reporting the incidence or lack of knowledge a TBI event transpired. In addition, mTBIs are heterogeneous in nature with no determined impact threshold, can present no loss of consciousness, and may show no damaging effects by brain imaging; however, there may be exigent and short-term impairment of neurologic function [84,92,94,117]. Certain neurodegenerative diseases such as CTE have been associated to rmTBI events by positing that a recurring insult to the brain may trigger a cascade of events leading to the onset of pathological abnormalities responsible for CTE. CTE was first described as punch-drunk syndrome or dementia pugilistica in studies from retired boxers, and since then, CTE has been identified in other contact sports, military personnel, and physical abuse cases. Evidence suggests the severity of the disease depends on the length of time individuals are engaged in contact sports or military service and the number of traumatic injuries that occur [63,77,80,84]. Moreover, research suggests that following a mTBI event with an additional mTBI in this vulnerable time-period or so-called secondary impact syndrome could be much more deleterious. CTE is a slow-progressing tauopathy demonstrated by the unique distribution of NFTs, which are composed of aggregated tau protein, in the brain with other pathological changes that lead to psychiatric and cognitive alterations. Tau protein is assumed to following a nucleation-polymerization model of amyloidogenesis and has exhibited

prion-like properties in disease. Questions still remain about what number of mTBIs, energy or level of impact, and role of induction and progression of tau pathology occurring over time regarding neurodegenerative tauopathies, like CTE. This aim will assess the effect of rmTBI on the formation of misfolded tau seeds that will lead to early development, spreading, and exacerbation of tau pathology. The main goal for this aim is to determine the effect of rmTBI on the formation of seeding-competent tau aggregates utilizing a contact sports athlete/CTE-like animal model. rmTBI was induced in Tg P301S tau mice by a modified mild, closed-head weight-drop impact model with a varied number of impacts, intervals between rmTBI, and ages upon evaluation. Neurobehavioral sequelae was assessed utilizing various behavioral tasks longitudinally to analyze the changes due to rmTBI and aggregate formation. Tau pathology was assayed by histology using various conformational specific methods and biochemical techniques analyzing the formation of early tau aggregates and anatomical spreading in the brain following rmTBI.

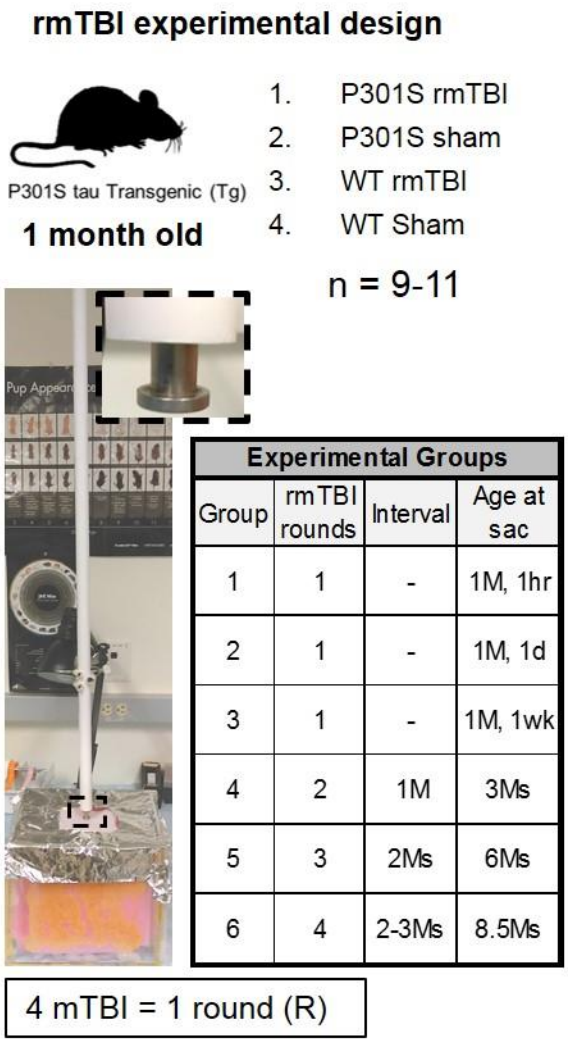

Figure 14. Experimental design for repetitive mild TBI. rmTBI was performed using a modified weight-drop method similar to the Wayne State method. 4 mTBIs were administered in 1 day (denoted as 1 round) over the head. As a control, sham mice were anesthetized and experienced the same fall through the platform but with no impact. Experimental groups were impacted at 1 month, 5 days old with varied rmTBI rounds over different time-points. Animals were sacrificed at: 1 hour (1 rmTBI round); 1 day (1 rmTBI round); 1 week (1 rmTBI round); 3 months (2 rmTBI rounds); or 6 months (3 rmTBI rounds) post-rmTBI event (Groups 1-5). Longitudinally studied mice sacrificed at 8.5 months of age had 4 rounds rmTBIs (16 total mTBI impacts in time) spread over time to assess exacerbation of tau pathology in an active athlete paradigm (Group 6). The groups (n = 9-11) assessed were P301S rmTBI, P301S sham, WT rmTBI, and WT sham mice.

Results

Four mTBIs were administered in 1 day (denoted as 1 round) over the head emulating multiple mild impacts or "second impact" syndrome. As a control, sham mice were anesthetized and experienced the same fall through the platform but with no impact. P301S and WT littermate mice were placed in experimental groups as noted in Figure 14, which included: P301S with rmTBI, P301S sham, WT with rmTBI, and WT sham (n = 9-1l for each time period). The described groups were exposed to the modified mild, closed-head weight-drop / sham treatment

at 1 month, 5 days and sacrificed at 1 hour (1 rmTBI round); 1 day (1 rmTBI round); 1 week (1 rmTBI round); 3 months (2 rmTBI rounds); 6 months (3 rmTBI rounds); or 8.5 months (4 rmTBI rounds) post-rmTBI event. No animals exhibited any gross anatomical disturbances, i.e. skull fractures or edema/hematoma when sacrificed, verifying the mild impact treatment. Neuropsychiatric behavioral tests (Splash test, Nesting, and Open field test), motor testing (RotaRod), and learning and memory assessment (Barnes maze, reversal learning) were performed before sacrifice. Tau pathology was determined by histology targeting different tau conformational structures and quantification in distinct brain regions as well as biochemical ELISA for insoluble tau levels from hemisected brains.

rmTBI triggers transient behavioral impairments along with augmented tau aggregation at early time-points

Following 1 round of rmTBI or sham induction, naïve P301S and WT were sacrificed 1 hour (hr), 1 day (d), or 1 week (wk) following impacts. Respective behavioral examinations were performed before sacrificing the groups, and tau pathology was assessed by histological and biochemical methods. Figure 15A reveals P301S and WT rmTBI mice impaired artificial grooming 1 hour and 1 day after rmTBI, yet there was no significant difference after 1 week (1hr and 1d, $p < 0.05$; 1wk, $p > 0.05$). P301S and WT rmTBI displayed lower overnight nesting scores 1 day and 1 week after rmTBI compared to controls ($p < 0.05$), respectively (Figure 15B). There was no difference in rmTBI and sham mice with latency to fall in RotaRod after 1 week after treatment ($p > 0.05$) (Figure 15C) as well as in percentage of time in the open field for open field testing (data not shown). When assessing the 1 hour, 1 day, and 1 week P301S rmTBI groups by ANOVA in grooming performance, the 1 week P301S rmTBI mice performed significantly better than the 1 hour and 1 day groups ($p < 0.0001$) (Figure 15D). 1 hour WT rmTBI mice exhibited significantly lower grooming time compared to the 1 day and 1 week post-rmTBI groups

comparing within the groups ($p < 0.0001$). There was no difference within the different time-point group analysis of the P301S sham and WT sham mice in Splash test (data not shown). The general neurobehavioral reaction from 1 hour to 1 day following rmTBI event may be due to the direct effects of the initial impact or a post-concussive like syndrome as both P301S and WT rmTBI had lowered performance, despite genotype. However, WT rmTBI mice may improve neuro-functionally slightly better following concussion in comparison to P301S rmTBI mice assayed by within group analysis of Splash test. P301S and WT rmTBI mice appear to begin an eventual recovery in behavior by the 1 week mark. Overall, these results suggest that rmTBI causes early, transient behavioral changes, independently from tau aggregation, hinting recovery may be slower in Tg tau mice as well as a progressive recovery in behavior at about 1 week post-rmTBI.

Figure 15. Behavioral examination of early time-point rmTBI-induced P301S and WT Mice. (A) P301S (*) and WT rmTBI ($) mice reveal impaired artificial grooming 1 hour and 1 day after rmTBI (1hr and 1d, $p < 0.05$; 1wk, $p > 0.05$). **(B)** P301S and WT rmTBI display lower nesting scores 1 day and 1 week after rmTBI compared to controls ($p < 0.05$). **(C)** There was no difference in rmTBI and sham mice with latency to fall in Rota-Rod after 1 week after treatment ($p > 0.05$) **(D)** P301S rmTBI mice may potentially recover slower following rmTBI treatment as within group analysis posits both 1 hour and 1 day time periods show significant differences to the 1 week mark ($p < 0.001$); however, WT rmTBI only show significant difference at the 1 hour time-point ($p < 0.05$); ($^{*}p < 0.05$, $^{**}p < 0.01$, $^{***}p < 0.001$). Data is expressed as means ± SEM.

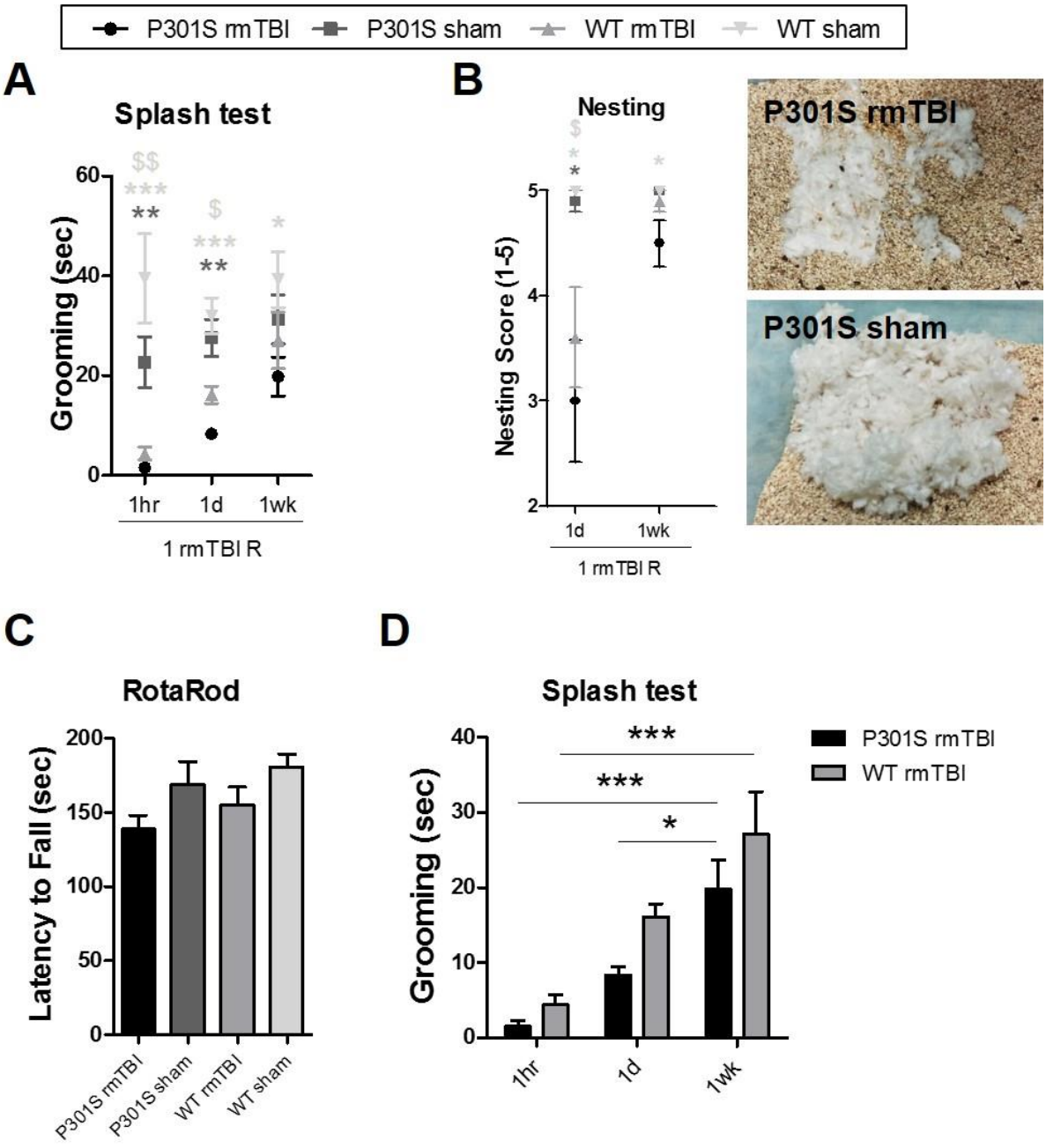
P301S rmTBI
P301S sham
WT rmTBI
WT sham
A
Splash test
Grooming (sec)
1hr
1d
1wk
1 rmTBI R
B
Nesting
Nesting Score (1-5)
1d
1wk
1 rmTBI R
P301S rmTBI
P301S sham
C
RotaRod
Latency to Fall (sec)
P301S rmTBI
P301S sham
WT rmTBI
WT sham
D
Splash test
Grooming (sec)
P301S rmTBI
WT rmTBI
1hr
1d
1wk

Astonishingly, when assessing these young rmTBI Tg tau mice by histology, we were able to detect a small, but detectable amount of tau aggregates in brain with more prevalence than age-matched sham mice. Representative images unveil positive and morphologically pertinent tau by AT8, MC1, and Gallyas silver staining in P301S rmTBI mice 1 hour (Figure 16A), 1 day (Figure 16B), and 1 week (Figure 16C) after TBI induction compared to respective age-matched P301S sham mice in similar undetected areas. Pathological tau accumulation was detected in the piriform and rhinal cortices, entorhinal cortex, cingulate gyrus/retrosplenial granular cortex, hippocampal area, hypothalamus along with dorsal areas of the thalamus, midbrain/pons, and tegemental area of the medulla in P301S rmTBI mice. Interestingly, some reactive tau was proximal to ventricles, such as 4th ventricle or Sylvian aqueduct, and a fair amount of deposition was noted in the dorsally located cingulate gyrus/retrosplenial granular cortex – brain regions just below the impacted closed-head skull. When the cortex and amygdala (CTX), hippocampal area (HPa), diencephalon (Di), and brain stem (BS) were quantified using AT8 for pTau in 4 distinctive coronal areas, P301S rmTBI mice exhibited elevated tau deposition compared to P301S sham animals: 1 hour (fold change (FC) in CTX: 7.72*; $p < 0.05$), 1 day (FC in CTX: 3.78*, HPa: 8.01, BS: 9.83*; $p < 0.05$), and 1 week (FC in CTX: 2.93*, HPa: 1.72, BS: 5.28*; $p < 0.05$) following rmTBI induction (Figure 17A). MC1 immunostaining revealed elevated conformational-dependent PHF tau in P301S rmTBI in comparison to P301S sham mice following: 1 hour (FC in CTX: 40*, HPa: 1.60; $p < 0.05$), 1 day (FC in CTX: 6.03*, HPa: 3.70, BS: 9.41*; $p < 0.05$), and 1 week (FC in CTX: 5.27*, HPa: 5.17, BS: 6.07*; $p < 0.05$) time-points (Figure 17B). AT8 and MC1 immunostaining revealed no detected tau in the diencephalon in the early-stage P301S sham mice; in addition, there was no detected NFT formation by Gallyas silver staining in any brain region in the 1 hour, 1 day, and 1 week P301S sham mice. Finally, the opposite hemisected brain was homogenized (10% w/v), ultra-centrifuged to retrieve the formic acid, insoluble protein fraction, and assayed

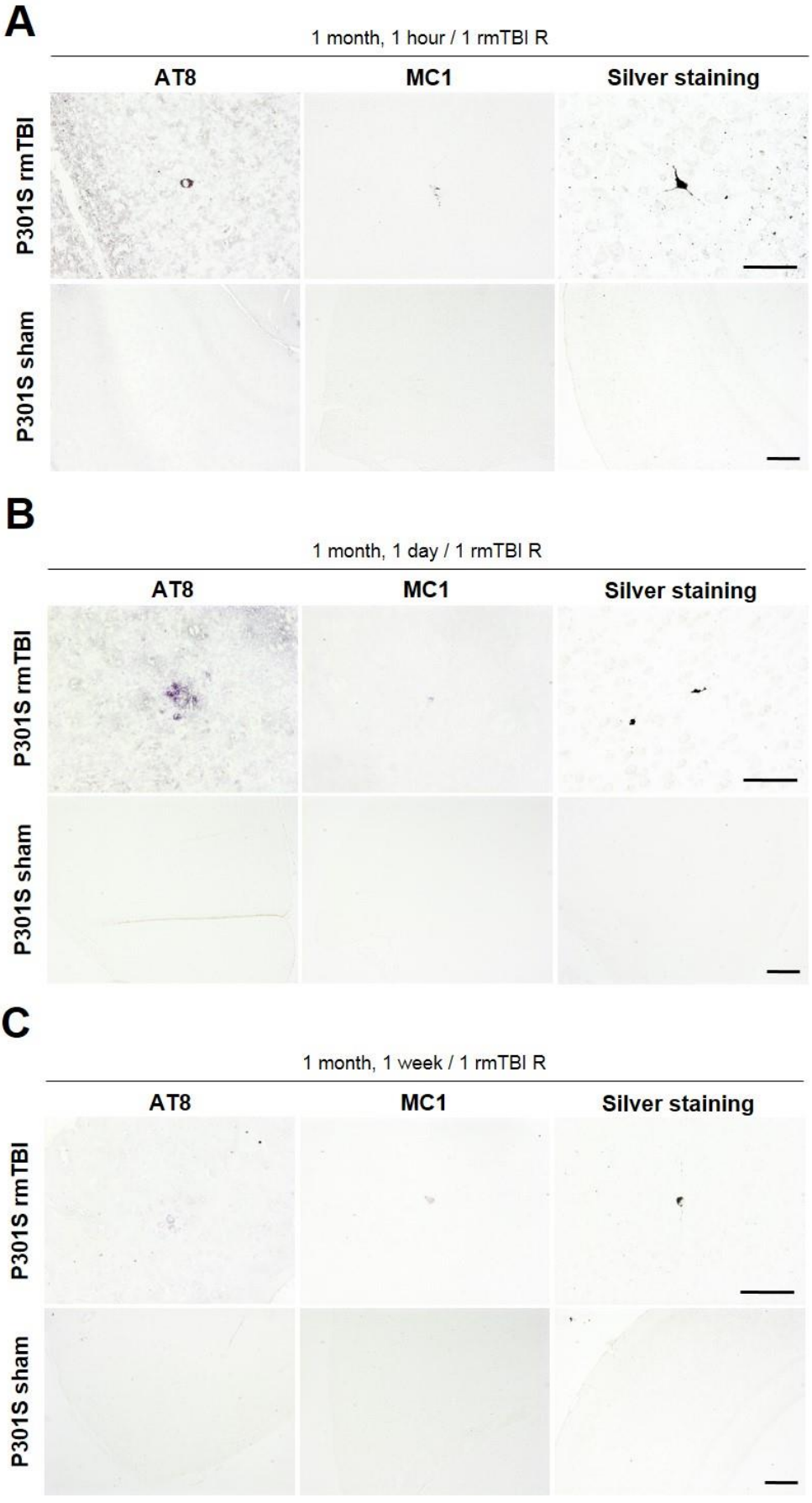
A
1 month, 1 hour / 1 rmTBI R
AT8
MC1
Silver staining
P301S rmTBI
P301S sham
B
1 month, 1 day / 1 rmTBI R
AT8
MC1
Silver staining
P301S rmTBI
P301S sham
C
1 month, 1 week / 1 rmTBI R
AT8
MC1
Silver staining
P301S rmTBI
P301S sham

Figure 16. Histological analysis of tau pathology in P301S rmTBI mice 1 hour, 1 day, and 1 week subsequent to rmTBI. Representative images of AT8 (left panel), MC1 (middle panel), and Gallyas silver staining (right panel) in P301S rmTBI and sham mice 1 hour after rmTBI induction **(A)**, 1 day after rmTBI **(B)**, and 1 week after rmTBI **(C)** versus age-matched P301S sham controls. Scale bar: 100 μm, 300 μm.

by ELISA. As shown in Figure 17C, each early time-point P301S rmTBI group displayed approximately ±1.5-fold increase of insoluble pathological tau in comparison to their respective age-matched P301S sham group (1hr FC: 1.63^{**}, 1d FC: 1.44^{*}, 1wk: 1.44^{*}; $^{*}p < 0.05$, $^{**}p < 0.01$). Thus, these results speculate that rmTBI can trigger accelerated tau deposition, as early as 1 hour along with the presence of different tau conformations, in comparison to sham animals by histological and biochemical analysis.

Figure 17. Histological and biochemical quantification of tau pathology in 1 hour, 1 day, and 1 week P301S rmTBI mice. (A) Quantification of AT8 burden at 1 hour, 1 day, and 1 week in P301S rmTBI and P301S sham mice. **(B)** P301S rmTBI and age-matched P301S sham mice MC1 burden quantifications at early time-points. **(C)** Early stage P301S rmTBI and P301S sham mice insoluble tau was analyzed by ELISA. ND: not detected. (*p < 0.05, **p < 0.01).

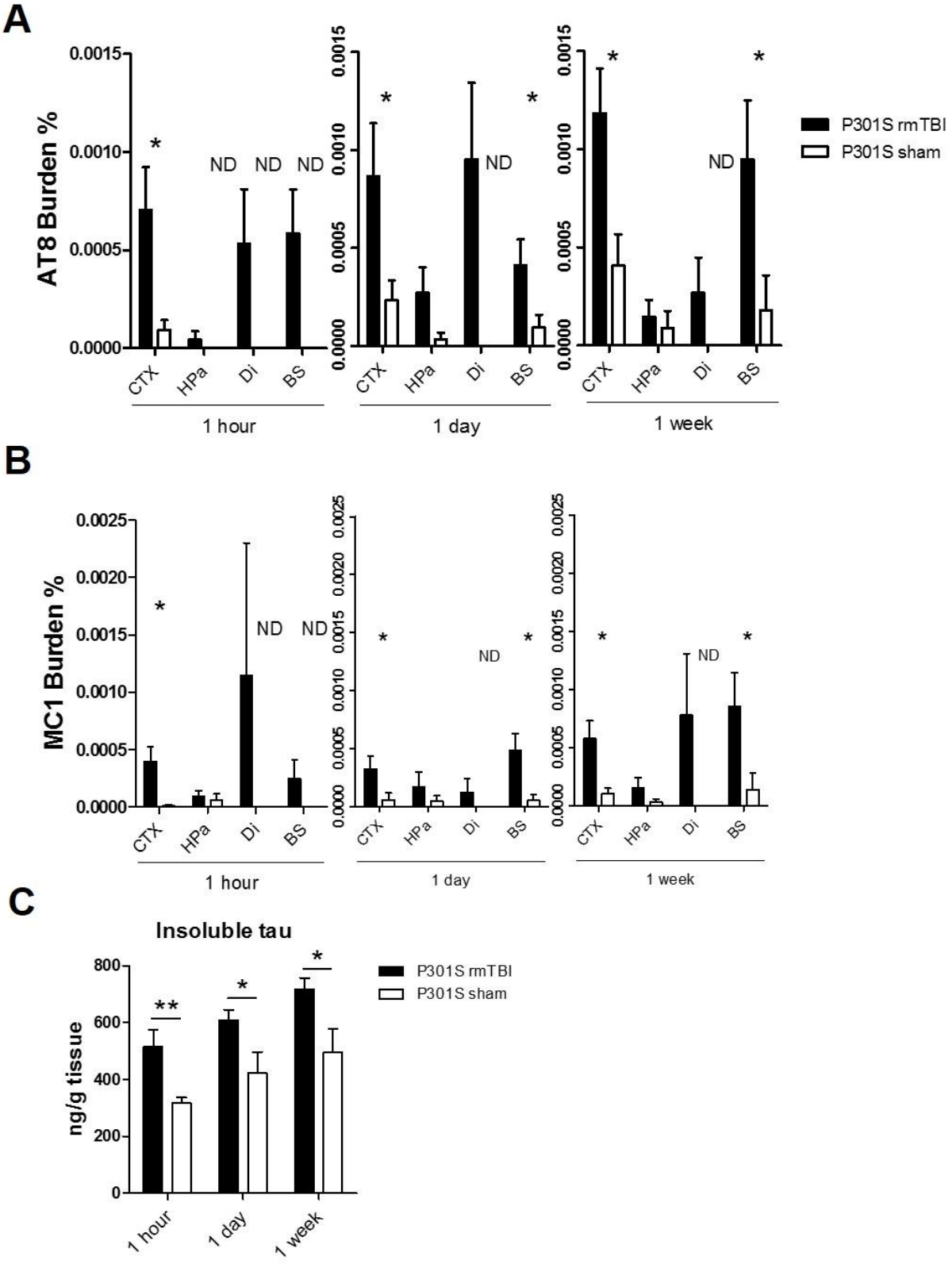
A
AT8 Burden %
0.0015
0.0010
0.0005
0.0000
*
ND ND ND
*
ND
*
*
ND
*
CTX HPa Di BS
1 hour
1 day
1 week
P301S rmTBI
P301S sham
B
MC1 Burden %
0.0025
0.0020
0.0015
0.0010
0.0005
0.0000
*
ND ND
*
ND
*
*
ND
*
CTX HPa Di BS
1 hour
1 day
1 week
C
Insoluble tau
ng/g tissue
800
600
400
200
0
**
*
*
1 hour
1 day
1 week
P301S rmTBI
P301S sham

Recurrent rmTBI intensifies cognitive impairment and tau aggregation over time

In addition to assessing the possibility of early triggered tau formation following rmTBI, we investigated the effect of multiple rmTBI events on tau pathology over time in brain and on behavior. P301S rmTBI, P301S sham, WT rmTBI, and WT sham groups (n = 9-1l for each time period) were subjected to a modified closed-head, mild weight-drop model at varied times and intervals and sacrificed at 3 months (3m) with 2 rmTBI rounds, 6 months (6m) with 3 rmTBI rounds, or 8.5 months (9m) with 4 rmTBI rounds (Figure 14). Behavioral assessment, histology, and biochemical analysis was performed as stated previously. One ancillary phenotypic characteristic of the Tg tau P301S mouse model is the probability of a fairly rapid hindlimb paralysis at later ages [110]. 8.5 month old P301S rmTBI mice exhibited 4 mice with hindlimb paralysis, which presented an inability to utilize their hindlimbs, hunch-backed posture, and difficulty feeding, with only one mouse having paralysis in the sham group; animals were immediately sacrificed upon paralysis discovery and not utilized for behavioral testing. Therefore, 8.5 month old P301S rmTBI mice had more paralytic animals than age-matched sham animals.

Approximately 2 weeks after the final rmTBI/sham treatment, non-cognitive assessing tasks (Splash test, Nesting, Open Field test, and RotaRod) was performed before sacrificing at either 3 months, 6 months, or 8.5 months. Splash test assessment by one-way ANOVA showed a lowered performance in P301S rmTBI at 3 months ($p < 0.05$), 6 months ($p < 0.05$), and 8.5 months ($p > 0.05$, ns) (Figure 18A). Nesting scores revealed lowered nesting abilities at the later stage time-points, as well (3m, $p > 0.05$; 6m, $p > 0.05$; 9m, $p < 0.05$) (Figure 18B). There was no significant difference in groups at any time-point for the percentage of time spent in the open field in Open Field testing (data not shown). Motor function by RotaRod testing was noted to be attenuated in P301S rmTBI at 3 months ($p < 0.01$), 6 months ($p < 0.01$), and 8.5 months ($p < 0.01$) (Figure 18C). However, despite diminished behavioral performance in these non-cognitive

associated tasks by the P301S rmTBI mice at later time-points, there was no significant difference between P301S rmTBI and WT rmTBI. Thus, progressing tau aggregation and rmTBIs over time revealed lowered neuropsychiatric and motor functions yet may not be the absolute definitive factor in non-cognitive behaviors.

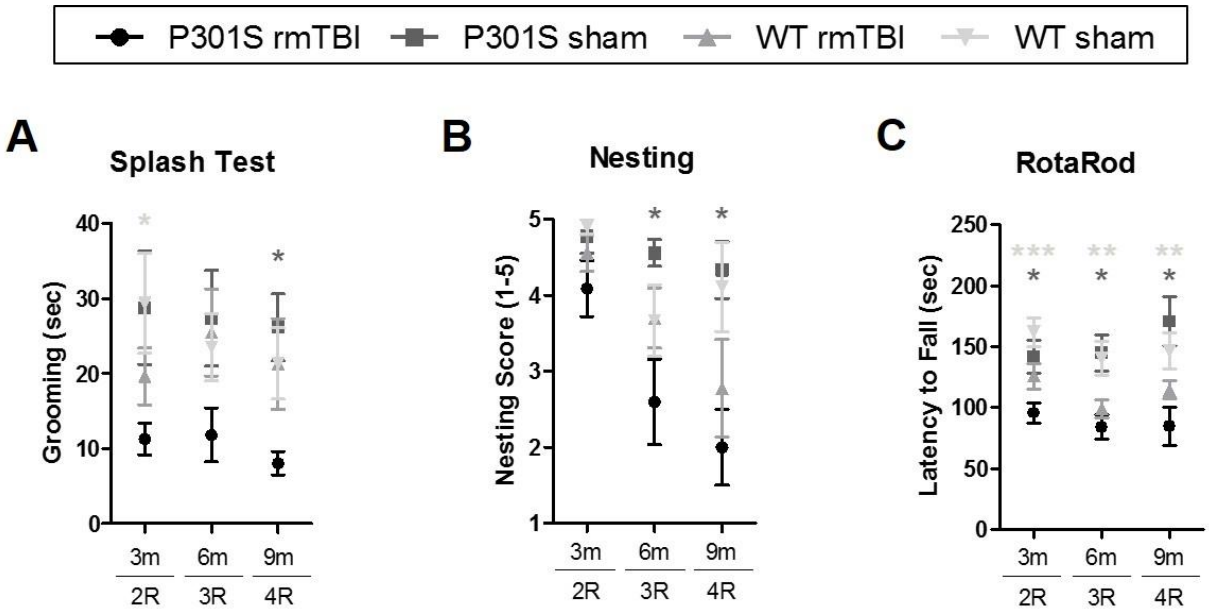

Figure 18. Psychiatric and motor behavior of late stage P301S and WT mice subjected to rmTBI or sham. Splash test, Nesting, and RotaRod was performed in all groups before sacrificing 3 months, 6 months, and 8.5 months. **(A)** Splash test assessment exhibited an overall lowered performance in P301S rmTBI at 3 months ($p < 0.05$), 6 months ($p < 0.05$), and 8.5 months ($p > 0.05$, ns). **(B)** Nesting scores revealed lowered nesting abilities at the later stage time-points (3m, $p > 0.05$; 6m, $p > 0.05$; 9m, $p < 0.05$). **(C)** There was a difference in motor performance by rmTBI treatment with P301S rmTBI demonstrating a significant impairment versus sham treated mice at 3 months ($p < 0.01$), 6 months ($p < 0.01$), and 8.5 months ($p < 0.01$). (*$p < 0.05$, **$p < 0.01$, ***$p < 0.001$). Data is expressed as means ± SEM.

Following neuropsychiatric and motor assessment, spatial learning and memory was tested by Barnes maze and reversal learning in all groups before sacrificing at 3 months (2 rmTBI rounds), 6 months (3 rmTBI rounds), and 8.5 months (4 rmTBI rounds). All groups at all time-

points improved performance in the training process over time in Barnes maze ($p < 0.0001$). Figure 19A demonstrated impaired navigation abilities in P301S rmTBI mice at the later time-points compared to aged-matched controls by analyzing the Barnes maze learning curve, respectively (3m, $p < 0.001$; 6m, $p < 0.01$; 9m, $p < 0.001$). Furthermore, in Figure 19B, 3 days after the final maze trial, P301S rmTBI revealed exacerbated long-term memory (LTM) by demonstrating a longer time to discover the escape hole in comparison of P301S sham, WT rmTBI, and WT sham mice at 3 months ($p < 0.01$), 6 months ($p < 0.001$), and 8.5 months ($p < 0.001$). Example traces of LTM assessment corresponding to the average primary latency of each group at each time-point are shown in Figure 20. P301S rmTBI mice revealed an approximately more randomized search pattern as compared to the other groups showing a more serial or spatial search pattern. When the escape hole was placed approximately 180 degrees from the previous static quadrant, late stage P301S rmTBI animals had a more difficult time disassociating the preceding escape hole and discerning the location of the novel escape hole by reversal learning (3m, $p < 0.05$; 6m, $p > 0.05$; 9m, $p < 0.01$), despite no significant difference as a function over time ($p < 0.0001$) (Figure 19C). In addition, 3 months and 6 months old P301S rmTBI engendered more total errors while navigating the arena compared to controls (data not shown). Moreover, there was no significant difference among the groups at each time-point examined measuring velocity (mm/sec) in the learning curve of the Barnes maze suggesting successful removal of paralyzed P301S mice and comparable locomotor activity ($p > 0.05$, ns; data not shown). These results suggest that the combinatorial effect of rmTBI and progressing tau deposition over time may play a larger role in cognitive learning and memory assayed by Barnes maze with reversal learning.

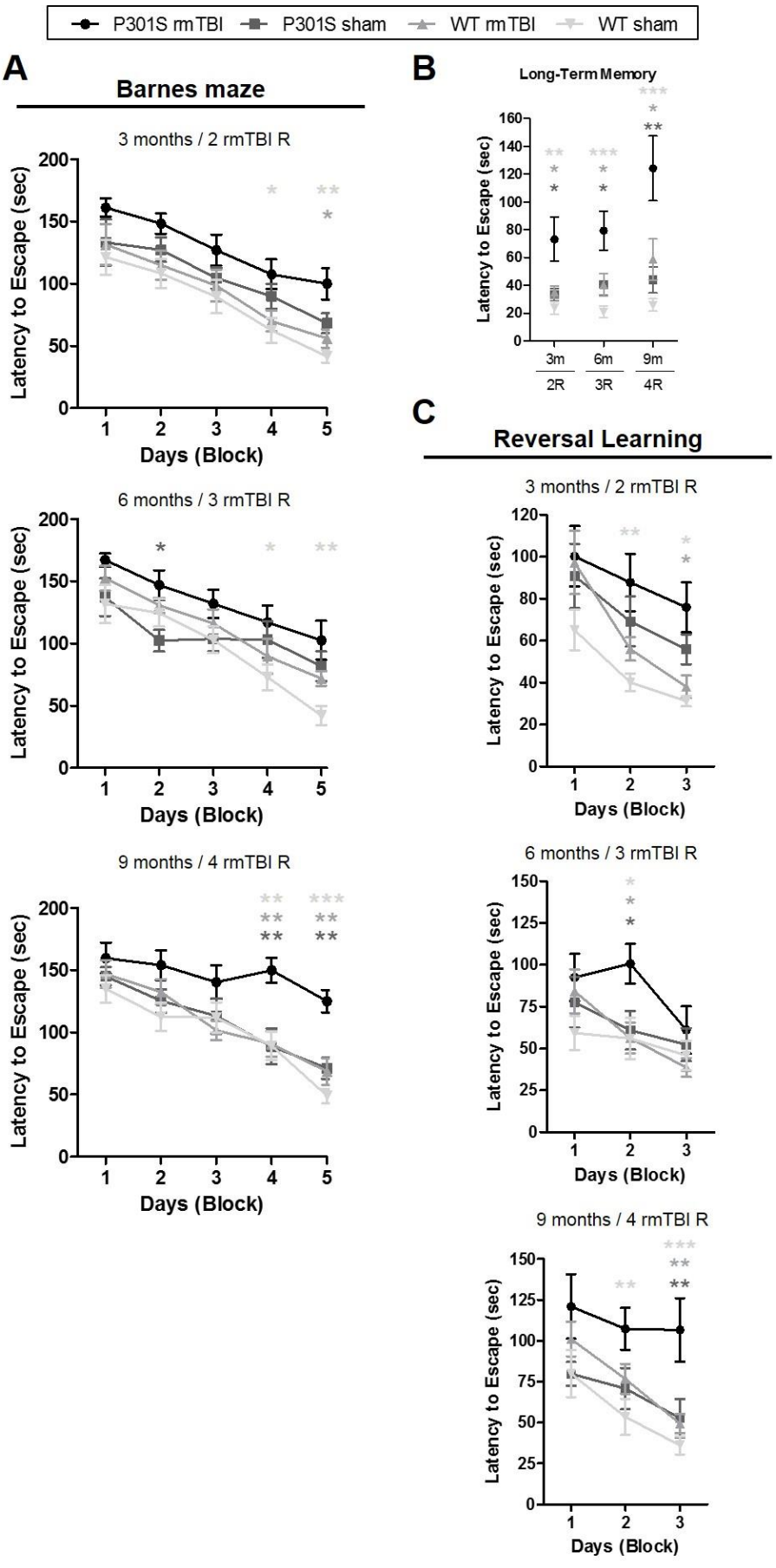
P301S rmTBI
P301S sham
WT rmTBI
WT sham
A
Barnes maze
3 months / 2 rmTBI R
6 months / 3 rmTBI R
9 months / 4 rmTBI R
Latency to Escape (sec)
Days (Block)
B
Long-Term Memory
Latency to Escape (sec)
3m
6m
9m
2R
3R
4R
C
Reversal Learning
3 months / 2 rmTBI R
6 months / 3 rmTBI R
9 months / 4 rmTBI R
Latency to Escape (sec)
Days (Block)

Figure 19. Cognitive assessment of late stage P301S rmTBI mice. (A) P301S rmTBI demonstrated impaired learning in the Barnes maze compared to age-matched controls at later time-points (3m, $p < 0.001$; 6m, $p < 0.01$; 9m, $p < 0.001$). **(B)** P301S rmTBI mice had impaired memory when assessed in long term memory versus age-matched controls at later time-points (3m, $p < 0.01$; 6m, $p < 0.001$; 9m, $p < 0.001$). **(C)** P301S rmTBI mice exhibited impaired performance when the escape hole was reversed compared to controls at later stages after rmTBI (3m, $p < 0.05$; 6m, $p > 0.05$; 9m, $p < 0.01$); (*$p < 0.05$, **$p < 0.01$, ***$p < 0.001$).

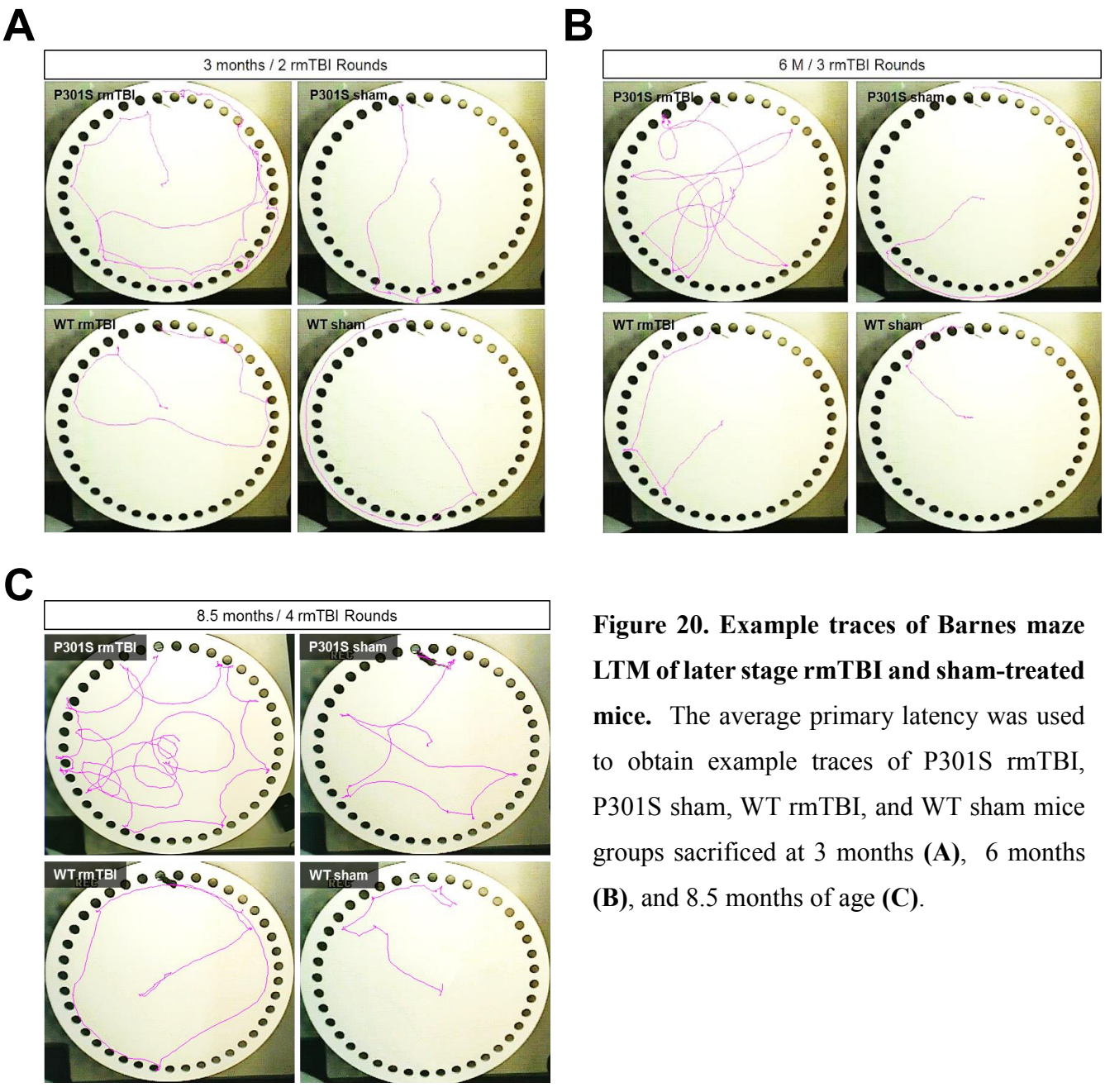

Figure 20. Example traces of Barnes maze LTM of later stage rmTBI and sham-treated mice. The average primary latency was used to obtain example traces of P301S rmTBI, P301S sham, WT rmTBI, and WT sham mice groups sacrificed at 3 months **(A)**, 6 months **(B)**, and 8.5 months of age **(C)**.

Tau pathology was determined following rmTBI induction at later time-points by histological analysis utilizing AT8 for pTau, MC1 for conformational-dependent PHFs, and Gallyas silver staining for NFTs. 3m (Figure 21A), 6m (Figure 21B), and 9m P301S rmTBI mice (Figure 22) presented robust and progressive tau pathology in 4 distinct coronal brain sections compared to their respective age-matched controls.

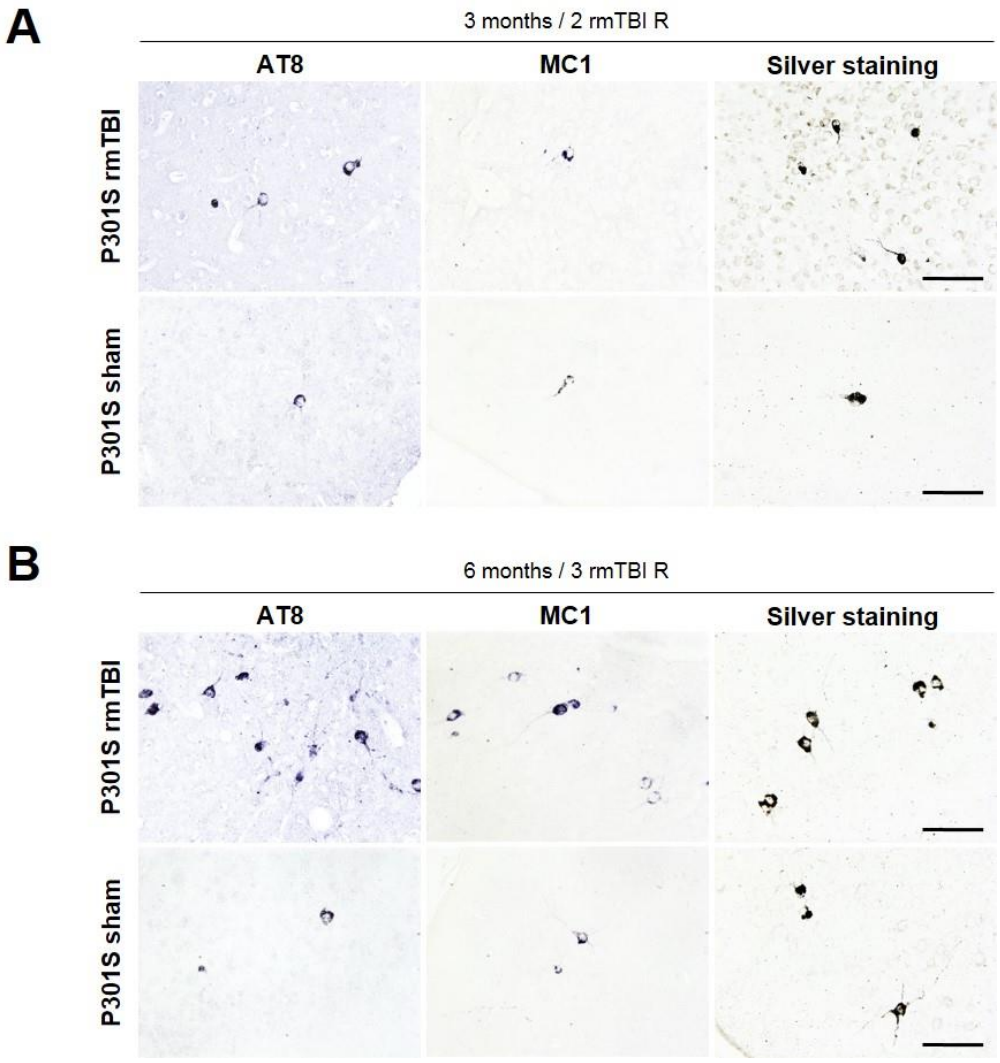

Figure 21. Tau histology in P301S rmTBI and P301S sham mice at 3 and 6 months of age. Demonstrative images of AT8, MC1, and Gallyas silver staining of P301S rmTBI and P301S sham mice at 3 months, 2 rounds of rmTBI **(A)**, and 6 months, 3 rmTBI rounds **(B)**. Scale bar: 100 μm, 30 μm.

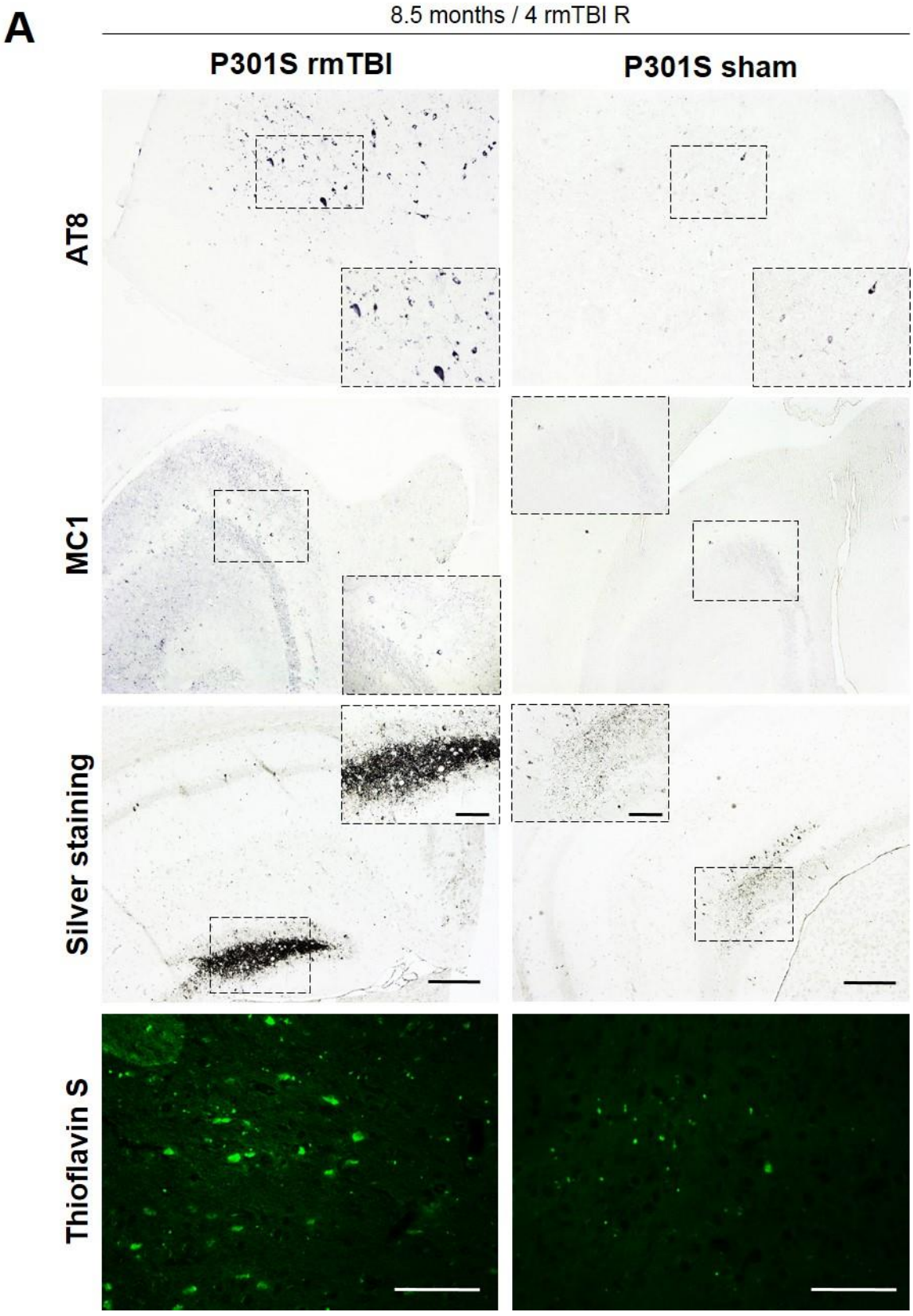
A
8.5 months / 4 rmTBI R
P301S rmTBI
P301S sham
AT8
MC1
Silver staining
Thioflavin S

Figure 22. Tau histology in P301S rmTBI and P301S sham mice at 8.5 months of age. Example images of AT8 (top panel), MC1 (second panel), Gallyas silver staining (third panel), and Thioflavin S staining (last panel) in brain of P301S rmTBI and sham mice at 8.5 months of age. P301S rmTBI animals exhibit a much more robust tau pathology in brain compared to P301S sham. Scale bar: 100 μm, 30 μm.

In Figure 23A-D, cortex/amygdala, hippocampal area, diencephalon, and brain stem were quantified for total percentage burden of AT8, MC1, and Gallyas silver staining in all later stage Tg tau groups. Following 2 rmTBI rounds, 3 month old P301S rmTBI mice demonstrated augmented pathological tau conformers compared to age-matched P301S sham mice by AT8 (FC in CTX: 1.83*, HPa: 4.55*, Di: 2.27, BS: 2.30*; $^{*}p < 0.05$), MC1 (FC in CTX: 2.17*, HPa: 4.58*, Di: 4.29**, BS: 3.83*; $^{*}p < 0.05$, $^{**}p < 0.01$), and Gallyas silver staining (FC in CTX: 2.53*, HPa: 4.06*, Di: 7.45**, BS: 7.57**; *p < 0.05, **p < 0.01). Six month old P301S mice treated with 3 rmTBI rounds had elevated pathological tau AT8 burden versus age-matched sham animals (FC in CTX: 3.30*, HPa: 5.87*, Di: 2.26*, BS: 2.05*; $^{*}p < 0.05$), MC1 burden (FC in CTX: 2.71*, HPa: 3.29*, Di: 2.47*, BS: 1.85**; $^{*}p < 0.05$, $^{**}p < 0.01$), and Gallyas silver staining (FC in CTX: 2.69**, HPa: 1.57**, Di: 2.29*, BS: 3.54**; $^{*}p < 0.05$, $^{**}p < 0.01$). Indeed, P301S rmTBI sacrificed at 8.5 months old with 4 rmTBI rounds exhibited the most grandiose tau pathology compared to their respective Tg sham mice by histological analysis of AT8 (FC in CTX: 1.31, HPa: 2.75*, Di: 1.43, BS: 2.62*; $^{*}p < 0.05$), MC1 (FC in CTX: 1.92, HPa: 2.92*, Di: 1.71, BS: 2.73*; $^{*}p < 0.05$), and Gallyas silver staining (FC in CTX: 1.81*, HPa: 2.64**, Di: 2.24, BS: 2.58*; $^{*}p < 0.05$, $^{**}p < 0.01$). Thioflavin S (ThS) positive-staining was also identified and followed the same trend as the silver staining (Figure 22); moreover, WT rmTBI and WT sham animals in all groups did not display any positive, morphologically-relevant tau staining using the same techniques here (data not shown). Supporting our histopathological results, hemisected brains were homogenized by 10%

w/v and ultra-centrifuged to obtain the formic acid fraction to assay insoluble tau levels by p^{S199} ELISA from the 3m, 6m, and 9m P301S rmTBI/sham treated mice (n = 10/time-point and group). Insoluble tau aggregates were seen to be exacerbated in P301S rmTBI mice compared to age-matched P301S sham mice at 3 months (FC: 1.21, $p < 0.05$), 6 months (FC: 1.53, $p < 0.01$), and 8.5 months of age (FC: 1.49, $p < 0.05$) (Figure 23D). Ultimately, P301S rmTBI mice at later time-points displayed burgeoning and amplified pathological tau of disparate structural conformations, such as pTau, PHFs, and NFTs, by histological quantifications and insoluble tau levels by ELISA in brain in comparison to age-matched P301S sham rodents.

Figure 23. Assessment of tau pathology in P301S rmTBI mice over time. Quantification of images of AT8, MC1, and Gallyas silver staining in cortex/amygdala (CTX), hippocampal area (HPa), diencephalon (Di), and brain stem (BS) of P301S rmTBI and sham mice over time. **(A)** Late-stage P301S rmTBI mice display exacerbated hyperphosphorylated tau AT8 burden in brain compared to P301S sham mice. **(B)** MC1 burden was augmented following rmTBI in P301S mice at 3 months, 6 months, and 8.5 months of age. **(C)** Quantification of Gallyas silver staining for NFTs revealed higher levels in brain in the late stage P301S rmTBI mice compared to age-matched P301S sham animals. **(D)** Insoluble pathological tau was noted to be intensified in P301S rmTBI mice compared to age-matched P301S sham mice at 3 months, 6 months, and 8.5 months old. (*$p < 0.05$, **$p < 0.01$). Data is expressed as means ± SEM.

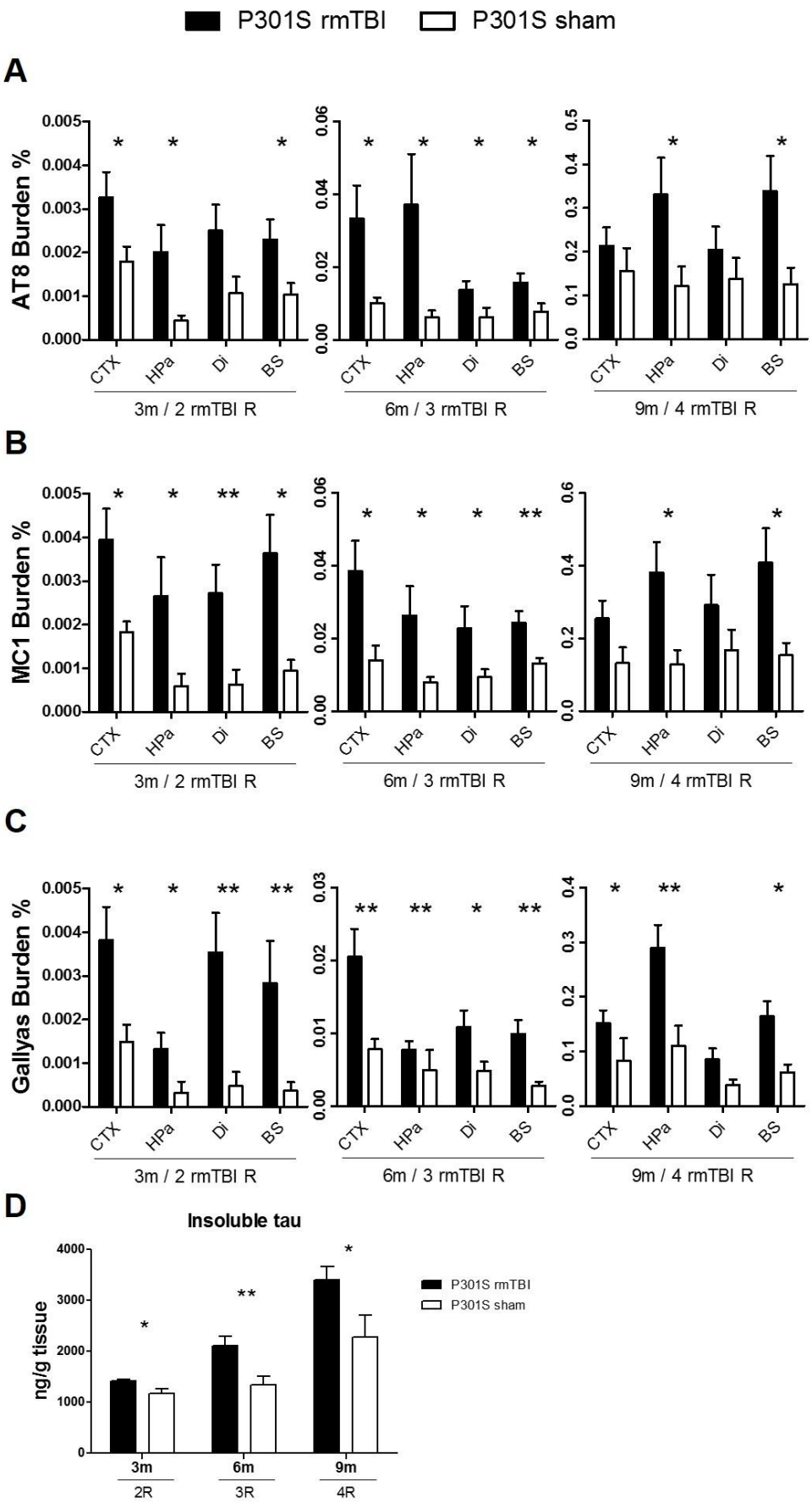
P301S rmTBI
P301S sham
A
AT8 Burden %
CTX
HPa
Di
BS
3m / 2 rmTBI R
6m / 3 rmTBI R
9m / 4 rmTBI R
B
MC1 Burden %
C
Gallyas Burden %
D
Insoluble tau
ng/g tissue
3m
6m
9m
2R
3R
4R

P301S rmTBI mice have elevated insoluble tau aggregates and accelerated model-related aging consequences

Additionally, if the insoluble tau ELISA levels from all of the groups are plotted over time comparing P301S rmTBI and P301S sham animals using linear regression, there is an approximate 1.5-fold increase of insoluble tau per month following the rmTBI paradigm as performed here ($p < 0.001$; $F_{(1,112)} = 12.41$) (Figure 24A) – assuming animal survival and continuous aggregation, i.e. not reaching a plateau phase. Incorporating the slope of the P301S rmTBI and sham animals indicates an overall accretion of insoluble tau levels thereby increasing the predicted age of the P301S rmTBI mice compared to sham mice. Moreover, analyzing the difference of the slopes for AT8 (Figure 24B), MC1 (Figure 24C), and Gallyas silver staining (Figure 24D) for the total summed burden of all groups, P301S rmTBI exhibit significant differences in MC1 ($p < 0.01$; $F_{(1,118)} = 10.64$) and Gallyas ($p < 0.01$; $F_{(1,118)} = 8.75$) overall burden, while AT8 overall burden showed a trend ($p > 0.05$; $F_{(1,118)} = 2.75$), as compared to P301S sham rodents over time. The auxiliary table revealed significant differences in the slopes of P301S rmTBI and sham mice in individual quantified brain regions with the most noteworthy differences seen among MC1 and Gallyas silver staining along with HPa and BS regions. Finally, the P301S Tg mouse model has reported neuronal loss at 9-12 months of age as studied previously [110]; thus, neuronal loss in 9m P301S rmTBI and sham mice was assessed by immunohistochemistry by anti-cleaved caspase-3 antibody, an apoptotic marker of cell death, and quantified in the prior described brain regions to study the potential acceleration of the Tg mouse model due to rmTBI. As described in Figure 24E, P301S rmTBI rodents at 8.5 months old had worse neuronal cell death in comparison to age-matched P301S sham mice (FC in CTX: 2.01^{*}, HPa: 3.21^{*}, BS: 3.67^{*}; $^{*}p < 0.05$). These concomitant results posit aggravated insoluble tau levels along with accelerated

progression of the Tg mouse model and age-related neuropathology following rmTBI events over time.

Figure 24. Neuropathological consequences of rmTBI manifest in transgenic tau mice over time. Collected data was plotted as a linear regression, and the slopes of the P301S rmTBI and P301S sham mice were compared. **(A)** Assessing insoluble pathological tau, P301S rmTBI mice had approximately 1.5-fold increase of tau aggregates over time compared to P301S sham ($p < 0.001$). Moreover, the predicted age in terms of this deposition of the P301S mice was elevated due to rmTBI treatment. Quantification of all groups of the specific brain regions were summed and plotted along with the slope of the line for burden of AT8 ($p > 0.05$) **(B)**, MC1 ($p < 0.01$) **(C)**, and Gallyas silver staining ($p < 0.01$) **(D)**. Additionally, distinct brain region data for AT8, MC1, and Gallyas silver staining was tested by linear regression, and the significance between the slopes of the P301S rmTBI and P301S sham mice was compared as shown in the ancillary table. **(E)** Anti-cleaved caspase-3 antibody was used to assess apoptotic cell loss in 8.5 month old P301S rmTBI and sham mice. Tg tau rmTBI rodents displayed a significant amount of neuronal loss compared to sham mice. Not detected (ND); (*$p < 0.05$, **$p < 0.01$). Scale bar: 100 μm. Data is expressed as means ± SEM.

A P301S rmTBI P301S sham

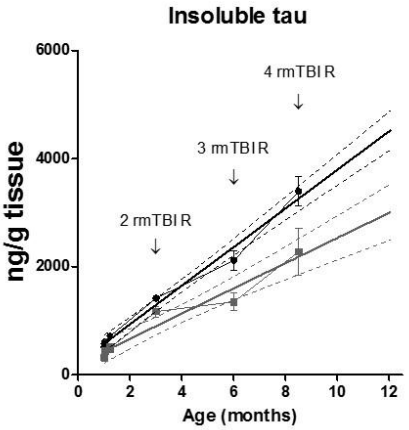

pS199 ELISA Insoluble Tau					
Age	P301S rmTBI	P301S sham	Fold Change	Predicted Age (m)	Age Difference (m)
1	576.9	432.5	1.33	1.62	0.62
2	934.5	665.9	1.40	3.15	1.15
3	1292.1	899.3	1.44	4.68	1.68
4	1649.7	1132.7	1.46	6.22	2.22
5	2007.3	1366.1	1.47	7.75	2.75
6	2364.9	1599.5	1.48	9.28	3.28
7	2722.5	1832.9	1.49	10.81	3.81
8	3080.1	2066.3	1.49	12.34	4.34
9	3437.7	2299.7	1.49	13.88	4.88
10	3795.3	2533.1	1.50	15.41	5.41
11	4152.9	2766.5	1.50	16.94	5.94
12	4510.5	2999.9	1.50	18.47	6.47

B

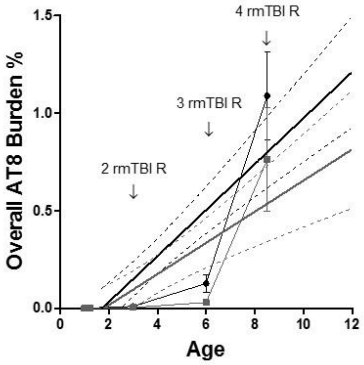

C

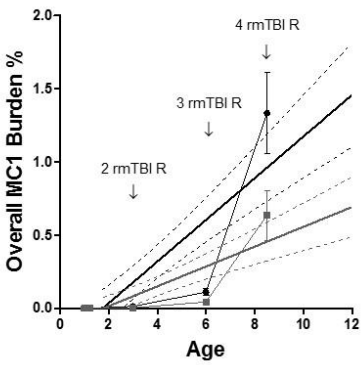

D

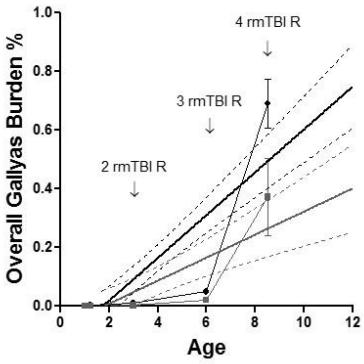

	AT8	MC1	Gallyas
Overall	0.1, ns	$p < 0.01$	$p < 0.01$
	$F_{(1,118)} = 2.75$	$F_{(1,118)} = 10.64$	$F_{(1,118)} = 8.75$
CTX	0.07, ns	$p < 0.01$	$p < 0.01$
	$F_{(1,116)} = 3.42$	$F_{(1,117)} = 10.65$	$F_{(1,117)} = 7.36$
HPa	$p < 0.001$	$p < 0.0001$	$p < 0.0001$
	$F_{(1,117)} = 14.13$	$F_{(1,118)} = 17.38$	$F_{(1,118)} = 17.34$
Di	0.31, ns	$p < 0.05$	0.054, ns
	$F_{(1,117)} = 1.02$	$F_{(1,117)} = 4.22$	$F_{(1,118)} = 3.80$
BS	$p < 0.01$	$p < 0.001$	$p < 0.0001$
	$F_{(1,118)} = 8.37$	$F_{(1,117)} = 14.25$	$F_{(1,118)} = 20.17$

E

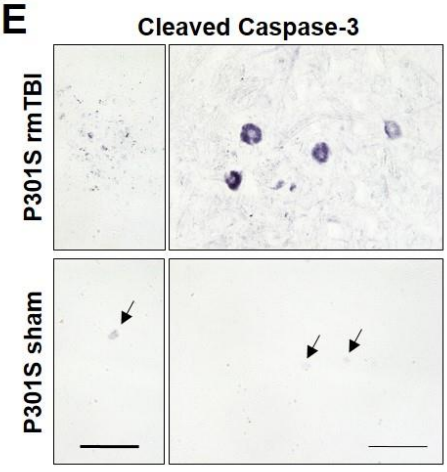

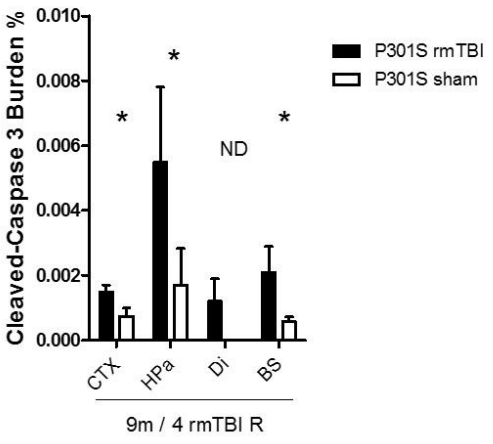

CHAPTER 4

Investigate the seeding capability of rmTBI-induced seeds by *in vivo* bioassay.

Rationale

The seeding-nucleation polymerization process has been reproduced *in vivo* in various Tg animal models of AD by bioassay, even using minute amounts of pre-formed seeds [43–49,118]. This method of assaying seeding capability by *in vivo* bioassay originated with prion diseases following the prion principle. One efficient way to study seeding capabilities of a certain substrate is to inoculate the material containing pre-formed misfolded seeds *in vivo* into naïve mice and examine the acceleration and/or deposition of pathology and clinical symptoms compared to animals that were not challenged. Exogenous infusion of tau seeding-competent material, whether synthetic or homogenized brain inocula, into rodent models to evaluate seeding capability, spreading, and further tau pathology has been performed previously [43–49]. In this study, brain homogenate collected from the previous P301S rmTBI and control mice were intracerebrally (i.c.) injected into naïve mice to sensitively assay the seeding ability of rmTBI-induced tau aggregates. Results from previous experiments dictated the earliest time-point (1 hour) of triggered tau formation and a canonical, tau-laden brain region (entorhinal cortex) that provided the inocula for the bioassay. Moreover, the extracted entorhinal cortex (EC) homogenate from the 1 hr grouped mice was i.c. injected into 2.5 month old hTau mice, which express non-mutated, normal human tau [119]. Utilizing different EC inocula, hTau injected mice were then assayed in animal behavior and histology as done above to examine the effect of specific tau seeds in inducing and exacerbating tau pathology.

Inocula for the *in vivo* bioassay was selected from the earliest determined time-point tau deposition was identified from previous experiments, which was 1 hour post-rmTBI. The EC, an area that displayed detectable tau pathology by histology and is acknowledged as an initial affected region of tau deposition in AD [60,61], was excised from the hemisected frozen brain (n = 3) and homogenized (10% w/v) for i.c. injection into 2.5 month old normal humanized tau (hTau) mice (n = 5/group). Thus, the following experimental groups for the *in vivo* bioassay included: 1) hTau mice injected with 1hr P301S rmTBI EC homogenate, 2) hTau mice injected with 1hr P301S sham EC homogenate, 3) hTau mice injected with 1hr WT rmTBI EC homogenate, and 4) hTau mice injected with Aged P301S (10-11 months old / n = 3) EC homogenate as a positive control. Unilateral 10 uL hippocampal injections of the various inocula was performed in naïve hTau mice and sacrificed at 9 months old. Behavioral examinations and tau histology was completed, as done previously. Thus, by the sensitive method by *in vivo* bioassay of early rmTBI-induced tau seeds, we evaluated the seeding competency of rmTBI-induced tau seeds in hTau mice.

Results

hTau-Aged P301S and hTau-P301S rmTBI inoculated mice reveal impaired learning and memory.

Naïve hTau mice were inoculated with: Aged P301S EC substrate (hTau-Aged P301S), 1hr P301S rmTBI EC substrate (hTau-P301S rmTBI), 1hr P301S sham EC substrate (hTau-P301S sham), or 1hr WT rmTBI EC substrate (hTau-WT rmTBI). Anxiety/depression-like behavior was tested by Splash test, Nesting, and Open Field test starting at about 6 months after the injection. Figure 25A-B shows no significant difference among the different inoculated hTau mice for Splash test and nesting abilities ($p > 0.05$, ns), respectively; furthermore, there was no significant difference in Open Field testing, as well ($p > 0.05$, ns; data not shown). Motor function assessment

was examined by RotaRod thereafter, and there was no significant difference among the groups ($p > 0.05$, ns) (Figure 25C). Remarkably, hTau-Aged P301S and hTau-P301S rmTBI mice revealed impaired spatial navigation learning abilities in the Barnes maze learning curve compared to their respective controls (Figure 25D) ($p < 0.05$). All groups displayed significant learning abilities during the training process as a function of time ($p < 0.0001$). Long-term memory assessment of primary latency and total errors made during the trial revealed significant impairments of hTau-Aged and hTau-P301S rmTBI mice particularly to hTau-WT rmTBI mice (Figure 25E-F) ($p < 0.05$; $p < 0.01$, respectively). When the platform was placed in a novel area 180 degrees from the previous position for reversal learning assessment, hTau-Aged P301S and hTau-P301S rmTBI mice demonstrated impaired ability to finding the novel escape hole as compared to hTau-P301S sham and hTau-WT rmTBI mice (Figure 25G) ($p < 0.01$). Overall, hTau-Aged P301S and hTau-P301S rmTBI inoculated mice presented impaired learning and memory compared to respective control groups.

Figure 25. Behavioral testing of inoculated 9 month old hTau mice. Anxiety/depressive-like behavior, motor function, and cognition was examined in hTau-Aged P301S, hTau-P301S rmTBI, hTau-P301S sham, and hTau-WT rmTBI mice. There was no significance in performance in Splash test ($p > 0.05$) **(A)**, Nesting ($p > 0.05$) **(B)**, or RotaRod ($p > 0.05$) **(C)** among the injected hTau animals. **(D)** hTau-Aged P301S ($) and hTau-P301S rmTBI mice (*) had impaired spatial navigation learning abilities as shown in the Barnes maze learning curve compared to their respective controls ($p < 0.05$). LTM primary latency ($p < 0.05$) **(E)** and total errors ($p < 0.01$) **(F)** demonstrated impairments in recalling the escape hole in hTau-Aged P301S and hTau-P301S rmTBI mice. **(G)** Reversal learning of the escape hole showed that hTau-Aged P301S and hTau-P301S rmTBI animals could not sufficiently discover the novel escape hole as compared to hTau-P301S sham and hTau-WT rmTBI mice ($p < 0.01$). (*$p < 0.05$, **$p < 0.01$, ***$p < 0.001$). Data is expressed as means ± SEM.

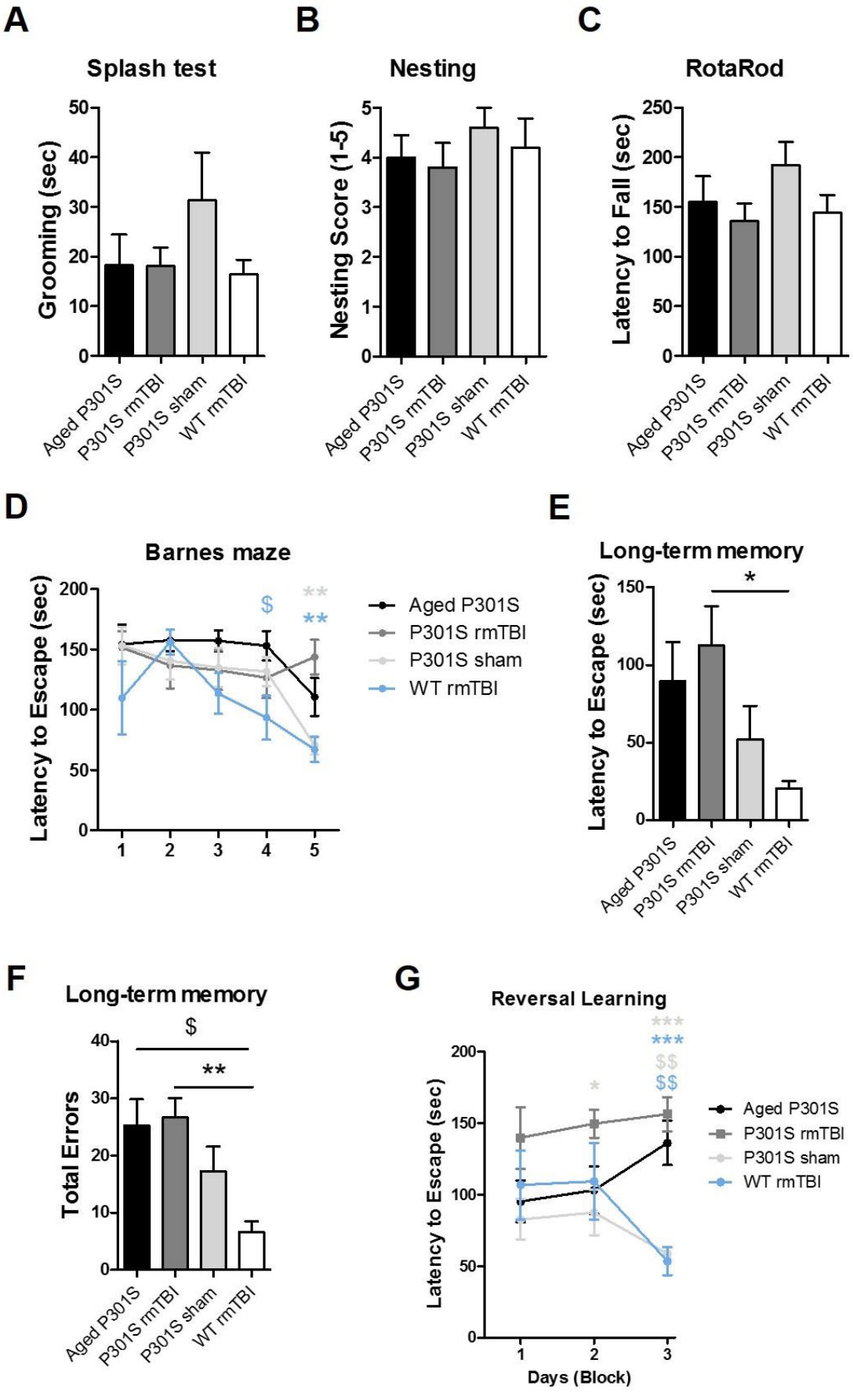
A
Splash test
Grooming (sec)
50
40
30
20
10
0
Aged P301S
P301S rmTBI
P301S sham
WT rmTBI
B
Nesting
Nesting Score (1-5)
5
4
3
2
1
0
Aged P301S
P301S rmTBI
P301S sham
WT rmTBI
C
RotaRod
Latency to Fall (sec)
250
200
150
100
50
0
Aged P301S
P301S rmTBI
P301S sham
WT rmTBI
D
Barnes maze
Latency to Escape (sec)
200
150
100
50
0
1
2
3
4
5
$
**
**
Aged P301S
P301S rmTBI
P301S sham
WT rmTBI
E
Long-term memory
Latency to Escape (sec)
150
100
50
0
*
Aged P301S
P301S rmTBI
P301S sham
WT rmTBI
F
Long-term memory
Total Errors
40
30
20
10
0
$
**
Aged P301S
P301S rmTBI
P301S sham
WT rmTBI
G
Reversal Learning
Latency to Escape (sec)
200
150
100
50
0
***
***
$$
$$
*
1
2
3
Days (Block)
Aged P301S
P301S rmTBI
P301S sham
WT rmTBI

hTau-Aged P301S and hTau-P301S rmTBI mice demonstrate exacerbated AT8 and MC1 tau burden.

After sacrificing all groups of 9 month old hTau inoculated animals, 6.5 months following EC homogenate injection, AT8 and MC1 immunohistochemistry was performed in 5 distinct coronal sections, and overall immunopositive burden was quantified in CTX, HPa, Di, BS, and cerebellum (Cb). Figure 26A illustrates AT8 (left panel) and MC1 (right panel) in hTau-Aged P301S, hTau-P301S rmTBI, hTau-P301S sham, and hTau-WT rmTBI mice. In all mouse groups, faint or weak AT8 and MC1 immunostaining could be detected chiefly in: piriform cortex and claustrum, superior cortex, entorhinal cortex, amygdala, hippocampal area, diencephalon, brainstem, and cerebellum. In the CA1/pyramidal layer of the HPa, among other areas, a plethora of diffuse AT8-positive punctates and thread-like structures were seen to be more robust in hTau-Aged P301S and hTau-P301S rmTBI compared to hTau inoculated P301S sham and WT rmTBI mice. Yet, some AT8 immunostaining similar to the classical somatodendritic tau morphology was seldom detected – mostly in hTau-Aged P301S mice - as seen in the enclosed inset from the hippocampal CA3 stratum lucidum (Figure 26A, inset). In the right panel, hTau-Aged P301S and hTau-P301S rmTBI mice revealed an interesting, yet aggravated MC1 immunostaining mostly in the granule layer of the cerebellum as compared to controls. This faint staining and morphology may resemble early tau aggregate processes or a pre-tangle state, and the cellular location of these pTau inclusions seems to emulate distal segments of basal dendrites, apical dendrites, and proximal dendrites making its way to the neuronal soma as described previously [120]. AT8 and MC1 abnormal tau, although a little more intense, was noticed in neuronal cell bodies in the brain, as well, in areas such as in basolateral amygdala and brain stem regions.

Furthermore, when quantifying these brain regions for AT8 and MC1 burden, hTau-Aged P301S and hTau-P301S rmTBI mice showed elevated pTau and conformational-dependent PHF

immunostaining, respectively. One-Way ANOVA assessment of AT8 immunostaining revealed significant overall differences in CTX ($p < 0.01$), HPa ($p < 0.01$), and BS ($p < 0.05$) (Figure 26B). Post-hoc analysis measured elevated pTau in hTau-Aged P301S versus hTau-P301S sham (FC in CTX: 3.51^{**}, HPa: 6.27^{**}) and hTau-WT rmTBI (FC in CTX: 3.12^{**}, HPa: 5.64^{**}, BS: 1.80^{*}), and hTau-P301S rmTBI mice had significant AT8 tau compared to hTau-P301S sham (FC in HPa: 5.39^{*}) and hTau-WT rmTBI (FC in HPa: 4.85^{*}, BS: 1.68^{*}) (Figure 26B). Moreover, Figure 26C shows MC1 burden quantification estimated significant overall differences in CTX ($p < 0.001$), HPa ($p < 0.05$), BS ($p < 0.05$), and cerebellum ($p < 0.01$). Multiple comparison testing confirmed hTau rodents inoculated with Aged P301S EC inocula had augmented MC1 burden in comparison to hTau-P301S sham (FC in CTX: 2.87, HPa: 3.59) and hTau-WT rmTBI mice (FC in CTX: 2.80^{**}, HPa: 3.62^{*}, Cb: 3.60^{*}). The hTau-P301S rmTBI group also had higher MC1-positive staining against hTau-WT rmTBI in the cerebellum (FC: 2.87^{*}). Overall, hTau-Aged P301S mice were determined to have a more aggressive tau pathology followed by animals inoculated with the 1 hour P301S rmTBI EC homogenate as compared to 1 hour P301S sham and WT rmTBI inoculated hTau animals by AT8 and MC1 immunohistochemistry in brain.

Figure 26. AT8 and MC1 tau immunohistochemistry and quantification in inoculated hTau rodents. (A) Example images utilizing AT8 and MC1 antibodies for hTau-Aged P301S, hTau-P301S rmTBI, hTau-P301S sham, and hTau-WT rmTBI mice in hippocampus. **(B)** Quantification of AT8 burden % revealed significant overall differences in CTX ($p < 0.01$), HPa ($p < 0.01$), and BS ($p < 0.05$) in hTau animals, yet hTau-Aged P301S and hTau-P301S rmTBI mice yielded significant differences in distinct brain regions by post-hoc analysis. **(C)** Quantification of MC1 burden % in brain presented significant overall differences in CTX ($p < 0.001$), HPa ($p < 0.05$), BS ($p < 0.05$), and cerebellum ($p < 0.01$). Animals injected with Aged P301S inocula had significant increase in MC1 immunostaining compared to hTau-P301S sham and hTau-WT rmTBI mice, while hTau-P301S rmTBI had a significant increase in the cerebellum compared to hTau-WT rmTBI mice. (*$p < 0.05$, **$p < 0.01$). Scale bar: 100 μm. Data is expressed as means ± SEM.

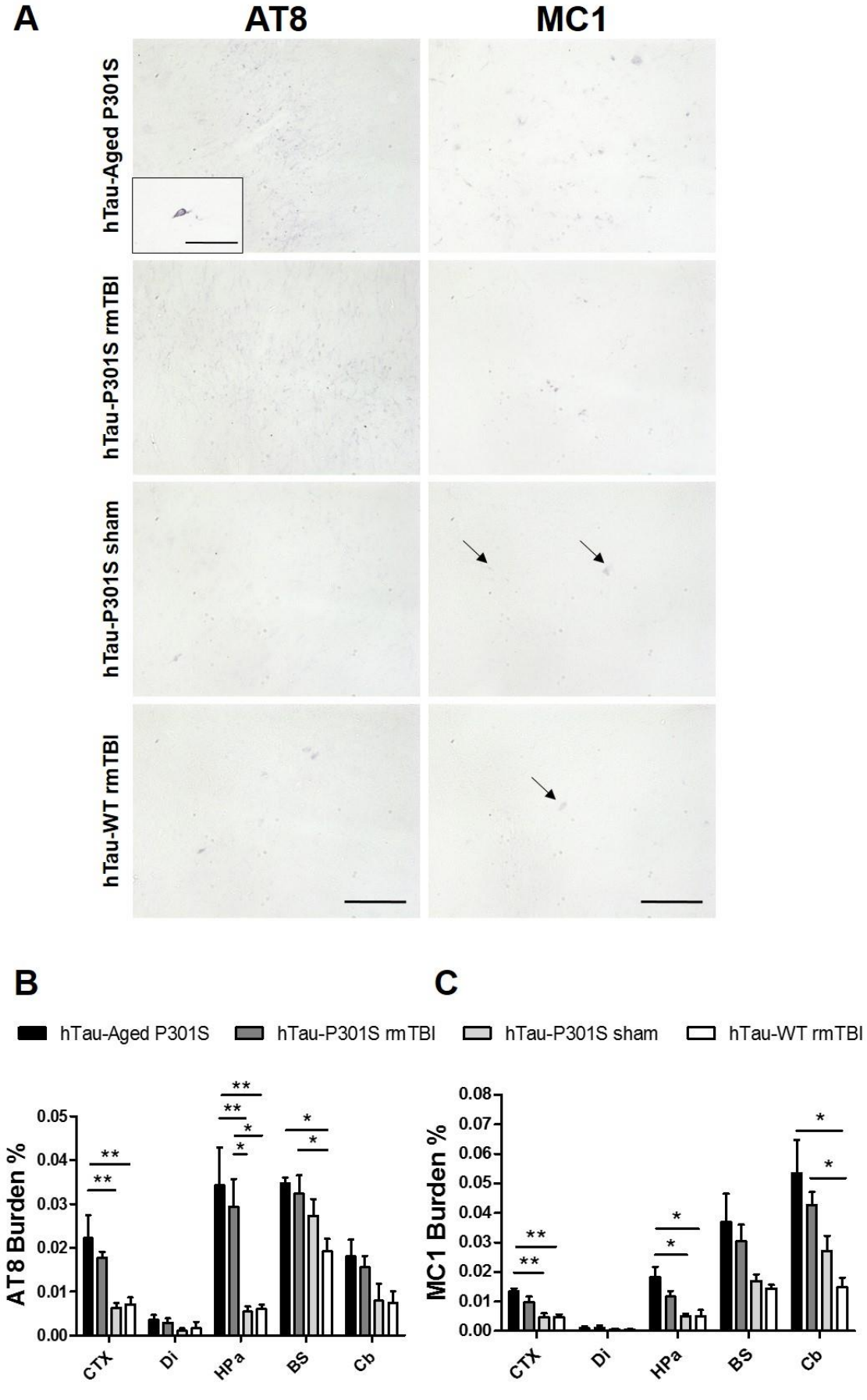
A
AT8
MC1
hTau-Aged P301S
hTau-P301S rmTBI
hTau-P301S sham
hTau-WT rmTBI
B
C
hTau-Aged P301S
hTau-P301S rmTBI
hTau-P301S sham
hTau-WT rmTBI
AT8 Burden %
MC1 Burden %
CTX
Di
HPa
BS
Cb

Tau seeds from Aged P301S and P301S rmTBI material demonstrate efficient seeding ability.

Finally, all inoculated hTau groups were assessed for tangle pathology induction following injection by classical Gallyas silver staining in various coronally sliced sections. All hTau injected mouse groups, although not all animals, displayed Gallyas positive staining in CTX around the inoculated area as exampled in hTau-P301S sham mice (Figure 27A). Interestingly, these argyrophilic inclusions in the surrounding CTX histopathologically bear resemblance to glial tau pathology found in certain 4R-specific tauopathies, such as progressive supranuclear palsy (PSP), corticobasal degeneration (CBD), and argyrophilic grain disease (AGD) [121–123]. Figure 27B shows the corpus callosum (cc) separating the CTX and HPa in hTau-P301S rmTBI mice having an argyrophilic collection of numerous, irregular-shaped grains or particles along the white matter fibers. This was mostly seen in Aged P301S and P301S rmTBI inoculated mice – only one mouse exhibited this type of pathology in the hippocampal alveus and cc in the hTau-P301S sham animals. Figure 27C further supports the presence of glial tangles as argyrophilic coiled bodies as well as rod or thread-like deposits were located in abundance in the fimbria fornix of mostly hTau-Aged P301S mice followed by hTau-P301S rmTBI animals. This type of silver impregnation reaction was not seen in the Tg tau sham or WT rmTBI hTau-inoculated mice. Despite glial-like tau pathology, hTau-Aged P301S (Figure 27D) and hTau-P301S rmTBI mice (Figure 27E) revealed Gallyas-positive silver staining neuronal tangles within the HPa. No argyrophilic tau pathology, whether neuronal or glial, was found by silver impregnation in the HPa in hTau-WT rmTBI mice (Figure 27F); additionally, 10 month old untreated hTau mice (n=3) also displayed no argyrophilic tau pathology in brain (Figure 27G). Silver staining burden in the HPa was determined to be significant among the groups ($p < 0.05$), while hTau-Aged P301S mice had significantly enhanced Gallyas silver staining ($p < 0.05$) with a strong trend in the hTau-P301S

rmTBI mice ($p = 0.0524$) in comparison to hTau-P301S sham mice as shown in Figure 27I. To further validate the presence of neuronal tangles in hTau-Aged P301S and hTau-P301S rmTBI animals, Thioflavin S (ThS) staining was performed in all hTau injected groups. Structures delineated as glial tangles in 4R-related tauopathies – and as viewed in this study – are thought to be ThS-negative [122,124,125], while neuronal tangles still are ThS-reactive. Figure 28A-B indicate ThS-positive neuronal aggregates in the hippocampus of hTau-Aged P301S and hTau-P301S rmTBI mice, while hTau-P301S sham and hTau-WT rmTBI animals exhibit ThS-negative reactivity in HPa and even in cortical areas that typically reveal Gallyas silver staining (Figure 28C-D). All together, these results suggest uniquely induced tau pathology in the HPa that exhibits efficient seeding from the Aged P301S and P301S rmTBI EC inocula.

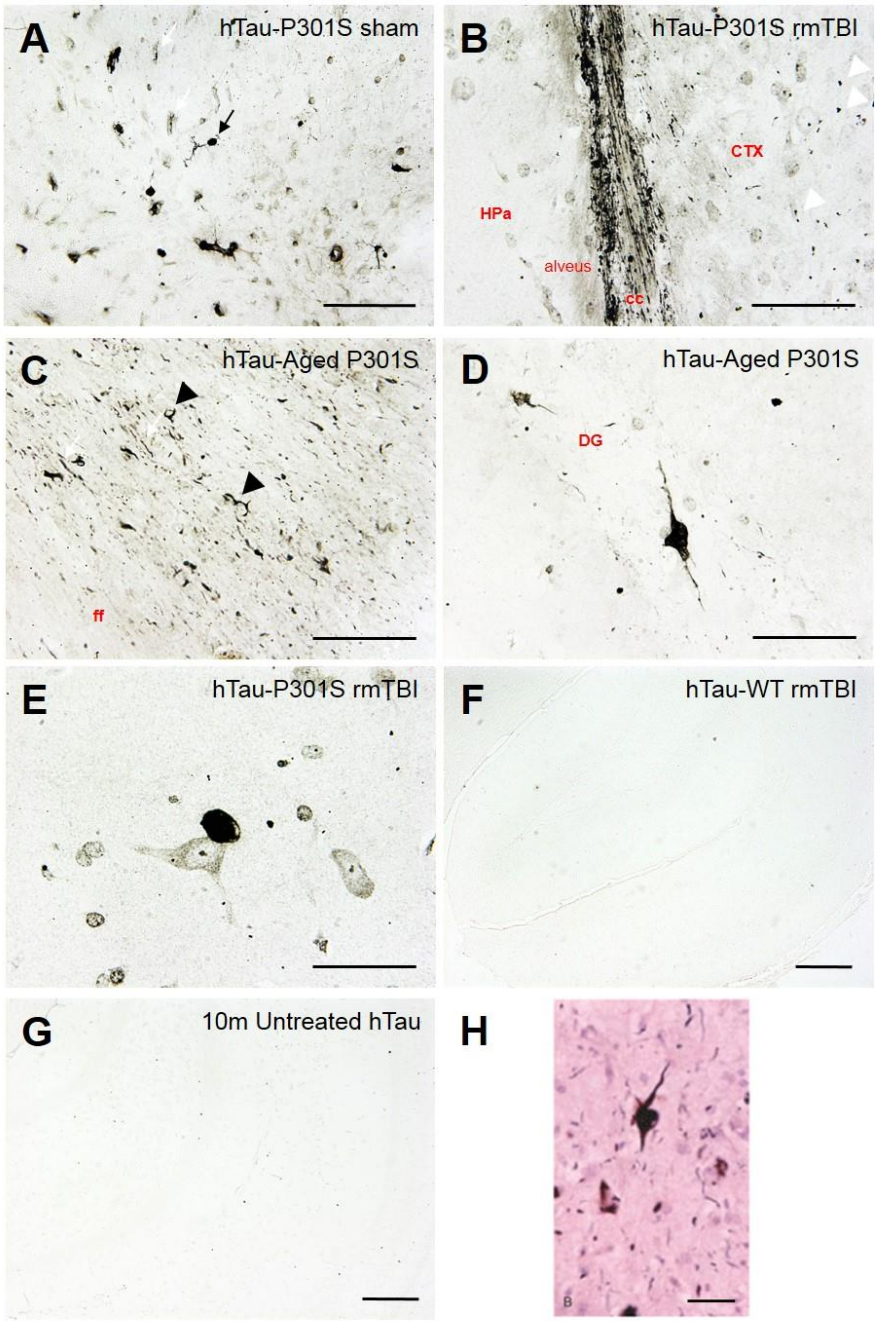
A
hTau-P301S sham
B
hTau-P301S rmTBI
CTX
HPa
alveus
cc
C
hTau-Aged P301S
ff
D
hTau-Aged P301S
DG
E
hTau-P301S rmTBI
F
hTau-WT rmTBI
G
10m Untreated hTau
H
I
Hippocampal Area
Gallyas Burden %
0.25
0.20
0.15
0.10
0.05
0.00
*
0.0524
ND
Aged P301S
P301S rmTBI
P301S sham
WT rmTBI

Figure 27. Gallyas silver staining in injected hTau mice. (A) In some of the experimental hTau animals, there was silver-positive inclusions that were similar to glial tau pathology noted in 4R-related tauopathies, such as PSP, CBD, and AGD. Argyrophilic staining, as exampled by irregular rod or thread-like structures (white arrows) and microglia-like morphological deposits (black arrow), was detected around the injected cortical area as shown in a hTau-P301S sham mouse. **(B)** Argyrophilic inclusions or irregular grains (white arrowheads) infiltrate the white matter tracts of the corpus callosum (cc) and alveus of the hippocampus (HPa) as shown in a hTau-P301S rmTBI mouse, which was more prevalent in hTau-Aged P301S and hTau-P301S rmTBI animals. **(C)** Associated glial tau pathology, which resembled threads (white arrows) and coiled bodies (black arrowheads), could be detected in the fimbria fornix (ff) as displayed in a hTau-Aged P301S mouse. This occurred only in the hTau-Aged P301S and –P301S rmTBI mice. Only hTau-Aged P301S **(D)** and hTau-P301S rmTBI mice **(E)** generated neuronal tangle pathology as observed in the hippocampus. **(F)** This induced tau pathology was not identified in the HPa of hTau-WT rmTBI, nor any argyrophilic staining was detected in aged untreated hTau mice **(G)**. **(H)** Human brain affected with AGD exhibit glial and neuronal tangle pathology; the NFT here is morphological very similar to the NFT pathology found in hTau-Aged P301S and hTau-P301S rmTBI mice. **(I)** Gallyas quantification in the HPa posited a significant difference among the groups by one-way ANOVA ($p < 0.05$), while hTau-Aged P301S mice had a significantly higher burden compared to hTau-P301S sham mice with hTau-P301S rmTBI exhibiting a strong trend ($p = 0.0524$). (DG) = dentate gyrus; (ND) = not detected. (*$p < 0.05$). Scale bar: 300 μm, 100 μm, 50 μm. Data is expressed as means ± SEM. **(H):** Ferrer, I., Santpere, G., van Leeuwen, F.W., 2008. Argyrophilic grain disease. Brain 131, 1416–1432. Permission to use the licensed content was obtained from Oxford University Press and Copyright Clearance Center.

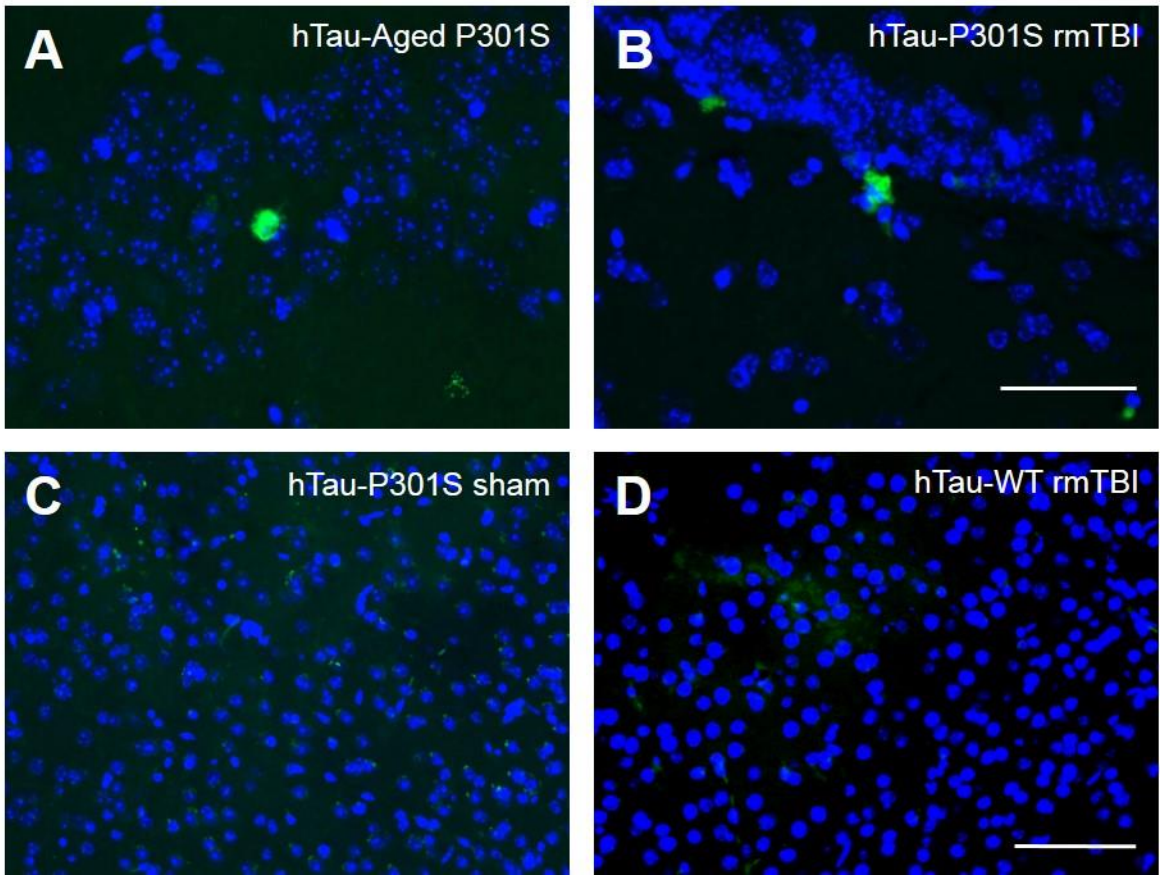

Figure 28. Thioflavin S (ThS) staining in injected hTau mice. Further support for the presence of neuronal tau aggregate pathology induced in hTau mice from the Aged P301S and P301S rmTBI EC homogenate was performed by ThS staining. Glial tangles are suggested to be negative for ThS staining. ThS-positive staining could be identified in the targeted inoculation area of hTau-Aged P301S **(A)** and hTau-P301S rmTBI mice **(B)** as shown in the hippocampal granule cell layer. Cortical areas of hTau-P301S sham mice **(C)** and hTau-WT rmTBI mice **(D)**, which generally proved argyrophilic, do not display ThS staining, as well. Scale bar: 100 μm, 50 μm.

CHAPTER 5

Discussion

There have been copious assertions of TBI as a strong risk factor for neurodegenerative diseases involved with protein misfolding, aggregation, and accumulation, such as AD and CTE. Indeed, the molecular mechanistic effects of both TBI and neurodegenerative diseases resemble very similar properties. Anomalous tau and tau aggregates have been detected following TBI events and is canonical in diverse tauopathies in brain. More so, recent research implicates multiple, continuous traumatic impacts, perhaps those involved in contact sports and military settings, to tauopathies, like AD and CTE. Neuropathological tau is believed to consist of characteristics redolent of the prion protein in prion diseases and has been suggested to be "prion-like". Moreover, tau is posited to follow a nucleation-polymerization process to ultimately form NFT amyloid structures composed of hyperphosphorylated tau as well as tau can spread through the brain transsynaptically through the brain functional connectome. A paragon for tau spreading assessing the degree of intensity and kinetics of disease-related tau has been described in AD by Braak staging and in CTE from the McKee laboratory, previously. In this current study, we assessed the effect of repetitive mild TBI in engendering early pathological tau formation as well as exacerbating tau aggregation in brain with additional rmTBIs over time and subsequent neurobehavioral consequences; moreover, we addressed if these initial rmTBI-tau aggregates represented seed competency by *in vivo* bioassay.

In the early time-point assessed groups (1 hour, 1 day, and 1 week post-induction), Tg and WT naïve animals treated with rmTBI exhibited altered neurobehavioral performance by measurement of artificial grooming in the Splash test - specifically 1 hour to 1 day after. Particularly, 1 hour after rmTBI not only was the grooming time attenuated, but overall participation in the task was diminished as measured by distance travelled and immobility (data not shown). This result was most likely due to the effect of the direct impacts presenting short-term impairment in neurological function evidenced by immobility, perhaps due to pain, or even

a dazed state / dizziness in some animals. This response can be found in concussed individuals and is known to be resolved in days' time [117]. However, the 1 day Tg and WT rmTBI mice revealed lowered performance in artificial grooming, not due to a lack of participation in the task (data not shown), as well as overnight nesting. This may be explained by the residing or lingering effect of the TBI initiating a post-concussion-like syndrome in the rmTBI animals. In TBI cases, this syndrome consists of headache, dizziness, fatigue, irritability, and principally compromised memory and concentration, but its exact frequency is not known [78,80,94,126,127]. These symptoms may persist longer than the transient symptoms, as seen in the 1 hour rmTBI mice, and may reflect altered neurotransmitter function and generally correlate with the duration of post-traumatic amnesia [128].

Nevertheless, rmTBI-induced animals then begin to progressively recover to normal behavioral function after 1 week as indicated by Splash test, Nesting, open field, and RotaRod. One week P301S rmTBI mice did demonstrate lowered performance among the groups in artificial grooming and nesting and no significant difference in motor capabilities. Although recovery rates are assuredly individualized, there appears to be a 7-10 day period of a heightened susceptibility to re-injury, thus activities with high concussion exposure are recommended to be avoided for at least 1 week [117]. When assessing the P301S and WT rmTBI with-in subject testing over these times, only P301S rmTBI revealed a significant difference between the 1 day and 1 week mark perhaps indicating a rate of slower recovery as compared to WT rmTBI and respective sham controls, yet more experimental emphasis is warranted. Moreover, additional behavioral results at later time-points (3m, 6m, and 9m) in P301S mice following rmTBI attested to the presence of tau aggregation and may have a more substantial role in learning and memory, which should be assessed at the early time-points. Still, no full recovery, or even a slower recovery, from symptoms 1 week after mTBI may occur, as indicated even at the high-school age level [129], and

the triggered TBI-induced secondary neuro-molecular events, such as the formation of pathological tau, may be associated with symptom recovery rate.

Further, our study assessed the early formation of tau deposition in P301S mice at 1 hour, 1 day, and 1 week with or without rmTBI events by histological and biochemical methods. For histological analysis, four coronal sections, which included regions as CTX, HPa, Di, and BS, were assayed utilizing AT8, MC1, and Gallyas silver staining. AT8 recognizes specific phosphorylation sites that is associated to pre-tangle or tangle hyperphosphorylated tau. MC1 detects a distinct conformation of tau, believed to be pre-tangle PHFs, by targeting the N-terminal (amino acids 5-15) and the third microtubule binding region (amino acids 312-322) of tau, and Gallyas silver staining is a classical technique canonical for NFT and NP thread detection. P301S rmTBI mice did exhibit a small, but detectable and elevated amount of conformation-specific tau aggregates in the quantified CTX, HPa, Di, and BS regions by AT8, MC1, and Gallyas silver staining histological procedures. Following a two-step fractionation and obtaining the insoluble formic acid fraction from brain homogenate, biochemical ELISA demonstrated that each early time-point P301S rmTBI group displayed approximately ±1.5-fold increase of insoluble pathological tau in comparison to their respective age-matched P301S sham group. Overall, these results suggest that rmTBI can trigger early and accelerated tau formation in brain following 1 hour, 1 day, and 1 week.

Primarily, tau deposition was seen to follow what normally transpires spatiotemporally in the P301S mouse model (i.e. piriform and rhinal cortices) regardless of treatment. Conversely, P301S mice with rmTBI did demonstrate more tau deposition just below the area of impact (i.e. cingulate gyrus/retrosplenial cortex) and in regions not detected typically in the P301S mice at this young of age (i.e. the hypothalamus in the diencephalon), as exampled by the Tg sham mice here. An explanation for this could be described by an altered tropism due to the direct effect of

the rmTBI, where it produced tau assemblies in regions not distinctly identified in a naïve P301S mouse resulting in spontaneous tau formation. Although, it may be debatable if this mild of impacts could produce a pertinent contrecoup injury to engender tau formation in a ventral portion of the brain such as the hypothalamus after impact. Tropism can be distinguished by the localization of proteinaceous deposits within the brain and by the pattern of disease that is produced, which may lead to functional clinical symptoms, and this has been well described in prion diseases where distinct prion strains dictate different tropisms in brain and peripheral organs [130–134].

Alternatively, the result of multiple mild traumas to the head may create a thriving cellular microenvironment that can aid in the accelerated formation and spreading of tau through the functional synapses in the brain. Therefore, the intrinsic Braak-like staging and spreading of tau in the P301S mouse model could be accelerated. Areas canonical for the origination of pathological tau seeds, described by Braak and Braak such as the EC and/or BS [60,61,120], could form seeding competent tau much earlier, as discovered in this study, which spread much more thoroughly and effortlessly following rmTBI. For example, tau seeds generated in the EC could very well travel by functional neuronal efferent projections, such as cingulate cortex, hippocampus and amygdala (both which also project to the hypothalamus) and others, at a more exigent rate following rmTBI – all brain regions exhibiting tau deposition by histology in the early time-point P301S rmTBI mice. It has been posited that seeding may actually be an earlier event in pathology by assessing different Braak stage brains and seeding ability [111]. To further complicate the issue, since this is a dynamic phenomenon, these results could be a concomitant effect of both spontaneous formation and accelerated spreading. An example, while the intrinsic spatiotemporal pattern of tau in the P301S mouse model is commencing, rmTBI-induction was seen to engender pathological tau just above the impact area, the cingulate and retrosplenial

cortices, which could then have tau spread to functional neuronal connections, such as deep layers of the EC and HPa, among others. Remarkably, early tau deposits can be usually detected in more superficial layers (layers II-IV); however, pathological tau could be found in deep layers of the EC, even at 1 hour post-rmTBI. Thus, the molecular mechanism responsible for the divergent neurotropism of tau formation and spreading following rmTBI remains to be elucidated and more clarifying experiments are warranted.

In addition to the spontaneous formation and/or accelerated spreading of pathological tau subsequent to rmTBI in brain parenchyma, there could be release and/or generation of tau seeds in the periphery that could then propagate tau aggregation and spreading in the brain. This may be evidenced by the finding of pathological tau in early stage P301S rmTBI mice appearing in areas proximal to ventricles, i.e. abnormal tau immunopositive staining in layers V-VI in the EC or in the oriens layer of the hippocampus near the ventrally extending lateral ventricles (Figure 16A, P301S rmTBI AT8) or in the hypothalamus where the 3rd ventricle would be present. The interstitial fluid (ISF), cerebrospinal fluid (CSF), and blood plasma collectively make up the extracellular fluid of the brain and spinal cord. The brain parenchyma is surrounded by ISF together with related vasculature and tissues as well as CSF that fills the ventricles within the brain and the spaces on its outer surfaces, and the ISF/CSF has multiple functions for the brain from solute volume and osmolality regulation, waste clearance, and buoyancy and cushioning, and others, respectively [135]. Indeed, detectable protein aggregates, such as Aβ and tau, are found in these biological fluids and are currently being assessed as a diagnostic marker for PMDs, like AD [74,75,83,136–143]. Alongside detection and diagnosis for diverse PMDs, biological fluids are being targeted in TBI cases, as well; one study demonstrated that tau levels in CSF from fatal TBI patients expressed over a 1,000-fold increase compared to various neurological-diseased and non-diseased controls, and a cleaved and reduced sized form of tau protein was detected in these brain

injured patients [83]. Tau found in ISF and CSF may be independent from cellular death and is not known if it is released in a free, soluble form or if it is packaged into small membrane vesicles, such as exosomes [144].

Moreover, proteinaceous deposits may be removed from the brain by various clearance systems, including: transport across the blood-brain barrier, astroglial-mediated ISF bulk flow or also known as the glymphatic system, and the meningeal lymphatic vessels. Impairments in this waste clearance system has been described in Aβ [145,146] and tau [147,148] in rodent models, even after TBI. Following TBI, glymphatic pathway function was dramatically reduced to around 60%, and knock-out of aquaporin-4, astroglial water channels important for CSF-ISF exchange and clearance, in mice subjected to TBI revealed impaired glymphatics, promotion of tauopathy, neuroinflammation, and neurodegeneration [148]. The initial formation of tau in peripheral fluids, like CSF, ISF, and blood plasma, after rmTBI is not unfathomable. In CTE, the irregular and patchy tau distribution, which is disparate from tauopathies like AD, is identified early in the sulcal, perivascular and periventricular, and subpial depths – all areas associated with CSF/ISF flow and glymphatic/lymphatic systems [63,79–81,84,89,94]. Thus, the presence of tau in biological fluids following TBI can be detected and perhaps promoted by such mechanisms as impaired circulating fluid clearance.

Additionally, one theory that may occur following TBI is a slosh effect of CSF/ISF in the head; the concept of slosh has been investigated in liquid dynamics and is the motion of a given liquid's free surface within a container, where energy transfer occurs among the various boundaries. The CSF that surrounds the brain may act as a safeguard converting focally applied external stress to compressive stress because the fluid follows the outlines of the sulci and gyri of the brain and distributes the force in a uniform fashion, but the CSF is unable to wholly prevent shearing forces from being transmitted to the brain, especially when rotational forces involved.

The slosh effect could be mitigated by the tension of neck muscles, such as omohyoid muscle, bracing for an impact; this can be thought of when a professional boxer is prepared to sustain a force of enormous magnitude by tightening the neck muscles, but an unexpected blow may lead to more deleterious consequences, perhaps such as that from a hook punch [149]. Reduction of a slosh effect can also be described in nature as woodpeckers, although somewhat controversial [150,151], are thought to have protective mechanisms from the effects of repetitive TBI by possible shock absorbing anatomical structures, i.e. hyoid bone and a unique tongue [149]. The significant and/or continuous stresses of a slosh effect could play a role in tau aggregation as exampled by the discovery of CTE pathology in instances that may not involve direct allisions or collisions to the head, such as military personnel affected by IED explosions or head bangers associated to heavy metal music [84]. Certainly, if complications such as sleep deprivation and wakefulness and epilepsy demonstrate increased ISF/CSF tau, then it is reasonable to assume that ISF/CSF tau would be augmented in the severity spectrum of TBIs [152,153]. Thus, it cannot be ruled out that the first misfolded tau seed could occur in the ISF/CSF, perhaps due to fluid dynamics from the injury, and penetrate into the brain parenchyma and spread through the functional connectome; this could explain the unique distribution of tau pathology in CTE (i.e. detection in subpial and sulci tissue in early stages). Future studies will be performed to detect pathological tau in CSF following TBI.

In all likelihood, tau, whether in a pathological state or not, may be released by diffuse axonal injury (DAI) after repetitive mild TBI and make its way into the circulating fluids and/or parenchyma. Whether by primary or secondary effects, this DAI may be due to the literal shearing of axons and axoskeleton components or from axonal swellings or bulbs that consequently burst after injury. Ultimately, both can result in impaired axonal transport and buildup and/or lysis of proteins and enzymes leading to accumulation of neuropathological substrates and toxicity along with axonal disconnection and synaptic issues. Axonal injury due to trauma can be measured by

amyloid precursor protein (APP) and neurofilament proteins (NFs). APP is present in axons at high concentrations and is transported by fast axonal transport, and NFs, which are coassembled of light, medium, or heavy chain corresponding to molecular weight, are important structural scaffolds for neurons providing mechanical stability and shaping axonal diameter through the number and spacing of NFs [63–65,74–78,102,154]. DAI is thought to be an early event in TBI as *in vitro* dynamic stretch injury of cortical axons revealed microtubule disruption as early as 2 minutes followed by axonal varicosities hours later [152]; in addition, detection for axonal injury has been identified in adult human tissue within ~6-10 hours after head injury [155–157] and as early as 35-45 minutes in children following a motor vehicle accident [158]. Axonal injury by APP has been seen to persist even up to 1 year along with Aβ deposits by fluid percussion injury in rats [159]. Nevertheless, the formation of Aβ perhaps due to DAI is very common in TBI cases, even appearing 2 hours after an incident [160], and may be attributed to an over-accumulation or a reservoir of the substrates known to generate toxic Aβ that then are easily lysed from the dilated bulb and into the brain parenchyma – tau could follow this same event [63,65,74,78,102,154,159]. Interestingly, some research suggests that experimental rotational head injury is proportional to the extent of rotational head motion, severity of DAI (particularly in the BS), and, in turn, the duration of coma as well as degree of neurological impairment; thus, it may be needed to study loss of consciousness in TBI and tau pathology for future studies [161,162]. Nevertheless, DAI could be an early molecular mechanism that allows tau protein to be unbound to microtubules and expelled into the extracellular space to enter circulating fluids or spread through the brain parenchyma.

Next, we asked the question if rmTBIs were continual over time as the animal aged what would happen to pathological tau progression and resultant neuro-behavior. Naïve P301S and WT animals were rmTBI or sham-treated at varied impact numbers and intervals and sacrificed at later

stages: 3m (2 rmTBI rounds), 6m (3 rmTBI rounds), and 9m (4 rmTBI rounds). Behavioral examination was assayed using tests that would emulate some of the clinical aspects of CTE; thus, tasks associated to non-cognitive behavior (Splash test, Nesting, Open field, and RotaRod) as well as cognitive assessing behavioral tasks (Barnes maze with reversal learning) were performed in P301S rmTBI, P301S sham, WT rmTBI, and WT sham mice before sacrifice. Once again, histology using AT8, MC1, and Gallyas silver staining was implemented for assessing tau pathology in different brain regions as well as measurement of insoluble pathological tau levels in brain by ELISA. First, the P301S mouse model is known to exhibit prompt hindlimb paralysis accompanied by a hunch-backed posture and difficulty feeding at later ages; at least 80% are noted to die by 12 months of age [109,110]. Following 4 rmTBI rounds, 8.5 month old P301S rmTBI mice had more paralyzed mice (4) compared to age-matched P301S sham animals (1). There can be difficulties when assessing rodent behavior in mouse models of AD; however, this is a fascinating result because it mimics what is seen in prion diseases, human and animal cases, where infection is substantial and fatal resulting in death, thus rmTBI seems to accelerate this canonical phenotype of paralysis that would lead to its demise.

When assessing the psychiatric and motor aspects of the animals treated with or without rmTBI over 3m, 6m, and 9m, P301S rmTBI mice had lowered performance in the Splash test and Nesting assessment for anxiety/depressive-like behavior. Likewise, One-way ANOVA revealed worsening motor function by RotaRod in late stage P301S rmTBI mice, even showing significance versus P301S and WT sham mice from 3m to 9m. However, there was no significant difference in these psychiatric and motor tests between P301S rmTBI and WT rmTBI mice at any age. These results posit that rmTBI-induced tau may not be the only underlying factor for this type of behavior, yet it is not known if these results would be sustained if various experimental features were altered, such as: an extended age, augmenting impact force or number, shorter

interval from impacts, among others. Thereafter, all animals and groups were examined by utilizing the medial temporal lobe-dependent Barnes maze task. P301S rmTBI at 3m, 6m, and 9m of age demonstrated impaired learning when investigating the primary latency to the escape hole over time compared to controls, and when LTM was measured 3 days after training, the P301S rmTBI mice at all late time-points exhibited significant impairment remembering where the escape hole was statically placed compared to all age-matched P301S sham, WT rmTBI, and WT sham controls. Representative images of the trace for all groups emulate the average primary latency to the escape hole in LTM. P301S rmTBI exhibited a randomized search pattern, while the control animals followed a more serial or spatial approach. Further, when the escape hole was moved to a novel area, the Tg tau rmTBI animals once again had difficulty discovering the newly placed escape hole, thereby indicating an impairment to disassociate the previously learned information and apply this to a novel context as in reversal learning.

Since developed by Carol Barnes in 1979, the Barnes maze is one of the most widely used, standard tasks to assess rodent spatial reference memory and hippocampal/medial temporal lobe (MTL) function [163–165]. Studies of the canonical patient H.M., effect in aging or diseases such as AD, and multiple animal lesion and imaging studies verify that the HPa and MTL are imperative for memory function [163,164,166,167]. The Barnes maze results explored in this study determine that the combinatory effect of burgeoning tau accumulation and rmTBI induction diminish spatial learning and memory signifying impairment in the hippocampus and MTL brain regions in the P301S rmTBI mice, even as early as 3 months of age. Moreover, in the reversal learning, where the escape hole position is changed to 180° from its previous testing location, the animal then has to learn that the former is no longer rewarded and adjust their strategy to resolve the issue. If an improvement in performance is not observed, this means that cognitive flexibility is distorted [163,168]. Studies that address reversal learning discovered involved brain regions are the

oribitofrontal cortex, medial prefrontal cortex, nucleus accumbens, and perhaps basolateral amygdala [168]. Once more, P301S rmTBI animals spent a longer time identifying the novel-situated escape hole compared to age-matched controls referring to disturbed cognitive flexibility and executive function. Notably, these are mostly all brain regions that are intimately neuronally connected and where tau accumulation can generally appear in tauopathies, as well as in the experiments performed here.

The significant difference between P301S rmTBI and the respective controls in the cognitive-associated Barnes maze with reversal learning task relay that rmTBI along with progressing tau pathology may play a more deleterious role in learning and memory. Tau aggregates in brain have been noted to correspond with clinical outcomes, neuronal degeneration, and disease severity better than Aβ aggregation in AD [169], yet other intricacies could be involved that lead to the behavioral consequences: time exposed to pathological tau protein, levels of the protein, the structural state or mislocation occurrence, and other factors. Seeding ability of tau has been correlated with a higher Braak stage and negative Mini-Mental State Exam [111]. Indeed, current AD therapy studies are shifting targets from Aβ to tau protein to hopefully delay or prevent AD [170]. Compounds directed to tau aggregates or anti-tau immunotherapy have shown to lower tau aggregates in brain and improve behavior [170,171]. Tau reduction by anti-sense oligonucleotides alleviated tau inclusions and seeding as well as neuronal loss in Tg tau mouse [172]. Cheng et al. demonstrated that complete ablation or partial reduction of tau prevented deficits in spatial learning and memory after a repeated mild frontal impact TBI model [173].

Tau protein could play a large role in neuronal networks as neuronal/synaptic activity can: stimulate the release of tau and spreading of tau pathology, induce tau phosphorylation, and relocate tau to the dendritic spines [42,174–176]. Reduction of tau protein prevented cognitive decline, synaptic impairment, and spontaneous epileptiform activity from the synergistic effect of Aβ and

Fyn in multiple hAPP mouse models as well as ameliorated seizure activity induced in Aβ/Fyn overexpressing mice [177,178]. The absence of tau protein prevented Aβ-induced impairment of long-term potentiation (LTP) with involvement of the GSK-3β kinase in hippocampal cultures [179]. Hyperphosphorylated tau was elevated in the dentate granule cells and mossy fibers in pharmacologically epileptic-induced 3xTg-AD mice compared to controls [180]. Over-expressed hTau-A152T tau Tg mice demonstrated abnormal brain oscillations that was corrected by genetic ablation of the MAPT gene and doxycycline inducible-expression [181]. Neuronal vulnerability, which could transpire to even brain region susceptibility, could be an issue along with pathological tau and spreading affecting neuronal types differentially[182] and may be amplified following TBI; two possibilities could occur: 1) the selective vulnerability is due in part to its intrinsic properties or 2) vulnerability may be due to their connectivity [183]. This could be why, agreeing with Braak staging, specific brain regions are compromised in disease, such as AD, and some are spared of neuropathological repercussions.

In AD, brain areas predominantly affected by tau pathology are those involved in higher-order cognitive functions, areas/neuronal connections vulnerable in aging, as well as those that take the longest time for reaching maturity during development [8,9,11,60,61]. A repetitive form of TBI may well engender a deleterious microenvironment, or even accelerating age-related molecular mechanisms, in the brain that can facilitate tau aggregation and propagation. Tauopathies are age-related and progressive, where tau pathology sequentially spreads over time, yet a TBI event could form tau pathology in a short time – or even in children – and these early tau aggregates could lead to disease onset and irreversible progression. Widespread protein insolubility and aggregation has been suggested as a natural part of aging [184,185], which could influence PMDs, and this reaction could be accelerated after TBI beginning with tau due to tau's response to damage and/or stress in brain.

To study the effect of varied rmTBI induction on tau pathology, histological procedures utilizing AT8, MC1, and Gallyas silver staining were employed. Although tau pathology was advancing along with age, Tg tau rmTBI mice showed a more robust pathology in brain as compared to Tg tau sham mice at 3, 6, and 8.5 months of age. P301S mice displayed positive staining with classical somatodendritic morphology as well as punctate and thread-like tau, which seemed more advanced in the assessed regions following rmTBI; for example, at 8.5 months old, P301S rmTBI mice had interesting infiltration of Gallyas-positive staining in the dentate hilus compared to sham mice (Figure 22, Gallyas inset). Thioflavin S staining of the groups exhibited the same trend in Gallyas silver staining. Overall quantifications demonstrated exacerbated and disseminated tau pathology, including various distinguished structures, in the P301S rmTBI mice compared to age-matched P301S sham mice at later stages, as denoted by fold-change (FC) evaluated below:

- AT8:
    - 3 months, 2 rmTBI R (FC = 1.83-4.55)
    - 6 months, 3 rmTBI R (FC = 2.05-5.87)
    - 8.5 months, 4 rmTBI R (FC = 1.31-2.75)
- MC1:
    - 3 months, 2 rmTBI R (FC = 2.17-4.58)
    - 6 months, 3 rmTBI R (FC = 1.85-3.29)
    - 8.5 months, 4 rmTBI R (FC = 1.71-2.92)
- Gallyas silver staining:

- 3 months, 2 rmTBI R (FC = 2.53-7.57)
- 6 months, 3 rmTBI R (FC = 1.57-3.54)
- 8.5 months, 4 rmTBI R (FC = 1.81-2.64)

For the most part, HPa and BS show some of the higher fold-changes by histology, which may translate to what is revealed by the Barnes maze results as well as the increased paralysis in the 9m rmTBI group. Finally, following fractionation protocols of 10% brain homogenate to obtain the formic acid, insoluble protein fraction, biochemical ELISA measurements determined significant augmented pathological insoluble tau in P301S rmTBI mice versus P301S sham mice at 3 months (FC = 1.21), 6 months (FC = 1.53), and 8.5 months of age (FC = 1.49). There was no measurements detected in WT rmTBI and WT sham mice tested at 8.5 months old by p^{S199} ELISA (data not shown).

Transgenic tau rmTBI and sham results were assessed from all early and later time-point groups by insoluble tau ELISA levels and summed brain areas of histology using linear regression and determining the effect of rmTBI on tau pathology as well as the potential equivalent age to P301S sham mice by the slope of the line. There was an approximate 1.5-fold increase of insoluble tau by ELISA per month – assuming animal survival and continuous aggregation; moreover, the predicted age of the P301S rmTBI mice compared to sham mice showed an accretion in age, following the rmTBI paradigm as executed in this study. The difference of the slopes for AT8, MC1, and Gallyas silver staining for the total summed burden of all groups demonstrated P301S rmTBI had differences as compared to P301S sham rodents over time. Breaking the overall burden back down to individual brain regions, P301S rmTBI mice revealed significant differences to P301S sham animals with noteworthy differences seen among MC1 and Gallyas silver staining along with HPa and BS regions. These results determined that P301S rmTBI had more aggregated

PHF/NFT tau pathology in the brain. The HPa and BS may be more vulnerable areas to tau pathology or even act as a hub for tau propagation and spreading as well as correlate with the behavioral and phenotypic results following rmTBI over time. The P301S mouse model is reported to have neuronal loss at 9-12 months of age [110]. Quantification of anti-cleaved caspase-3, one apoptotic marker of cell death, determined that P301S rmTBI mice sacrificed at 8.5 months old, earlier than the 9-12 months mark, had more neuronal degeneration in comparison to age-matched P301S sham mice. Higher levels were seen in the HPa and BS, once again, which may correlate to tau aggregates and behavior. These results posit intensified insoluble tau levels along with accelerated model/age-related neuropathology following rmTBI events over time.

If we extrapolate these data, following the rmTBI paradigm studied here, there is an elevated presence of aggregated tau and neuronal death in the brain, markedly in the HPa and BS, which may then translate to the observed learning and memory deficits and paralysis in the P301S rmTBI animals. It has been suggested that tau spreading and aggregation is age and brain region dependent. For example, the Hyman laboratory deduced that mice, virally expressed with human tau in the EC, had more tau spreading in the hippocampus and adjacent cortical regions and EC neurons in older mice than young, yet viral vector introduction in the striatal caudoputamen (CPu) left the mice unaffected by tau spreading, despite the age [186]. As conferred previously, these results hint to region/neuronal vulnerability, where there may be an integral difference in neuronal populations in the EC versus CPu that may promote tau aggregation and spreading, or the regional environment / cell autonomous conditions, as there is a difference in tau kinases and phosphatases in the EC versus CPu [186]. TBI could very well magnify these aspects related to tau misfolding and aggregation, but it is yet to be determined if the formation of a pathological tau seed strictly in an anomalous region, not prominent for tangle pathology, could occur and spread throughout the

brain. It still cannot be ruled out that some regions/neuronal cells may have the ability to degrade tau longer before succumbing to tau accumulation.

Moreover, could TBI, as in the association of rmTBI with CTE, actually engender the formation of multiple types of seeds or conformers as delineated by different tau strains? The "strain" terminology in terms of proteopathies originated from prion diseases where the self-propagating PrP^{Sc} protein can have differing structural heterogeneity (i.e. size and conformation) or conformational variants that results in maladies with diverse features: clinical symptoms, affected brain regions, seeding or sequential spreading, preference to specific cells to affect, and/or toxicity [4,7,34,38,99,113,115,130–132,134]. This could be one explanation for the various tauopathies and atypical sequential pattern of tau neuropathology, distinguished tau morphology, and clinical symptoms. Clavaguera et al. was able to recapitulate the corresponding pathological lesions from inoculated tauopathies (AD, tangle-only dementia, AGD, PSP, CBD, and Pick's disease) in ALZ17 mice and were able to serially propagate this seeding material *in vivo* [43]. The laboratory of Marc Diamond measured tau seeding by the Förster resonance energy transfer (FRET)-flow cytometry tau biosensor cell assay from multiple brain regions and Braak stages in human AD samples and observed extensive seeding activity, noticeably in regions projected to unaffected by pTau deposition, and in detergent-insoluble fractions that were not detected by tau ELISA [111]. Thus, this implies there may be multiple types of soluble and insoluble tau seeds in the diseased human brain; moreover, this too could be happening in TBI cases. Purified and synthetic tau oligomers and PHFs have been used to seed endogenous tau in rodents, as well [46,47,51,100]. Indeed, recent research utilizing cryo-microscopy at high resolution has discovered that CTE (3 cases) demonstrated distinct filamentous structures from AD and PiD cases, and over 97% of the CTE protofilaments comprised of a conserved fold were different from AD and PiD [71,187–189]. Thus,

manifestation and dissemination of distinct conformers of assembled tau may underlie different tauopathies and could be present following TBI events.

The discovery of prions acting virtually alike to a virus with infectious properties and as a causative agent of prion diseases, or transmissible spongiform encephalopathies, was a transformative innovation in the scientific field. Subsequently, this idea was translated to various PMDs that were thought to have a transmissible component or shared "prion-like" mechanisms. This could be demonstrated in animal models by an *in vivo* bioassay where the seeding-nucleation model could be propagated *in vivo* by inoculation of seed-containing material (i.e. an aberrant proteinaceous brain homogenate) and generate similar pathologic features or a significant attenuation of the nucleation or lag phase of seeding in the circumstance if there is endogenous components in the animal model. Thus, seeding is observed as a significant shortening of the incubation period or acceleration in the onset of the inherent arising disease. Akin to prion diseases, seeding assessment of AD by *in vivo* bioassay was performed originally in marmosets followed by intensive evaluation in rodent models; these results gave strong support for the protein-only hypothesis in disease [34,37,190,191]. Indeed, exogenous inoculation of a tau seeds (i.e. synthetic tau or brain homogenates from human tauopathies or transgenic tau mice) determined resultant tau deposition was not limited to the injection site, but had spread beyond to functionally connected brain regions in human tau transgenic mice and even in non-genetically modified WT mice [43–49]. Seeding could also be detected in parallel by serially diluted amyloidogenic Aβ brain homogenate *in vivo* [118].

To address if the earliest rmTBI-induced tau (1 hour post-rmTBI) was seeding competent, we excised and made an entorhinal cortex brain homogenate and inoculated mice expressing normal human tau (hTau) to analyze any acceleration of endogenous pathology or induction of insoluble tau *in vivo*. Results from the prior experiments dictated the earliest time-point (1 hour)

of triggered tau formation and a canonical, tau-laden brain region (entorhinal cortex) that provided the inocula for the bioassay. The EC is an area canonical for tau pathology and as an initial affected region of tau deposition in AD [60,61]. The extracted EC homogenate from the 1 hr P301S and WT rmTBI or sham-grouped mice was i.c. injected into 2.5 month old hTau mice; these animals observe progressive formation of soluble tau over time, not as robust as the P301S model, but no tangle formation [119]. EC inoculated hTau injected mice were then assayed in animal behavior and histology as done previously to examine the effect of rmTBI-induced tau seeds in prompting NFTs and exacerbating tau pathology at 9 months of age. The following experimental groups for the *in vivo* bioassay included: 1) hTau mice injected with 1hr P301S rmTBI EC homogenate, 2) hTau mice injected with 1hr P301S sham EC homogenate, 3) hTau mice injected with 1hr WT rmTBI EC homogenate, and 4) hTau mice injected with Aged P301S EC homogenate as a positive control.

As completed previously, hTau-EC injected animals were assayed in psychiatric and motor abilities. There was no significant difference in performance among the groups for Splash test, Nesting, Open field test, or RotaRod suggesting the different EC homogenates had no effect on these relative behaviors. Nonetheless, examining Barnes maze with reversal learning, hTau-Aged P301S and hTau-P301S rmTBI revealed impaired cognitive capacities compared to controls in Barnes maze learning curve, LTM (primary latency and errors), and primary latency to the novel escape hole in reversal learning, respectively. These results were similar to what was seen beforehand that tau combined with rmTBI may play a more deleterious role in learning and memory and cognitive-associated brain regions as specific EC homogenates (Aged P301S and P301S rmTBI) were able to alter behavior in hTau mice evaluated by Barnes maze with reversal learning. Immunohistochemistry using AT8 and MC1 antibodies in hTau-Aged P301S, hTau-P301S rmTBI, hTau-P301S sham, and hTau-WT rmTBI mice was performed. All mouse groups

presented a faint or weak AT8 and MC1 immunostaining, which could be detected essentially in: piriform cortex and claustrum, superior cortex (deep cortical layers), entorhinal cortex, amygdala, hippocampal area, diencephalon, brainstem, and cerebellum, respectively. Soluble pre-tangle tau pathology is primarily non-argyrophilic and non-fibrillar; this weakly immunostained droplet-like inclusions in the hTau groups may be in a prefibrillar and pre-tangle state at 9 months of age. Immunopositive nuclei was also detected with better intensity in regions such as the amygdala and BS. This weak staining of AT8 and MC1 seems to be an intrinsic property of the hTau mouse model as missorting of tau has been reported at about 6 months of age utilizing the PHF-1 anti-tau antibody [119] and as older 10 month old untreated hTau mice exhibited the same type of immunoreaction (data not shown). Thus, abnormal tau seemed to be located in the distal dendritic segments / proximal dendrites as noticed by Braak et al [192] and therefore may exhibit a mislocalization of tau as an early step in tau pathogenesis. Some classic somatodendritic aberrant tau with AT8/MC1 immunostaining, as that of in the P301S mouse model, could be found in the HPa of hTau-Aged P301S mice, which had been reported much later (12-18 months) previously [119], thereby positing an acceleration of tau pathology in the hTau mice following Aged-P301S EC inocula.

Protein assemblies may be viewed in post mortem tissue and reveal visually striking pathological aggregates, yet this end-point result may not convey the conclusive pathogenic alteration of the specific protein. As in the case with tau protein, pre-tangle or oligomeric structures or precursor events may be directly responsible for the neurotoxicity accompanied with behavioral changes in disease. Soluble oligomers appear to be an intermediate on the pathway to fibrilization and/or amalgamate together to form fibrils, yet oligomers could lead to a different "off pathway" system - disparate from the nucleation-polymerization pathway; however, there is much difficulty determining the nature of protein misfolded intermediates/oligomers due to

unfavorable energy context resulting in a transient structural change. Mechanisms of oligomer toxicity suggested are: direct binding to molecules, pathway activation, oxidative stress, recruitment of cellular factors, generation of membrane permeating pores or binding to receptors, and/or overload of proteostasis machinery. Research has demonstrated that there is an inverse relationship between oligomer size and toxicity and have hydrophobic patches exposed, which may make them more capable seeders. Yet, there may be different types of oligomers (i.e. amorphous or disordered aggregates) with different: fates, stability, mechanisms of toxicity or even lack thereof, and propagation properties [4,14,193–195]. It cannot be ruled out that rmTBI could trigger the formation of "on-or-off pathway" neurotoxic tau oligomers, which are able to propagate *in vivo*, and can result in behavioral consequences as shown here in this study.

These samples were carefully quantified for AT8/MC1 burden intensity, and hTau-Aged P301S mice demonstrated the most significant effect with AT8 staining higher in CTX, HPa, and BS, and MC1 staining elevated in CTX, HPa, and Cb as compared to hTau-P301S sham and hTau-WT rmTBI mice, respectively. Hyperphosphorylated tau, indicated by AT8 immunostaining, was augmented in the HPa of hTau-P301S rmTBI mice as compared to hTau-P301S sham and hTau-WT rmTBI mice and in the Cb versus hTau-WT rmTBI mice by MC1 immunostaining. MC1 immunoreactivity was surprising in the Cb, mostly localized to the granular cell layer, but may be from the inherent characteristic of the hTau model, as untreated 10 month hTau mice had similar immunostaining; however, this also could serve as a portent for cerebellar motor-related issues as even later-aged hTau mice observe altered gait. These results are indicative of the amount and perhaps type of *de novo* tau seeds inoculated in the hTau mice having a deleterious effect by accelerating AT8/MC1-stained aberrant tau pathology in the hTau model. Aged-P301S inoculated hTau mice exhibited a more robust hyperphosphorylated tau and MC1-PHF pathology in brain, yet hTau-P301S rmTBI had elevated pTau in the hippocampal area, but significantly

only by AT8 immunostaining, representing significant, but early pathological changes, compared to respective controls. Longer incubations may be necessary to observe significant differences of PHF tau and/or other brain regions in hTau-P301S rmTBI.

Astonishingly, Gallyas silver staining of the injected hTau mice presented fascinating results. All groups, although not all animals, displayed argyrophilic Gallyas positive staining in the CTX proximal to the injected area and likely where the homogenate may have dispersed. This staining resembled glia-like morphology that was rod-like and punctate structures and some ameboid morphologies. Argyrophilic grain-shaped staining could be detected more often in hTau-Aged P301S and hTau-P301S rmTBI mice in the corpus callosum and trickling into the alveus of the HPa – although this occurred in one hTau-P301S sham mouse. Only hTau-Aged P301S and hTau-P301S rmTBI mice exhibited abnormal Gallyas positive staining similar to coiled bodies and neuropil thread-like structures in the fimbria fornix and stria terminalis. Argyrophilic staining could be examined in the hippocampal-targeted area much higher in hTau-Aged P301S rodents followed by hTau-P301S rmTBI mice, and no Gallyas staining in the internal hippocampal structures was noted in hTau-P301S sham and hTau-WT rmTBI mice and even 10 month old hTau untreated mice. The staining in the HPa of hTau-Aged P301S and -P301S rmTBI animals was ThS-positive and resembled neuronal morphology. The argyrophilic staining identified here can be determined from the inocula that produced an induced reaction, utilized in this study, as older untreated hTau mice do not show Gallyas positive tau or fibrillar tau as stated previously.

When quantifying Gallyas staining threshold density in the targeted HPa of the groups, hTau-Aged P301S animals had elevated Gallyas silver staining in the HPa as compared to hTau-P301S sham (one mouse) and undetected in hTau-WT rmTBI mice, whereas hTau-P301S rmTBI mice exhibited a very strong trend against hTau-P301S sham mice ($p = 0.0524$). It is evident that inoculation with the hTau-Aged P301S EC substrate, which most likely contains an exorbitant

amount of tau seeds and is seeding competent as seen in previous studies, provoked the formation of argyrophilic structures shown as an amalgamation of glial and neuronal tangles *in vivo,* while hTau-P301S rmTBI mice presented a similar effect at a lower level. It could be expected that the 1hr P301S sham inocula could reveal some seeding activity since there could still be capable and available endogenous tau seeds as conveyed in the P301S mouse model, as seeding activity could be reported earlier than previously expected in this Tg tau mouse model [45]. It is imperative to point out that only the hTau-Aged P301S and hTau-P301S rmTBI animals demonstrated what looked like soma-filled, neuronal argyrophilic inclusions (as well as ThS-positive) below the corpus callosum and alveus of the hippocampus, i.e. in the hilus of the dentate gyrus or CA1 regions of the HPa. In prion studies of zoonotic potential, the transmission barrier can manifest as a subsequent delay of etiology and/or as an incomplete attack rate which may predominantly be determined by the percentage of similarity between the prion PrP sequence and the novel host's PrP sequence; thus, this could be occurring in our experimental study in terms of different tau isoforms. This could explain why there was not a uniform attack rate among the groups, as well as individual mice showing a more robust reaction than others, when the P301S mouse (4R1N isoform) was introduced into the host hTau mouse (4R2N isoform); moreover, the amount levels and/or engendering of a different tau strain and/or folded conformation cannot be ruled out, as well. Ultimately, these results together posit successful seeding capability of the Aged-P301S and 1hr P301S rmTBI inocula demonstrated by an augmentation of AT8/MC1 tau pathology and induction of glial and neuronal tangle pathology – normally not present in the hTau mouse model.

Most significantly, argyrophilic inclusions were generated by EC inoculation in normal human tau mice, which has not been described in this mouse model [119], and, indeed, these silver-positive deposits attained in the injected hTau mice highlight intriguing results. Gallyas silver staining is a very useful staining technique in that it is able to react to PHF/NFT-tau and has been

determined to be a vital staining for tauopathies, like AD, and stated to react to only 4R tau isoforms, yet it has been a significant staining method for identifying glial fibrillary tangles (GFTs) and astrocytic inclusions (i.e. tufted astrocytes, astrocytic plaques) and glial cytoplasmic inclusions (GCIs) in related 4R tauopathies such as PSP, CBD, FTD, and AGD, and other NDs, like Multiple System Atrophy, respectively [196]. Incredibly, inoculation of EC substrate in the hTau mouse model generated what can be described as GFTs, much more aggressively in hTau-Aged P301S and hTau-P301S rmTBI mice, emulating some of the same silver impregnated, morphological neuropathology denoted in these particular 4R tauopathies [122,196–198]. Some of the glial tangles detected in these mice are described below. GCIs are composed of a meshwork of randomly arranged, loosely packed filaments with cross-sectional diameters of 20-30 nm; can entrap cellular organelles; are Thioflavin S-negative; and may reveal weak or negative immunostaining with various anti-tau and anti-PHF antibodies [196,199]. Argyrophilic thread-like structures or interfascicular threads can be seen as long, thin, wavy, and/or corkscrew-shaped filaments as well as may be oligodendroglial in nature [196]. Coiled bodies are composed of accumulations of fibrils measuring 10–20 nm in diameter ultrastructurally and appear as a fine bundle of filaments coiled around the nucleus [196,198,200,201]. Scattered inclusions and/or grains are small, about 4–8 microns, spindle shaped, rod-like, button-like or round protrusions in the neuropil and are thought to be located in dendrites and dendritic branches [122,196,197,200]. Fairly similar results have been described as *post-mortem* brains from PSP and CBD cases were inoculated in non-Tg mice, and only these particular 4R tauopathies induced astroglial and oligodendroglial tau inclusions [202]. It is not necessarily known which 4R isoform composes these described silver-responsive pathologies, but immunoreactivity of argyrophilic grains, coiled bodies, and pre-tangle neurons to non-phosphorylation-dependent antibodies to N-terminal and C-terminal tau suggest that full length tau (4R2N) is contained in these structures [203].

However, despite the presence of GFTs in the injected hTau groups, only hTau-Aged P301S and hTau-P301S rmTBI mice revealed neuronal NFT formation in the targeted HPa as demonstrated by argyrophilic neuronal morphology, as well as Thioflavin S-positive staining in hippocampal structures - below the corpus callosum and alveus of the hippocampus. ThS-positivity was not as rampant as that of the Gallyas silver-stained pathological consequences, but indication of Thioflavin S reactivity in the Aged P301S and P301S rmTBI injected hTau animals posits the occurrence of neuronal tangles, as glial-related tangles are dictated as ThS-negative [122,124,125]. It can be presumed the deleterious effect from the glial tau inclusions as argyrophilic deposition in the corpus callosum or alevus may alter axonal transport or could have an effect related to the learning and memory impairments exhibited as solely the hTau-Aged P301S and hTau-P301S rmTBI had glial tau in the fimbria fornix, which has been suggested to play a role in memory. It cannot be ruled out that these substrates may have transferred or even generated a novel strain of tau that may have involved different astroglial populations or triggered a distinct astroglial response. AT8/MC1 immunohistochemistry did not robustly detect these tau astroglial-like pathologies, which normally do show AT8/MC1-positive GFTs and GCIs in the various 4R tauopathies [124]. These argyrophilic inclusions may be later aggregation events where the AT8 epitope and MC1 detecting region may be rendered inaccessible or proteolytically degraded. Remaining experiments are to determine if this type of neuropathological response is an endogenous reaction that may be induced by really any kind of homogenate - as well as defining if this is indeed a novel tau strain by utilizing the diverse anti-tau antibodies that target specific phosphorylation sites of tau. Nevertheless, hTau-Aged P301S and –P301S rmTBI injected hTau mice reveal an induced Gallyas-positive neuronal and glial tauopathy, reminiscent of 4R-affiliated tauopathies, which therefore suggests a prolific seeding capability – even at estimated minute

quantities as predicted in the 1 hour P301S rmTBI EC homogenate - as compared to controls, yet transsynaptic spreading may occur more rampantly at much later ages.

Although tau exists principally in neurons, tau has been suggested to be present in astrocytes, microglia, and oligodendrocytes in lower levels, yet this same tau protein is reported to be involved in proteinaceous astrogliopathies in NDs related to protein misfolding and aggregation. More so, CTE is described to have neuronal and astroglial tau neuropathology in brain [84,89]. Thus, glial tangles may appear in a spectrum of morphologies in disease, but it is not uncommon or extraordinary in NDs. Astrocytes and glia are important for the neuroinflammatory response, among other functions, and has been suggested as an early pathological event and might promote the progression in NDs. A neuroinflammatory response to damage-associated molecular patterns can occur immediately following injury, and this response balances on a fine line between beneficial and deleterious. Following a TBI, inflammation is activated, yet can persist, as seen even in some human cases of up to 17 years [65,75,78,204–206], producing more harm. Other than responding to injury, astroglial cells could play a role in the transcellular spread of tau or may even react with neuronal tau pathology. Depleting microglia reduced tau propagation *in vitro* and *in vivo* [207]. Extracellular tau oligomers have been detected to abundantly and promptly accumulate in astrocytes where they disrupted intracellular Ca^{2+} signaling and Ca^{2+}-dependent release of gliotransmitters, especially ATP, and induced synaptic dysfunction [208]. Moreover, these results of tau uploading from astrocytes required APP [208], which could be altered from TBI events as in DAI or APP-filled axonal bulbs. Oligodendrocytes, which insulate neuronal axons with myelin sheaths, were seen to be involved in tau seeding and spreading; Ferrer et al. introduced various brain homogenates from diverse tauopathies into the corpus callosum in mice, and phospho-tau deposition, resembling coiled bodies and threads, was able to spread from the ipsilateral injection site to the contralateral side [209]. The results discovered here call for an understanding of this glial

tangle pathology that is found in various tauopathies, and the role of astroglial cells involvement in tau spreading remains unresolved.

CHAPTER 6

Conclusions and Future Directions

The effect of TBI on tau pathology was assessed *in vivo* over time following a moderate-severe TBI using the classical controlled cortical impact method and by rmTBI by means of a closed-head modified weight drop method emulating sub-concussive or concussive impacts. In addition, the seeding capability of the earliest generated rmTBI-induced tau seeds was assayed by *in vivo* bioassay. The central hypothesis of this study was that TBI would induce the early formation of tau misfolded seeds as well as exacerbate tau pathology and spreading throughout the brain by a nucleation-polymerization process, which would then lead to neurodegenerative changes relative to disease. In this study we observed:

Chapter 2: Determine the effect of moderate-severe TBI on the formation and spreading of tau pathology *in vivo*.

- TBI is involved in the early formation and spreading of pathological tau that could accelerate the progression and even induce the onset of tauopathy.
- TBI is able to induce tau deposition as early as 1 day post-TBI most significantly on the impacted side of the brain.
- TBI generates pathogenic tau aggregates than can spread from the initial impacted-site to the contralateral side of the impacted brain as tau pathology is observed 1 week after the event.
- Tau load continuously increases over time (1-2 months and 6 months post-TBI) indicating a progressive and spreading pathology - not just a local and restricted event.
- Tau spreading followed progression along the functional connectome of the brain suggesting the neuronal transport of tau aggregates from one brain area to another.
- Tg P301S tau mice demonstrated impaired learning and memory 6 months post-TBI, manifesting the effect of increased aggregated tau on clinical signs.

- TBI induced an altered tropism in tau deposition suggesting the possibility of a new tau strain that aggregates in a brain area that is usually not affected in P301S mice.

Chapter 3: Determine the generation and spreading of tau pathology and behavior following repetitive mild TBI *in vivo*.

- rmTBI causes early, transient behavioral changes, in both WT and Tg mice, due to the effects of the direct impact and/or a post-concussion syndrome. Normal functional recovery is slower in Tg mice compared to WT suggesting that tau aggregation may be involved in post-concussive pathology.
- There is a small, detectable amount of tau pathology of different conformations triggered as early as 1 hour after rmTBI, which is augmented compared to respective age-matched sham mice noted by histology and ELISA.
- Following multiple rounds of rmTBI, anxiety and motor coordination impairment are exacerbated in the P301S rmTBI mice, although the presence of tau may not be the only underlying factor, as there was no significant difference compared to WT rmTBI mice.
- Late stage P301S rmTBI mice (3 months, 6 months, and 8.5 months) displayed exacerbated tau pathology in brain by histological and biochemical assessment as compared to age-matched controls. Thus, multiple mTBI events were seen to exponentially intensify tau aggregation and spreading in all the brain regions analyzed.
- Our data indicates that insoluble tau levels in the P301S rmTBI mice increases over time, higher than in Tg control mice, augmenting age-associated deposition. Also, neuronal loss, another age-related neuropathology of the P301S mouse model, was exacerbated in P301S rmTBI suggesting rmTBI-induced tau aggregates cause cell death.

Chapter 4: Investigate the seeding capability of rmTBI-induced seeds by *in vivo* bioassay.

- hTau mice inoculated with Aged P301S or rmTBI-induced P301S extract showed learning and memory impairments, positing the deleterious effect of tau on behavior and suggesting the presence of tau aggregates in rmTBI-induced P301S mice.
- hTau bioassayed mice displayed increased abnormal aggregated tau burden in brain compared to controls corroborating the induction of tau aggregation in the inoculated samples, and its seeding capability in the host .
- hTau-Aged P301S and –P301S rmTBI injected mice reveal a remarkable induction and elevation of neuronal and glial tauopathy, reminiscent of 4R astroglial human tauopathies, which suggests seeding and spreading depends on the host model and the inoculum.

Altogether, based on these data, following TBI there can be an early triggering of pathological tau that can alter and/or accelerate the spatiotemporal progression of aberrant tau in the brain, which can lead to disease-associated manifestations. Indeed, TBI-induced tau seeds, even as early as 1 hour post-TBI, were seen to be seeding capable demonstrated by elevated abnormal tau burden and induction of argyrophilic glial and neuronal tau pathology by *in vivo* bioassay.

There are few translatable animal models that impeccably emulate a mild head impact/concussion-induced athlete or military personnel. This problem may stem from the deliberations on defining mild impacts/concussions, problems reporting and diagnosing, and heterogeneity of the TBI itself; however, animal models for mild TBI are expanding. Edwards III et al. described various experimental models for repetitive mild TBI and the effect of these on Aβ and tau pathology [63]. Depending on multiple reported elements, the research somewhat had consistent results demonstrating higher pTau deposition following mTBI; however, there is a need to explore and pool these models and results in detail to answer tenuous questions, i.e. the number of mTBIs to induce pathology, differences in the placement of impacted areas of the head, effect of loss of consciousness, age of onset, and more. In addition, novel animal models of TBI are still being investigated such as the modCHIMERA, which allows rotational acceleration to a cradled animal tested at 1.7 and 2.1 joules [210]. Moreover, *post-mortem* assessment of former military personnel engaged in blast exposure or military-related concussion as well as animal models of blast exposure indicate tau pathology after TBI suggesting that diverse injury types can provoke tau pathology in brain [77,94,106].

Nevertheless, to initiate rmTBI in this study, mice were treated by a modified, closed-head weight drop method, similar to the Wayne State weight drop animal model. This model fulfills mostly all criteria emulating a CTE-like/contact sports animal model with no severe damaging effect or invasive procedure as well as implementation of acceleration/de-acceleration and rotational forces due to a free-flowing head movement [63,211–214]. Free-flowing head models are yet to thoroughly explore tau deposition especially utilizing Tg animals. Angular acceleration may be more deleterious for the brain than straight linear forces [127], and a study on professional boxers revealed that hook punches, where the head is turned laterally, caused more concussions than parallel blows (i.e. jab punch) [215]. We used the lowest reported mass to our knowledge as our

method of mild, sub-concussive rmTBI induction in naïve anesthetized animals. This approach was scaled to previous studies that enumerated human concussions to rodents [126]. Four mTBIs were administered in 1 day (denoted as 1 round) over the head at varied time-points, consisting of 1 to 4 totaled rounds, reflecting multiple mild impacts and/or "second impact syndrome". This syndrome transpires following a concussion head injury or worse accompanied by a second head injury before symptoms associated with the first have cleared and can be cataclysmic for the brain [127]. Moreover, CTE diagnosis is highly associated to rmTBI signifying that the repeated exposure to brain trauma could be an enormous factor in tau development and progression. Indeed, in our study, consecutive mild impacts generated over time were seen to trigger early tau formation, exacerbate neuropathology over time, and impair learning and memory in P301S Tg tau mice. This novel experimental approach contributes to on-going mTBI/concussion studies, yet more studies are warranted at different combinations of ages of induction and intervals, augmenting weight forces and number of impacts, comparison of disparate impacted areas, methods of mTBI and animal models, and more.

As previously mentioned above, this study utilized the PS19 strain (P301S mutation) Tg mouse model for assessing tau aggregation. Although an acceleration and worsening of tau pathology can be measured, as performed in this study, this mouse model is non-physiological in nature as there is an overexpression of the human P301S mutant tau protein and 4R/1N tau isoform on the prion promoter, which may alter expression of MAPT in different brain regions. This model does not fully recapitulate human tauopathy maladies, although no animal model does so faithfully. Future rmTBI studies could incorporate: transgenic tau mice with green fluorescent protein (GFP), such as the T40PL-GFP Tg mouse from the laboratory of Virginia Lee, where pathological tau induction and propagation could be measured by tracking GFP following TBI induction [216]; Tg mouse models that express wild-type or normal human tau, which do not exhibit

tangle accumulation [109,119,217,218]; and a tau knock-in (KI) mouse, such as the KI of P301L observed at physiological levels of expression [219] with comparison to tau knock-out (KO) mice. Moreover, just as CTE and AD have a close 3R/4R tau isoform ratio, there could likely be different molecular conformers composed of both 3R/4R and solely 3R or 4R tau isoforms following TBI; thus, rmTBI studies could analyze models of various tau isoforms and/or mice including all putative 6 isoforms of tau [220,221]. In addition, future studies could include more natural mammalian models that could comprise some of the relevant brain morphology emulating humans, such as present sulci and gyri, since CTE-related tau is primarily detected in the depths of sulci and gyri in human cases.

Although we demonstrate that there is triggered formation and elevation of abnormal, seeding-capable tau deposition following rmTBI very early on that is able to uninterruptedly remain exacerbated over time complemented with cognitive impairment, the initial molecular mechanism remains to be elucidated. Figure 6 shows general molecular cascades that may be altered following TBI, whether resulting from the primary impact and/or secondary initiated pathways, such as neuronal excitotoxicity, Ca^{2+} overload, mitochondrial dysfunction, oxidative stress due to formation of free radicals, inflammation, and abnormal protein aggregation. The force from the direct, primary insult can perturb the cellular membrane, thereby spilling its contents into the extracellular space shocking the microenvironment and chronically triggering multiple, overlapping downstream pathways that begin to exhaust the brain. There are impairments in a myriad of neurotransmitter systems linked to mental and behavioral function including: glutamate, gamma-Aminobutyric acid (GABA), acetylcholine, and dopamine [78]. The activation of the glutamatergic system is a typical component following TBI. The brain is estimated to consume 20% of energy stores in the body, and neurons depend on a steady transport of glucose facilitated by glucose transporters (GLUTs), especially GLUT-1 and -3. Alteration in

GLUT-1 and -3 is reported in TBI [222]; a deficiency of GLUT-1 and -3 is noted in AD brains and correlates with hyperphosphorylation of tau and the density of NFTs [135,223]. After TBI, there is damage to the neuronal cell, which causes ionic imbalance by an efflux of K^+ and influx of Na^+ and Ca^{2+} as well as impaired glutamate release and re-uptake, in so doing causes an energy conundrum in the cell. This results in excessive extracellular glutamate which engenders an amplified and chronic membrane depolarization activating specific excitatory channels such as α-amino-3-hydroxy-5-methyl-4-isoxazolepropionic acid receptor (AMPA) and N-methyl-D-aspartate receptor (NMDA) as well as opening of Ca^{2+} channels. This chronic hyperexcitability due to copious glutamate downregulates glutamate receptors which can impair LTP and induce long-term depression, among other problems [76,78]. With the unrestrained Ca^{2+} influx and constant release of intracellular stores, there can be the over-production and over-activation of various phospholipases (i.e. calcineurin), proteases (i.e. calpains and caspases), and transcription factors (i.e. c-Jun and NOS). These molecules along with elevated Ca^{2+} can cause cytoskeletal demolition and dendritic spine shrinkage by: neurofilament compaction and microtubule disassembly; mitochondrial impairment, which can occur rapidly and persist (from less than 1 hour to 14 days) and where there is additional release of Ca^{2+} stores; oxidative stress from the formation of free radicals like reactive oxygen species and nitric oxide; formation of aggregate proteins such as pTau/NFTs and Aβ; and activation of neuronal cell death [78,224,225].

As discussed prior, neuroinflammation can respond immediately after TBI. Following TBI and/or a disturbance of the blood brain barrier (BBB), astrocytes and microglia can migrate and activate chemokines and cytokines to remove injury by-products and offer neuroprotection; however, this is another example of a mechanism that can become activated for too long and producing insidious effects. Indeed, pro-inflammatory cytokines - tumor necrosis factor, interleukin 1β, and interleukin-6 – were initiated within hours in a TBI mouse model [78,226], and

this negative inflammatory response can endure even up to 17 years after TBI [65,75,78,204–206]. To add to the complexity, various kinases and phosphatases entwined in tau phosphorylation are altered in TBI and tauopathies like CTE and AD, as well [227–229]. In addition, the incorporation and/or interaction of molecular cofactors and enzymes may play a role as estimated by the ultrastructural assembly of CTE filaments, which revealed a dense, hydrophobic cavity, not found in AD and PiD cases [187]. Future auxiliary immunohistochemistry utilizing APP and/or neurofilament-light will be performed to analyze the effect of axonal injury as an early pathological event and role in tau pathology following rmTBI, as noted in Figure 29.

Neurofilaments serve as major components of the axonal cytoskeleton, being the most abundant fibrillary piece of the axon, and are built by the intertwining of 3 protofibrils – one being 68-70 kDa neurofilament light chain (NF-L). NF-L is found highly in neurons of the brain, in particular the cortex and cerebellum, while also detected in the periphery. Importantly, NF-L has been studied as a marker of axonal injury and researched as a biomarker of damage in the brain for TBI and neurodegenerative brain disorders [227–231]. In Figure 29A, preliminary results utilizing anti-Neurofilament L antibody reveal normal immunofluorescent staining throughout the brain, as exampled by the CTX here, in both the 1 hour P301S rmTBI and sham mice. However, various brain regions, such as CTX and BS (inset), did identify NF-L positive ovoids or varicosities in the 1 hour P301S rmTBI mice prominently in the age-matched sham mice (Figure 29B). Interestingly, when assaying subcortical white matter of the corpus callosum (cc), 1 hour P301S sham exhibited no aberrant NF-L staining or morphology (Figure 29C), but 1 hour P301S rmTBI mice had prominent NF-L positive compacted beads or varicosities along the cc white matter tracts (Figure 29D) reminiscent to axonal damage as observed with such antibodies for DAI like APP or SMI-34 [83,155,157,204,210,233]. This immunoreactivity was not seen in 1 hour P301S sham mice. These preliminary results show impairments in axonal structure by NF-L immunofluorescent

staining of DAI in brain 1 hour after rmTBI in P301S mice. However, further studies are necessary to evaluate auxiliary molecular mechanisms involved in the results demonstrated in this study.

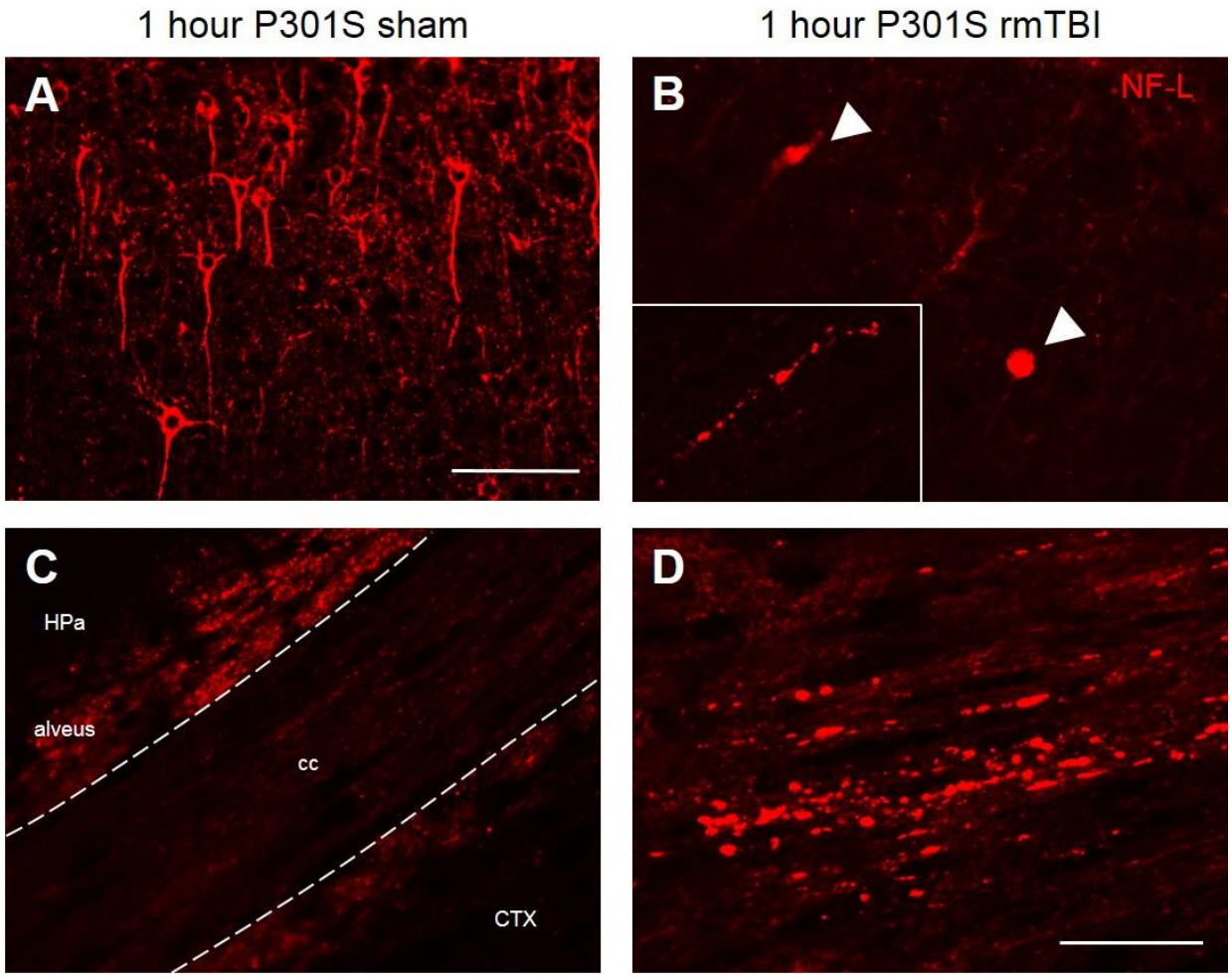

Figure 29. Early axonal injury detected by neurofilament light chain (NF-L) immunofluorescence in 1 hour P301S rmTBI mice. Anti-Neurofilament L antibody was used to determine presence of axonal injury 1 hour following rmTBI in P301S mice. **(A)** NF-L was highly identified in areas such as the cortex (CTX), as shown here, and cerebellum in rmTBI and sham-treated P301S mice. **(B)** 1 hour P301S rmTBI mice exhibited more prominent abnormal NF-L immunopositive large ovoids or varicosities (white arrowheads) in CTX and midbrain (inset). **(C)** NF-L staining was seen to be at WT control levels and show unbroken white matter tracts in the corpus callosum (cc) of 1 hour P301S sham mice. **(D)** 1 hour P301S rmTBI animals demonstrated NF-L positive varicosities akin to axonal injury all along the cc much more prevalently. HPa = hippocampal area. Scale bar: 100 μm, 30 μm.

Moreover, tau pathology is seen only in a subset of TBI cases - not unanimously; other studies are warranted to assess perhaps what pathways are involved or not involved in individuals that are resilient to the effects of TBI versus those that succumb to deleterious consequences in the brain.

We believe that an assortment of injuries and/or stresses to the brain can drive tau pathology, yet we inadequately know the exact biochemical profile of tau following injury – the effect of disparate and heterogeneous injuries, inclusion types formed, precise phosphorylation sites involved, the effect of the various tau isoforms, among others. Along with neurodegenerative tauopathies, TBI is a risk factor for diverse NDs and dementia and is associated to other protein aggregates, as well; thus, TBI could be classified as a polypathological trauma [235]. For example, TBI generated a higher incidence of PD in patients with TBI of all severities (0.58%) and even mTBI (0.47%) as compared to patient controls [236]. A unifying feature of TBI is the abnormal accumulation and potential concomitant accumulation, as within the same brain, of pathological proteins associated with NDs – tau, Aβ, alpha-synuclein, and TDP-43 [235]. Amyloid-beta deposition resembling early AD, diffuse plaques has been demonstrated in human TBI cases, even at younger ages, which indicates that TBI can reduce the age of when amyloid generation is typically observed [160,235]. Stein et al. analyzed 114 deceased athletes and veterans with CTE, which revealed Aβ accumulation increasing 2.7-fold for every decade in age for 52% of the subjects. In addition, CTE patients with Aβ had a trend for greater amount of concussions reported, elevated CTE stage prognosis, and higher frequency of dementia than CTE subjects without Aβ [66,87]. Other factors following TBI upon pathological protein accumulation and related NDs could include: injury severity and repetitive nature, survival time, patient age at injury induction, genotype (i.e. APOE genetics), and cognitive reserve [63,235]. Nevertheless, the

independent and dependent effect and/or interaction of these pathological proteins subsequent to TBI and risk to disease remain to be elucidated and could provide interesting future studies.

Could rmTBI be facilitating earlier and more aggressive neuronal tau mislocalization and spreading? Some of the early time-point P301S rmTBI mice revealed more punctate and thread-like tau immunoreactivity in brain, such as in apical dendrites in the EC. Undoubtedly, the classical soma-filled tau was detected in brain, as well, and yet as rmTBIs and time progressed, so did this punctate and thread-like tau pathology – especially in the EC and HPa. At the 8.5 month old age, some P301S rmTBI mice had this similar pathology as compared to age-matched P301S sham mice. Representative images of the EC utilizing AT8, MC1, and Gallyas staining of 8.5 month old P301S rmTBI mice reveal more robust punctate and thread-like positive tau compared to age-matched P301S sham mice (Figure 30A). This particular histological positive morphology could be area/region or cell type specific; for example, irregular punctate tau pathology was detected more often in the lateral EC and hilus of the dentate gyrus, while more thread-like, most likely due to axonal projections, was seen in CA1/CA3 of the hippocampus. The mislocalization of tau to the dendritic compartment is noted as an early pathological event in AD and has been provoked by Aβ accumulation and associated with dendritic degeneration [8,10,13,25,42,119,120,174], yet it is interesting to see this type of pathology so early on and even robustly at the late-stage in the P301S rmTBI mice. Initial tau-related deficits may develop as a result of synaptic aberrations caused by the accumulation of hyperphosphorylated tau within intact dendritic spines, where it disrupts synaptic function by impairing glutamate receptor trafficking or synaptic anchoring as shown by Hoover et al [41]. Indeed, this pathological dendritic tau could be a much more potent seeder and be a key cog in the spatiotemporal progression of tau in disease-afflicted brains. With the repetitive head impacts occurring over time, pathological tau, perhaps even localized in the axon or soma, could be fragmented engendering more available seeds, which

translocate to the dendritic compartment, or it cannot be ruled out that axonal injury or shearing, as shown in Figure 29, could allow free extracellular tau in the brain parenchyma, which may be up taken by neurons and begin the misfolding and aggregation process. Nevertheless, future studies are aimed to determine the compartmental localization of tau aggregates in rmTBI-treated and sham animals by double-labeled immunohistochemistry in consecutive slides using: AT8/NeuN (neuronal soma); AT8/MAP2 (neuronal axons); and AT8/anti-total tau (dendrites). Additional approaches to isolate the synaptosomes in the brain and detect number and tau levels by biochemistry will be done in parallel, as well.

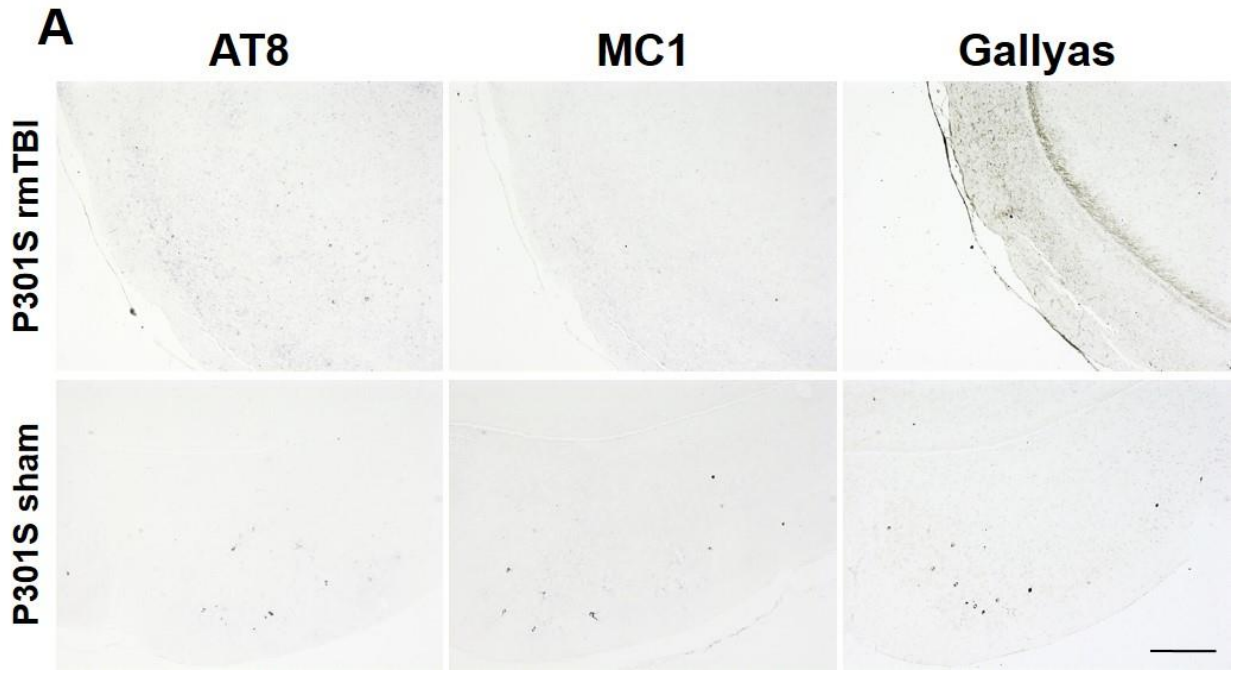

Figure 30. Potential mislocalization of tau following rmTBI. Example images show 8.5 month old P301S rmTBI mice reveal more robust punctate and thread-like positive tau compared to age-matched P301S sham mice by AT8, MC1, and Gallyas silver staining. Future directions can aim to determine the localization of pathological tau in rmTBI versus sham Tg tau animals.

Additionally, in terms of tau seeding capability, an ultrasensitive and specific FRET-based flow cytometry (fc) biosensor assay as a method to examine *in vitro* tau seeding has been developed in the laboratory of Dr. Marc Diamond at the University of Texas Southwestern (UTSW) in Dallas, TX [45,52,115,237–239]. This assay discriminates to tau seeds and shows sensitivity to ~300 fM of added tau seeds [45]. Previously, monoclonal FRET biosensor HEK293T cells were engineered to stably express the repeat domain P301S mutation that was fused to either cyan fluorescent protein (CFP) or yellow fluorescent protein (YFP), and when exposed to exogenous tau seeds (i.e. synthetic tau or disease-associated homogenate), this leads to tau reporter protein aggregation which emits a FRET signal and can be detected by fc. In the absence of proteopathic seeds, the cells maintain tau as a soluble monomer, and have no substantial background FRET [45,52,115,237–239]. Accordingly, while performing a visiting rotation at UTSW in the Diamond laboratory, we assessed the earliest time-points pathological tau was determined following rmTBI (1 hour and 1 day) in the P301S mice by the FRET-based fc biosensor assay. A novel generation of HEK cells that express the tau repeat domain P301S mutation fused to GFP/Pacific Blue were optimized for codon usage to diminish truncation of the tau protein (NK cells, unpublished) were utilized here. Permission for further presented results and usage (Figure 31) was obtained directly from Dr. Marc Diamond at UTSW.

Under a sterile fume hood, for usage, NK cells were trypsinized using 3 ml of trypsin-EDTA (0.25%) for 5 minutes (min), quenched with 9 ml of aspirated warm culture medium (DMEM+10% FBS), and transferred to a 15 ml conical tube after gentle re-suspension/washing. Ten µl of the cells sample along with trypan blue was loaded into a TC20 automated cell counter (Biorad, Hercules, CA) to obtain cell count measure. Cells were centrifuged at 1,000 x rpm for 5 min at room temperature (RT), and the cell pellet was resuspended in warm culture medium. A master mix of cells (culture media + Penstrep antibiotic) was made so that each well of two 96

well plates would contain 35,000 cells in 130 µl media. The NK cells were allowed to settle by leaving the plate undisturbed for 8 min at RT and then incubated overnight (o/n) at 37 °C, 5% CO_2. The following day, when tau biosensor cells were 60-65% confluent, NK cells were treated with 1 hour P301S rmTBI (n = 5), 1 hour P301S sham (n = 5), 1 day P301S rmTBI (n = 5), and 1 day P301S sham (n = 5) randomly selected 10% mouse brain homogenate. All samples were performed in triplicates and blinded to experimenters. Since standardized characterization of the novel NK cells to P301S brain homogenate was limited, a "naked" seeding assay was performed by serially diluting homogenates of 8 µL, 4 µL, and 2 µL in 1x PBS split between the triplicate wells. Seed transduction complexes were created by: incubating appropriate volume of Lipofectamine (Lipo) + Opti-MEM at RT for 5 min; 35 µL of this solution was placed in each diluted sample tube and incubated for 30 min at RT; 10 µL of Lipo + Opti-MEM was added in triplicate biosensor cell control wells; and 50 µL of samples was added per well for each triplicate. Cells were then incubated for 36 hours at 37 °C, 5% CO_2.

The next day cells were harvested for FRET-fc by first trypsinizing cells (50 µl) for 5 min in 37 °C incubator, quenched with 150 µl of aspirated culture media, and after resuspension, centrifuged at 1,000 x rpm for 5 min at RT. Media was carefully removed to not disturb the pellet, and 200 µL of 2% paraformaldehyde was incubated for 10 min at RT then re-centrifuged and paraformaldehyde removed. Cells were resuspended in 200 µL flow buffer for FRET-fc thereafter. FRET-fc was ran using BD LSR Fortessa instrument (special order - BD Biosciences, Haryana, India), and gating strategies utilized as explained in previous publications [45,52,115,237–239]. AmCyan signal appears in response to tau seeding with these NK cells. FCS files were obtained and analyzed by fc analysis programs FlowJo (FlowJo, LLC, Ashland, OR) and Community Cytobank [240]. Briefly, compensation was performed to avoid fluorescence spillover, and cell populations were taken through the appropriate gates to remove any debris, doublets, and false-

positives, as shown previously [237]. A FRET-positive polygonal gate was obtained by plotting the empty liposome-treated GFP/Pacific Blue cells on a FRET-positive (AmCyan) vs GFP bivariate plot, and this gate excluded most cells (~99%), such that background FRET was $\geq$ 1% of cells. Any events that shifted into this gate were considered FRET-positive and expressed as percentage of FRET-positive cells as indicated in Figure 31.

Thus, tau seeding by the FRET-based flow cytometry biosensor assay was performed in the earliest rmTBI and sham-treated P301S (1 hour and 1 day) diluted brain homogenates. As a whole, the tau seeding effect was not robust; however, minute tau seeding could be detected only in the early time-point P301S rmTBI-treated animals. The 8 μL brain homogenate dilutions, in all cases, seemed to produce a more toxic effect to the cells as noted under the microscope and debris identified by FRET-fc analysis. This has been reported to be cognizant of seed volume, as too high of crude sample volume may be toxic to these biosensor cells [237]. Cells treated without seed material (i.e., empty liposomes) revealed diffuse fluorescence, whereas cells treated with seed material had punctate and reticular intracellular inclusions as noted in the 4 μL and 2 μL dilutions having healthier cells and producing a better seeding effect. In Figure 31A, top panel, in the 1 hour P301S rmTBI and P301S sham mice (n = 5/each group), one P301S rmTBI mouse demonstrated prolific tau seeding at the 4 μL (average of triplicates = 0.68%) and 2 μL (average of triplicates = 0.73%) dilutions. This FRET-positive population was above FRET background and occurred in all triplicates with sufficient FRET events, while no seeding was detected in any 1 hour P301S sham mouse (data not shown). The 1 day-P301S examined groups once again revealed tau seeding activity in three 1 day P301S rmTBI mice in the 4 μL and 2 μL dilutions in all triplicates, as exampled by Figure 31A (2 mice shown, middle panel), while no reputable tau seeding occurred in any 1 day P301S sham mice (Figure 31A, lower panel). Although tau seeding did not occur in all early-staged P301S rmTBI mice, the number of FRET-positive events reported

was higher in P301S rmTBI versus sham animals, and when the average percentage of FRET-positive cells was quantified for the 1 day P301S rmTBI and sham mice, Student t-test demonstrated a significantly higher reported FRET-positive cell % in both 4 μL ($p < 0.05$) and 2 μL ($p < 0.05$) dilutions for the 1 day P301S rmTBI animals, respectively (Figure 31B). Thus, these preliminary results posit minute levels of seeding capable tau in the 1 hour and 1 day post-rmTBI P301S mice by the FRET-based fc biosensor assay. Further experiments are warranted to optimize this assay to assess the degree of tau seeding in P301S rmTBI and sham mice at the earliest time-points, such as: reducing the number of cells per well and extending the temporal measurement, identification of the best homogenate dilution or fraction, increasing the n-value of the groups, among others. Despite this, with the expected low levels of pathological tau seeds in the naïve P301S rmTBI and sham mice 1 hour and 1 day after induction and "naked" tau seeding assay approach taken here with these novel NK biosensor cells, these results are promising and support our hypothesis of the formation of exigent rmTBI-triggered and seeding proficient tau seeds.

Figure 31. *In vitro* FRET-based flow cytometry tau biosensor assay of 1 hour and 1 day post-rmTBI P301S mice. After following standard flow cytometry-gating methodology, a FRET-positive (AmCyan) versus GFP bi-variate plot was generated, and a FRET gate was constructed from empty liposome-treated cells, such that the background FRET is ≤ 1%. A cell population shift into the FRET gate would appear following treatment with tau seed-containing material. **(A)** Results show example plots of 4 μL and 2 μL brain homogenate (BH) dilutions, which demonstrate FRET-positive tau seeding in the 1 hour P301S rmTBI mice (top panel) and 1 day P301S rmTBI mice (middle panel), while no reputable tau seeding was detected in early time-point P301S sham mice (lower panel). **(B)** Student t-test was performed for the 4 μL and 2 μL dilutions of the 1 day P301S rmTBI and sham mice. Each dilution presented significantly higher percentage of FRET-positive cells in the 1 day P301S rmTBI mice compared to sham animals ($p < 0.05$), respectively. Data is expressed as means ± SEM. Experiments and data analysis performed by George Edwards III and Joshua Beaver, UTSW in Dallas.

A

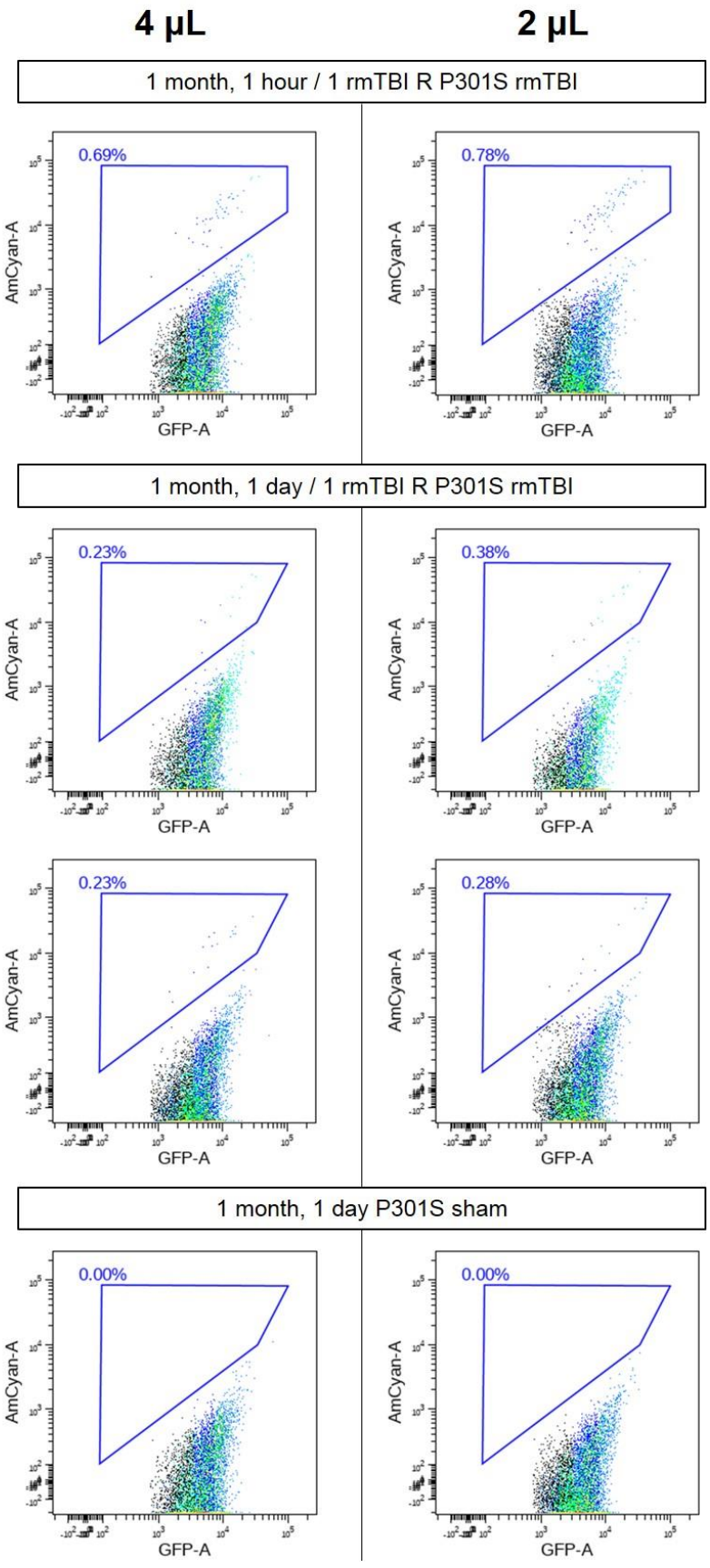
4 µL
2 µL
1 month, 1 hour / 1 rmTBI R P301S rmTBI
0.69%
0.78%
1 month, 1 day / 1 rmTBI R P301S rmTBI
0.23%
0.38%
0.23%
0.28%
1 month, 1 day P301S sham
0.00%
0.00%
AmCyan-A
GFP-A

B

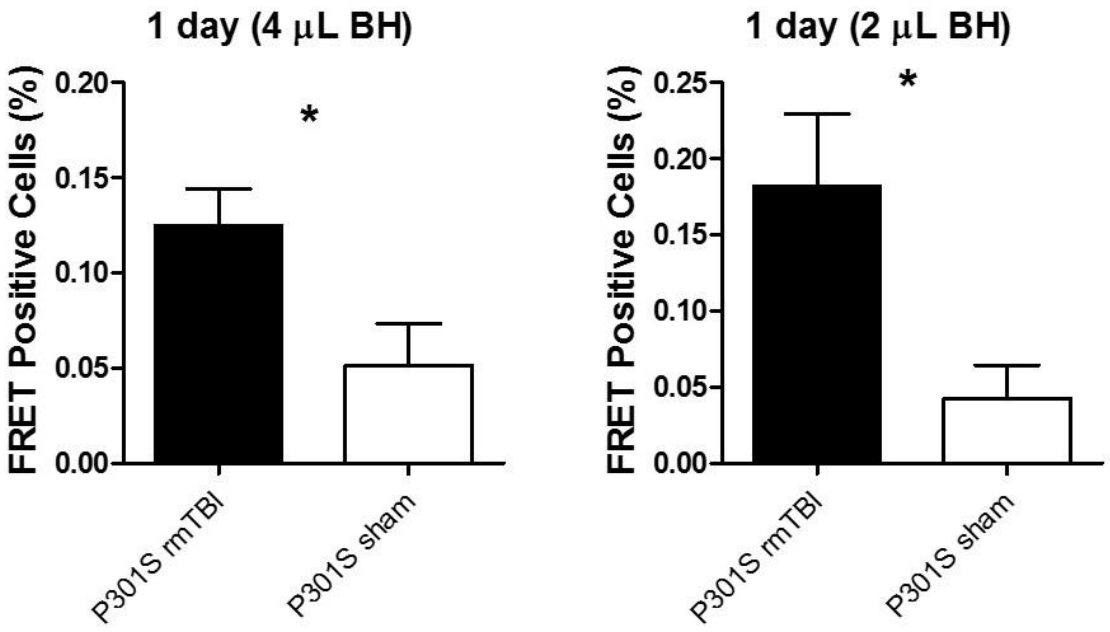

The results of the inoculated hTau animals exposed unexpected and intriguing findings. Indeed, the hTau injected animals used here demonstrated faint AT8 and MC1 immunostaining along with more punctated and thread-like morphology of tau, and yet these animals produced robust argyrophilic staining, which closely resembles glial tau pathology seen in tauopathies such as PSP, CBD, and AGD, in some arrangement. However, penetration into the targeted HPa of the inoculated material seemed to be better suited for the Aged P301S and P301S rmTBI EC homogenate, thereby generating GFT neuropathology, but also what may possibly be neuronal Gallyas and ThS-positive induced tau pathology in the normal human tau-expressing rodent. The seeding event examined in this study could very well be a combination of the host's intrinsic response and provided intracerebral inoculated substrate. Tauopathies show unique and heterogeneous clinical symptoms and neuropathology, despite the commonality of pathological tau protein distinguished *post-mortem* in each of these diseases. These features could be due to

tau aggregates forming distinctive structural conformations or strains, and this cannot be ruled out in this case. Future studies will look to illuminate these suggestions, such as the use of different phospho-tau antibodies that target different epitopes (i.e. AT100, AT180, AT270, etc.) as the distinct recognition by anti-tau antibodies of the seeded pathology is indicative of tau strains.

Finally, in recent publications, Dr. Claudio Soto's laboratory has shown promising results for technique, similar to what is achieved in PCR, for amplifying the nucleation-polymerization process *in vitro* by a method called protein misfolding cyclic amplification (PMCA). Results for an Aβ-PMCA for AD and α-synuclein PMCA for PD using human CSF posited this diagnostic approach to have high specificity and selectivity [241,242]. This same technology is being applied to tau protein with encouraging results. PMCA uses the functional property of misfolded oligomers that catalyze the polymerization of the monomeric protein as a way to amplify and detect them over time. Briefly, tau monomers are incubated with a tau-seeding component (i.e. synthetic oligomers or tauopathy homogenate or collected biological fluid), along with respective controls, and with Thioflavin T (ThT). Seeding efficiency of tau is then measured following multiple rounds of intermittent shaking/sonicating while over time ThT interacts with the polymerizing fibrils, thus shifting the ThT emission peak monitoring the kinetics of fibrillogenesis, as shown previously [241,242]. If the material is seeding-competent, tau-PMCA should display an attenuated nucleation phase, thereby demonstrating faster aggregation kinetics compared to controls. The main overall goal is to utilize the tau-PMCA as a diagnostic method or predictor for tau-affiliated NDs. In Figure 32A, preliminary results demonstrate an attenuation of the nucleation phase of tau fibril formation *in vitro* by a concentration-dependent manner. With a higher concentration of added pre-formed synthetic tau seeds, the reaction occurs faster thereby exigently reaching the exponential or polymerization phase measured by ThT fluorescence over time. This provides

good concentration separation and superior sensitivity that will be instrumental when assessing affected disease–related and TBI samples.

The goal of this future study is to efficiently detect tau aggregates after TBI by tau-PMCA in available brain and biological fluids, including CSF and blood plasma, to monitor the progression of tau pathology with disease onset. It is noted following a TBI event and in tauopathies, like AD, that tau levels are aberrant in biological fluids such as CSF [66,76,136,138,139,243]. Thus, the rmTBI-treated mice and respective controls indicated in Chapter 3 will be assessed by tau-PMCA utilizing brain, CSF, and blood collected at various time-points following impacts, different intervals between impacts, and age of termination (Table 3) to investigate whether rmTBI results in an increase of seeding-capable tau protein aggregates. Brain and CSF samples were collected from P301S rmTBI, P301S sham, WT rmTBI, WT sham mice at different ages at the terminal endpoints following rmTBI: 1 hour, 1 day, 1 week, 3 months, 6 months, and 8.5 months with varied rmTBI rounds. CSF extraction occurred by withdrawal from the cisterna

Table 3. Blood plasma and CSF collection in P301S and WT mice for future studies. This table shows a synopsis of the P301S and WT rmTBI and sham treated groups for fluid collection with varied number of rmTBIs, ages, and time after rmTBI. CSF will be collected through the cisterna magna in all groups at 1 hour, 1 day, and 1 week post-1 round rmTBI, 3 months after 2 rounds rmTBI, 6 months after 3 rounds rmTBI, and 8.5 months after 4 rmTBI rounds, respectively. In addition, to these points as well as the others listed, blood plasma was obtained by submandibular withdrawal and cardiac puncture as final collection technique. Blood was collected in 0.5 M EDTA and immediately centrifuged then snap frozen. Essentially, using these various time-points we can assess blood plasma following differing numbers of TBIs, ages, and time after TBI events focusing on early detection by tau-PMCA without over exacerbating the animal with multiple withdrawals. hour (h), day (d), week (wk), month (m).

Experimental Groups				Blood Withdrawal		CSF
Group	rmTBI rounds	Interval	Age at sac	# of Times	Age of animal, time after rmTBI #	Time
1	1	-	1m, 1hr	2	(1) pre-TBI; (2) 1m, 1hr after 1 rmTBI	1m, 1hr
2	1	-	1m, 1d	2	(1) pre-TBI; (2) 1m, 1d after 1 rmTBI	1m, 1d
3	1	-	1m, 1wk	2	(1) pre-TBI; (2) 1m, 1wk after 1 rmTBI	1m, 1wk
4	2	1m	3m	4	(1) pre-TBI; (2) 1m, 1hr after 1 rmTBI; (3) 2m, 1m after 1 rmTBI; (4) 3m, 1m after 2 rmTBI	3m
5	3	2ms	6m	4	(1) pre-TBI; (2) 3m, 1hr after 2 rmTBI; (3) 5m, 2m after 2 rmTBI; (4) 6m, 1m after 3 rmTBI	6m
6	4	2-3ms	8.5m	4	(1) pre-TBI; (2) 3m, 1hr after 2 rmTBI; (3) 6m, 3m after 2 rmTBI; (4) 8.5m, 2.5m after 4 rmTBI	8.5m

magna as described previously [244]. Blood samples were collected by submandibular withdrawal longitudinally and at terminal points by cardiac withdrawal at: before any TBI event as baseline, at 1 hour, 1 day, 1 week, 1 month, 2 months (1 rmTBI round), 3 months (2, 3 rmTBI rounds), 4 months (3 rmTBI rounds), 5 months (2 rmTBI rounds), 6 months (2, 3 rmTBI rounds), and 8.5 months (4, 5 rmTBI rounds). For plasma collection, whole blood was centrifuged at 3,000 rpm for 15 minutes, and the supernatant collected and snap frozen until use. Once again, tau monomers and ThT will be incubated with the biological fluids collected from all mice in SA2. During interval shaking fluorescence will be measured by fluorimeter over time. Overall, we will compare the detection of misfolded tau oligomers in brain, CSF, and blood in the absence or the presence of rmTBI by tau-PMCA and correlate associated histology, biochemical ELISA, and behavioral results to tau-PMCA detection. These results can assist to pinpoint an estimated time tau seeds form after rmTBI induction, levels of peripheral and parenchymal seeds, the number of TBI events initialized, the level of tau pathology and behavioral state of the animal at that stage.

Potentially, together this could give a diagnostic window in which treatments could be used to intervene following TBI.

Furthermore, future studies will aim for a translational approach by detection of abnormal tau seeds or aggregates in biological fluids in TBI and AD human samples. The detection of tau levels in biological fluids may show promise as a pertinent biomarker in individuals suffering from TBI and act as a portent for deleterious maladies to come. Diagnostic methods are warranted for TBI cases; furthermore, the tau-PMCA technology may demonstrate the capability to be used as an early indicator for other known tauopathies. Here, we will collect human biological samples of CSF and blood plasma taken from various individuals with a history of TBI and assess levels of tau seeds utilizing tau-PMCA. Samples will be obtained in collaboration with: Dr. Paul Schulz, the Director of the Memory Disorders and Dementia Clinic at UTHSC; Dr. Andrew Goldfine, Neurologist, Assistant Professor and Director of the Neurorehabilitation clinic after Traumatic Brain Injury at Stony Brook, New York; and Dr. Anat Beigon, Professor of Neurology at Stony Brook Neurosciences Institute. Samples will be collected from AD cases (with or without TBI), severe and mild TBI cases, and healthy controls (age 50 and under). Younger, healthy controls should have lower amounts of tau circulating in fluids compared to TBI affected patients that should produce a measurable effect of tau seeds. We will attempt to establish a relationship with TBI severity level and time since TBI, along with known confounding factors, to estimate whether misfolded tau protein oligomers correlated with a history of TBI at a cross-sectional population level. Preliminary results demonstrate the tau-PMCA's capability to detect tau seeding in P301S versus WT mice in brain (Figure 32B). When assessing human TBI, AD and CBD, and control CSF, the tau-PMCA indicated more accessible tau seeds in human TBI and tauopathy-related CSF as compared to control CSF comparing the rate of the aggregation curve (Figure 32C). This assay will provide high sensitivity in comparison to other assays that will aid in targeting tau seed

formation in relation to TBI and neurodegenerative diseases and is continually being optimized for future diagnostic capabilities.

We expect that the addition of biological fluids from P301S mice following rmTBI will contain pre-formed seeds that can accelerate the misfolding and aggregation reaction in tau-PMCA exhibited by an attenuated nucleation phase compared to control material and normal aggregation rates. We expect that using the specific and sensitive tau-PMCA, we can detect the earliest time-point in CSF and plasma following rmTBI that is seeding capable and correlate this to the animal's age, number of mTBIs, pathology by histology and biochemical assays, and behavior, thereby making a well-rounded diagnostic supposition. If our hypothesis is correct, the acceleration in tau pathology would indicate that rmTBI can initiate the formation of seed-competent tau aggregates that can propagate misfolding and aggregation in a "prion-like" manner and can use this to detect early aggregate formation and track disease progression by tau-PMCA. As we initiate trials and take a translational approach utilizing human samples, this will generate a significant impact in the TBI and tauopathy field. This will bring novelty to the field as no other study to our knowledge has measured tau levels following multiple rmTBI events longitudinally in CSF and blood to detect the formation of tau seeds and correlate this with clinical symptoms over time in humans and treated animals.

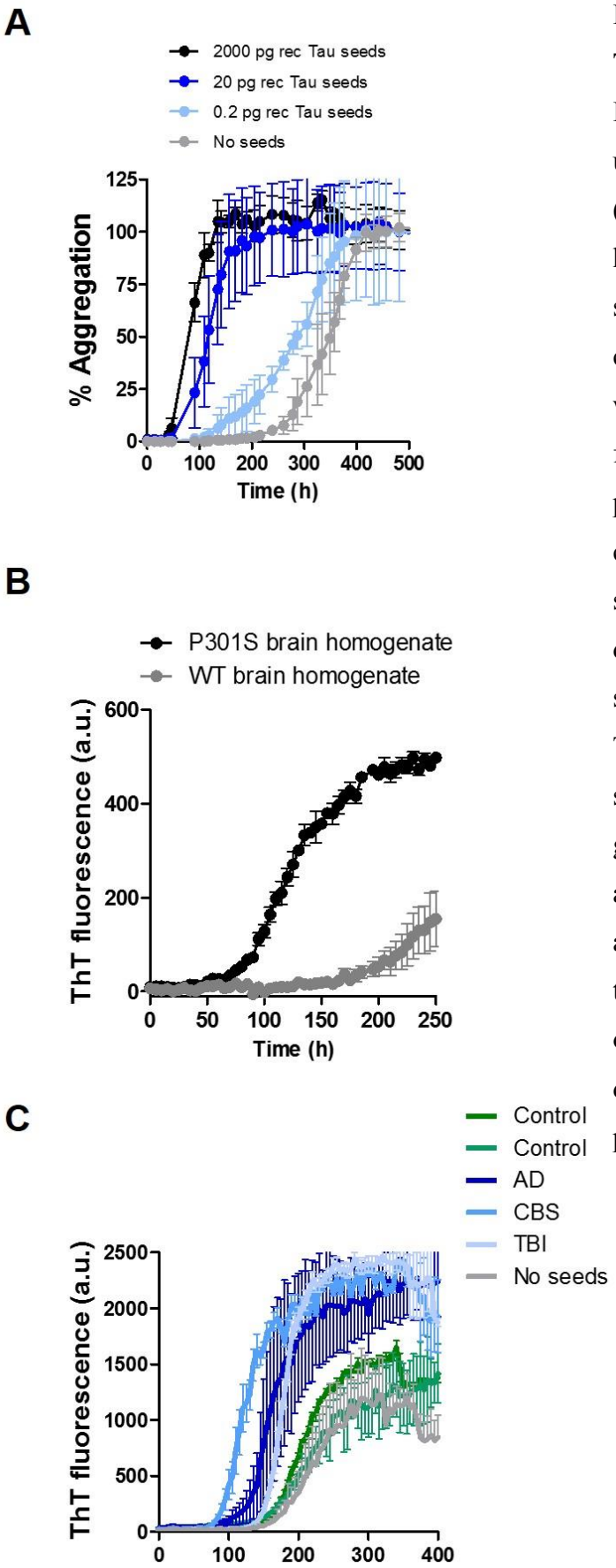

Figure 32. Potential diagnostics for TBI and tauopathies utilizing Tau-PMCA. Tau-PMCA was performed using tau monomers, synthetic tau seeds **(A)**, transgenic or WT brain homogenate **(B)**, or human CSF samples **(C)**, and ThT while using cyclic agitation over time. Aggregation was followed over time by ThT fluorescence. **(A)** Tau-PMCA displays prominent detectability and concentration dependence using synthetic tau seeds. **(B)** Tau-PMCA demonstrates the capability to detect tau seeds in mouse brain homogenate. **(C)** Tau-PMCA detected misfolded tau seeds in human patient TBI CSF generating a quicker aggregation curve along with Alzheimer's disease (AD) and Corticobasal syndrome (CBS) CSF than the respective controls measured over time. All assays were performed in duplicates. Experiments and figures prepared by Nico Mendez Dinamarca.

CHAPTER 7

Materials and Methods

This chapter contains portions from:

Edwards III G.A., Zhao J., Dash P.K., Soto C., Moreno-Gonzalez I. Traumatic brain injury induces tau aggregation and spreading. J Neurotrauma. 2019 Jul 18. doi: 10.1089/neu.2018.6348. [Epub ahead of print]

Animals

P301S transgenic mice (Prnp-MAPT*P301S P301SVle/J, Jackson Laboratory, Bar Harbor, ME) express the P301S mutant human microtubule-associated protein tau (MAPT) under the control of the mouse prion protein (Prnp) promoter. These animals accumulate pTau and NFT formation that can be detected around 6-9 months of age [109,110]. The expression of the mutant human MAPT is five-fold higher than the expression of the endogenous mouse MAPT. P301S Tg mice were used for Chapters 2 and 3. For Chapter 4, normal or WT human full length tau (4R/2N) hTau mice expressed on the Thy1.2 promoter were used to assess seeding capability by *in vivo* bioassay. hTau mice exhibit somatic mislocalization of tau at 6 months and have reported hyperphosphorylated tau that is increased with age (12-18 months), but no tangle formation [119]. Mice were double genotyped for all chapters. Animals were housed in groups of up to 5 in individually ventilated cages under standard conditions (22°C, 12h light–dark cycle) receiving food and water *ad libitum*. All animal experiments were carried out in accordance with the NIH regulations and approved by the committee of animal use for research at the University of Texas Health Science Center at Houston, McGovern Medical School.

Induction of TBI

For Chapter 2, groups of 3 month old P301S mice and wild-type (WT) littermates were anesthetized with isoflurane, placed on a stereotaxic apparatus with a face mask, and prepared for controlled cortical impact (CCI), as done previously to induce moderate to severe TBI [63,245,246]. Briefly, a midline incision was made, and a 5-mm-diameter craniotomy was performed on the right parietal cortex, midway between the Bregma and the Lambda with the medial edge of the craniotomy 1.0 mm lateral to the midline. A pneumatic impact device (Custom Design and Fabrication, Richmond, VA) was used to deliver an impact at 3.0 m/sec generating a 1.0 mm

deformation on the posterior cortex. The incision was closed, and animals were assessed in latency of foot, tail, and righting reflexes as previously described (Suppl. Figure 1A) [247]. Animals were allowed to completely recover in a warm chamber before being returned to their home cages. Sham-operated animals received all the analogous surgical procedures except for the craniotomy and impact. Animals were monitored thereafter daily for up to 2 weeks. TBI and sham groups were n = 4-6 at each time point and were randomly selected and placed in different time-point groups.

In Chapter 3, 1 month, 5 day old P301S Tg tau animals and WT littermates (n = 9-11/group) received a modified closed-head weight drop method, similar to the Wayne State weight drop method, and sacrificed either at 1 hour, 1 day, 1 week, 3 months, 6 months, or 8.5 months. Animal number for the groups was obtained by G-Power analysis [248,249]. This weight drop method emulates a contact sports athlete, and as examined by Kane et al, fulfills most criteria as a CTE-like model, better than others, thereby producing CTE-like results [63,211–214]. The proposed weight drop method engendered no severe damaging effect (i.e. skull fracture, edema, etc.) in mice with 95 g weight at 1 meter [211]. Here, we proposed using a mass of 18 g at 82 cm height as our method of rmTBI induction in anesthetized P301S and WT animals to study the early formation, spreading, and exacerbation of tau in brain following rmTBI. This method was the lowest reported weight utilized, to our knowledge. Animals treated with rmTBI were anesthetized by isoflurane induction and placed just below a ½ inch diameter PVC cylinder tube, which fit perfectly around the skull of the mouse, on a collapsible platform. The 18 g metal weight with a beveled end was securely tied from the top of the cylinder tube to prevent any unnecessary secondary impacts following initial insult. We performed the rmTBI with 4 impacts in one day (being 1 round) with 2 mild impacts given under anesthesia, a 1 hour interval, and 2 more impacts under anesthesia. Sham mice were anesthetized following the same as above, thereby

experiencing the same fall through the platform but with no impact. Overall, this procedure was scaled to fit human cases as previously reported [126]. Once again, as according to Figure 11, P301S and WT mice were rmTBI or sham-treated at 1 month, 5 days and sacrificed 1 hour (1 rmTBI round); 1 day (1 rmTBI round); 1 week (1 rmTBI round); 3 months (2 rmTBI rounds); or 6 months (3 rmTBI rounds) post-rmTBI event (Groups 1-5). Mice sacrificed at 8.5 months of age had 4 rounds rmTBIs (16 total mTBI impacts in time) spread over time to assess exacerbation of AD pathology in an "active athlete " paradigm. Sacrificing at 8.5 months of age was thought to be efficient, in our experience, due to the beginning of motor impairment phenotype that can occur at later months (as seen in our hands the earliest at 9 months) and due to robust tau pathology in the P301S model [109,110].

Behavioral analysis

For Chapter 2, Barnes maze was performed 6 months after CCI in both groups (transgenic and WT) as well as in the sham group, as previously described [3]. Barnes maze is a medial temporal lobe dependent task that evaluates spatial learning and memory. Barnes maze consists of a circular platform with 40 holes with one being an exit from the arena, and the animal uses spatial cues to discover the stationary escape hole in a 3 minute trial. Mice were trained on day 1 with 2 acquisition trials and then 4 trials per day for 4 days. 7 days later long-term memory (LTM) was assessed. Primary latency to the escape hole was used to assess learning and memory. Task performance was recorded and analyzed using the TopScan 2.0 tracking software (Clever Sys, Reston, VA). Behavioral analysis was done by a single experimenter blinded to subject identities.

For Chapters 3-4, Splash test was performed to assay anxiety/depressive-like behaviors in mice [250]. Briefly, animals were sprayed with 10% sucrose solution on the dorsal coat and allowed to freely roam a clean home cage for 5 minutes during which the time spent having cephalocaudal

motions of grooming was quantified. Nesting is a naturally conserved behavior and has been examined in anxiety-related studies. Overnight Nesting was performed by singly housing animals with *ad libitum* food and water and a nestlet (±2.50 g). In the morning, nesting scores were assessed from a 1 (no nest) to 5 (structurally complete nest) rank, as done previously [251]. Motor coordination and activity, grip-strength, and fatigue are all measurements that can be assessed by the commonly used behavioral task of RotaRod (Med Associates Inc., Vermont). Here, the animal was placed on a horizontal oriented, rotating cylinder that accelerated from 4 to 40 rpm. The latency to fall was quantified over 3 trials with 2 minutes interval rest in one day. 6 minutes was used as the final cut-off latency to fall measurement. In addition, one difficulty of the task is the rodent's desire to grip the rotating rod to prevent falling; thus, 2 consecutive rotations of the animal clinging was considered as a latency to fall measurement. The animals were aided for 30 seconds in the first trial to prevent unnecessary behavior (i.e. turning and false-positive falls/jumps). Open field assessment is a useful and simple task to analyze locomotion, exploration, and anxiety behaviors in rodents [252]. The open field apparatus is 44 x 44 cm Plexiglas square box, which was split into sixteen 11 x 11 cm squares for open field testing. The mouse was transported from outside the room into the behavioral testing room in a small box. The animal was placed in the middle of the apparatus with this box overturned, and the small box removed at the start of the trial. Open field testing was ran over a 5 minute trial. Barnes maze was ran similarly, as above, but the LTM assessment was ran 3 days after the final trial. After the LTM trial, reversal learning, also delineated as cognitive flexibility, was performed as 3 trials for a total of 3 days. The escape hole for reversal learning was placed approximately 180° degrees from the previously learned escape hole placement in these trials. The animals were allowed to explore the arena for up to 3 minutes to discover the novel escape hole. All tasks, except for RotaRod, were video recorded and tracking performed by TopScan 2.0 tracking software.

Histology

In Chapter 2, TBI and sham mice were sacrificed either 1 day, 1 week, 1-2 months, or 6 months following CCI trauma. Mice were sacrificed by CO2 inhalation and perfused trans-cardially with cold 5mM EDTA+PBS (1X). Brains were removed, post-fixed into 10% neutral buffered formalin fixative solution and embedded in paraffin. Paraffin-fixed brain tissue was sliced coronally by microtome obtaining 10-μm-thick serial sections and were processed for immunostaining, as previously reported [3]. After blocking the endogenous peroxidase activity with 3% H2O2-10% methanol for 20 min, sections were incubated overnight at room temperature in monoclonal AT8 phospho-PHF-tau pSer202+Thr205 antibody (1:100, ThermoFischer). Primary antibody was detected by incubating 2 hours with sheep anti-mouse HRP-linked secondary antibody (General Electric, Pittsburgh, PA), and peroxidase reaction was visualized using DAB Kit (Vector, Burlingame, CA) following the manufacturer's instructions. Finally, all sections were dehydrated in graded ethanol, cleared in xylene, and cover slipped with DPX mounting medium.

In Chapter 3, P301S and WT rmTBI and sham mice were sacrificed, as above, at 1 hour, 1 day, 1 week, 3 months, 6 months, and 8.5 months of age. In Chapter 4, normal human tau Tg (hTau) mice were perfused with 15 ml of PhosStop phosphatase inhibitors (Roche) and Complete protease inhibitors (cOmplete™ Protease Inhibitor Cocktail, Millipore Sigma) in 1X PBS, pH 7.4. Ten-μm-thick serial coronal sections were processed as above and incubated in AT8; MC1 - pre-tangle PHFs by targeting the N-terminal (amino acids 5-15) and the third microtubule binding region (amino acids 312-322) of tau (a gift from Peter Davies, 1:350); and Gallyas silver staining for NFTs, as done previously [253,254]. For ThS staining, tissue slices were incubated in 0.025% ThS solution for 10 min, as done previously [3]. For analysis of neuronal loss, anti- cleaved caspase-3 (Asp175) (5A1) rabbit monoclonal antibody (Cell Signaling Technology, Danvers, MA, 1:1000) as caspase-3 is a critical executioner of apoptosis. Primary antibody was incubated multiple days

and detected by incubating 2 hours with sheep anti-mouse/rabbit HRP-linked secondary antibody (General Electric, Pittsburgh, PA), and peroxidase reaction was visualized using DAB Kit. Preliminary results for NF-L immunofluorescent staining was obtained utilizing anti-Neurofilament L antibody (Millipore, Temecula, CA, 1:1000). After heat-mediated antigen retrieval in sodium citrate buffer (pH 6.0), the primary antibody was prepared in 2.5% goat serum + 1X PBS with 0.02% Triton X and incubated o/n. Secondary antibody goat anti-rabbit IgG (H+L) Alexa Fluor® 594 (Invitrogen) was used for fluorescent detection after cover-slipping with VECTASHIELD® Antifade Mounting Medium with DAPI (Vector Laboratories).

Image analysis and quantification

Pathological tau burden was quantified using AT8 antibody assessing the overall, ipsilateral (Ipsi) and contralateral (Contra) side of CCI impact of the cortex and amygdala (Ctx), hippocampal area (Hp), and brain stem (BS). Coronal areas assessed were based on anatomical connectivity and cytoarchitectural patterns. The area rostral to the impact covered Interaural (IL) ± 4.54 mm, Bregma (B) ± 0.74 mm – IL ± 3.46 mm, B ± -0.34 mm; the rostral impacted area was assessed from IL ± 2.74 mm, B ± -1.06 mm to IL ± 1.50 mm, B ± -2.30 mm; the caudal impacted area included IL ± 1.34 mm, B ± -2.46 mm – IL ± 0.00 mm, B ± -3.80 mm; whereas the caudal area to the impact was analyzed between IL ± -1.16 mm, B ± -4.96 mm and IL ± -3.16 mm, B ± -6.96 mm. 3-5 sample slides of every 10th section were examined under a bright field microscope (DMI6000B, Leica Microsystems, Buffalo Grove, IL, USA) and photomicrographs were taken with a digital camera (DFC310 FX Leica), imported into ImageJ 1.45s software (NIH), and converted to black and white images. Threshold intensity was used to quantify AT8 burden in brain. Threshold intensity was automatically adjusted to remove the background and held constant during quantification of all the analyzed animals. Burden was defined as the immunoreactive area per total area analyzed in percentage. Likewise, AT8 assessment was measured 5-7 slides of every

10th section and scored from no tau detected (0 score) to highest tau deposition (5 score). This semi-quantitative score was graded by the volume and abundance of AT8 immunoreactivity of disease-associated morphological tau adapted previously [46,100,255]. Score values were averaged and imported into a custom-designed heat map software to generate an overall view of tau deposition. The experimenter was blinded to the animal identities and groups during processing and subsequent quantification methods. For Chapters 3-4, the hemisected brain of mice was coronally sliced, and AT8, MC1, and Gallyas silver staining (3-5 sections) burden percentage was quantified as done above. Multiple brain regions were assessed in all groups: CTX, HPa, Di, BS, and Cb, respectively.

ELISA quantification

Additional 3 month old mice (n=3-4) were CCI-induced (Leica Impact One^{TM} Buffalo Grove, IL) or sham-induced by the same parameters above. TBI and sham mice were sacrificed after 1 day. The ipsilateral and contralateral sides of the brains were extracted from injured and sham mice. Brain hemispheres were homogenized at 10% w/v in PBS containing protease inhibitors as previously described [3]. Brain homogenates were centrifuged at 32,600 rpm for 1 h at 4°C in an ultracentrifuge (Beckman-Coulter). The supernatant was removed, and pellets were resuspended in 200 μL of 70% formic acid followed by sonication. Samples were centrifuged for 30 min under the same conditions, and the supernatant was collected and neutralized in 1 M Tris-HCl buffer, pH 10.8 to measure the fraction of insoluble tau in brain following TBI. Levels of phosphorylated tau at Ser199 were measured using Human tau [pS199] ELISA kit (Invitrogen) per manufacturer's instructions on an ELISA plate reader (EL800 BIOTEK). As for Chapter 3, the other half of brain from P301S rmTBI or sham animals (n = 10/group) sacrificed at 1 hour, 1 day, 1 week, 3 months, 6 months, and 8.5 months were assessed for insoluble pathological tau by ELISA. Before homogenization, the cerebellum was excised from the brain to possibly reduce the

dilution of any tau seeds, especially at the earliest time-points. Homogenization and obtaining the insoluble or formic acid fraction as well as performing the ELISA was done as discussed in Chapter 2.

Statistical analysis

Graphs are expressed as means ± standard error of the mean (SEM). For Chapter 2-3, data was tested for normal distribution by Shapiro-Wilk normality test. Student t-test was used to analyze normal data for histological burden and ELISA quantifications as well as non-parametric data was ran with Mann-Whitney test, respectively. For Chapter 4, the Kolmogorov-Smirnov normality test for was performed, due to a lower n-value, to assess data distribution. One-way analysis of variance (ANOVA) with Tukey's multiple comparison test or Kruskal-Wallis test with Dunn's multiple comparison test was utilized, where applicable, for Splash test, Nesting, Open Field test, and RotaRod behavior analysis as well as experimental hTau mice AT8, MC1, and Gallyas silver staining quantifications. In Chapter 3, comparison of pathological tau between P301S rmTBI and sham mice over time was performed by linear regression analysis, and slopes compared by GraphPad Prism 5.0 (GraphPad Software Inc., La Jolla, CA). Two-way ANOVA followed by Bonferroni post-test was used to analyze the Barnes maze learning curve as well as with reversal learning analysis, and one-way ANOVA with post hoc Tukey's multiple comparisons test was used for long term memory in all cases. Statistical analyses were performed using GraphPad Prism 5.0 software. Statistical differences for all tests were considered significant at the $p < 0.05$ level.

CHAPTER 8

Appendix

Bibliography

1. Dobson, C. M. Protein folding and misfolding. *Nature* **426**, 884–890 (2003).

2. Soto, C. Unfolding the role of protein misfolding in neurodegenerative diseases. *Nat. Rev. Neurosci.* **4**, 49–60 (2003).

3. Moreno-Gonzalez, I., Edwards, G., Salvadores, N., Shahnawaz, M., Diaz-Espinoza, R. & Soto, C. Molecular interaction between type 2 diabetes and Alzheimer's disease through cross-seeding of protein misfolding. *Mol. Psychiatry* **22**, 1327–1334 (2017).

4. Soto, C. & Pritzkow, S. Protein misfolding, aggregation, and conformational strains in neurodegenerative diseases. *Nat. Neurosci.* **21**, 1332–1340 (2018).

5. Morales, Rodrigo; Moreno-Gonzalez, Ines; Soto, C. Cross-Seeding of Misfolded Proteins: Implications for Etiology and Pathogenesis of Protein Misfolding Diseases. *PLoS Pathog.* **9**, e1003537 (2013).

6. Soto C.; Estrada L.; Castilla J. Amyloids, prions and the inherent infectious nature of misfolded protein aggregates. *TiBS* **31**, 150–55 (2006).

7. Jucker M.; Walker L.C. Pathogenic Protein Seeding in Alzheimer's Disease and Other Neurodegenerative Disorders. *Annu Rev Neurosci.* **38**, 87–103 (2015).

8. Arendt, T., Stieler, J. T. & Holzer, M. Tau and tauopathies. *Brain Res. Bull.* **126**, 238–292 (2016).

9. Lee, V. M.-Y., Goedert, M. & Trojanowski, J. Q. Neurodegenerative Tauopathies. *Annu Rev Neurosci.***24,** 1121-1159 (2011).

10. Wang, Y. & Mandelkow, E. Tau in physiology and pathology. *Nat. Rev. Neurosci.* **17**, 5–

21 (2016).

11. Gotz, J. Tau and Transgenic Animal Models. *Brain Res. Rev.* **35**, 266–286 (2001).

12. Iqbal, K., Liu, F., Gong, C.-X. & Grundke-Iqbal, I. Tau in Alzheimer's Disease and Related Tauopathies. *Curr. Alzheimer's Res.* **7**, 656–664 (2010).

13. Morris, M., Maeda, S., Vossel, K. & Mucke, L. The many faces of Tau. *Neuron* **70**, 410–426 (2011).

14. Nizynski, B., Dzwolak, W. & Nieznanski, K. Amyloidogenesis of Tau protein. *Protein Sci.* **26**, 2126–2150 (2017).

15. Cleveland, D. W., Hwo, S. Y. & Kirschner, M. W. Physical and chemical properties of purified tau factor and the role of tau in microtubule assembly. *J. Mol. Biol.* **116**, 227–247 (1977).

16. Kadavath, H., Jaremko, M., Jaremko, J., Biernat, J., Mandelkow, E. & Zweckstetter, M. Folding of the Tau Protein on Microtubules. *Angew. Chemie - Int. Ed.* **54**, 10347–10351 (2015).

17. Johnson, G. V. W. & Stoothoff, W. H. Tau phosphorylation in neuronal cell function and dysfunction. *J. Cell Sci.* **117**, 5721–5729 (2004).

18. Gong, C. X., Singh, T. J., Grundke-Iqbal, I. & Iqbal, K. Phosphoprotein phosphatase activities in Alzheimer disease brain. *J. Neurochem.* **61**, 921–27 (1993).

19. Kanemaru, K., Takio, K., Miura, R., Titani, K. & Ihara, Y. Fetal-type phosphorylation of the tau in paired helical filaments. *J. Neurochem.* **58**, 1667–1675 (1992).

20. Arendt, T., Stieler, J., Strijkstra, A. M., Hut, R. A., Ru, J., Zee, E. A. Van Der, Harkany,

T., Holzer, M., Ha, W., Schiller, F. & Jena, D.-. Reversible Paired Helical Filament-Like Phosphorylation of Tau Is an Adaptive Process Associated with Neuronal Plasticity in Hibernating Animals. **23**, 1–10 (2003).

21. Planel, E., Richter, K. E. G., Nolan, C. E., Finley, J. E., Liu, L., Wen, Y., Krishnamurthy, P., Herman, M., Wang, L., Schachter, J. B., Nelson, R. B., Lau, L.-F. & Duff, K. E. Anesthesia Leads to Tau Hyperphosphorylation through Inhibition of Phosphatase Activity by Hypothermia. *J. Neurosci.* **27**, 3090–3097 (2007).

22. Kopke, E., Tung, Y.-C., Shaikh, S., Alonso, A. D. C., Iqbal, K. & Grundke-Iqbal, I. Microtubule-associated Protein Tau. Abnormal Phosphorylation of a non-paired helical filament pool in Alzheimer's disease. *J. Biol. Chem.* **268**, 24374–24384 (1993).

23. Seubert, P., Mawal-Dewan, M., Barbour, R., Jakes, R., Goedert, M., Johnson, G. V. W., Litersky, J. M., Schenk, D., Lieberburg, I., Trojanowski, J. Q. & Lee, V. M.-Y. Detection of Phosphorylated Ser262 in Fetal Tau, Adult Tau, and Paired Helical Filament Tau. *J. Biol. Chem.* **270**, 18917–18922 (1995).

24. Šimić, G., Babić Leko, M., Wray, S., Harrington, C., Delalle, I., Jovanov-Milošević, N., Bažadona, D., Buée, L., de Silva, R., Giovanni, G. Di, Wischik, C. & Hof, P. R. Tau protein hyperphosphorylation and aggregation in alzheimer's disease and other tauopathies, and possible neuroprotective strategies. *Biomolecules* **6**, 2–28 (2016).

25. Chu, D. & Liu, F. Pathological changes of tau related to alzheimer's disease. *ACS Chem. Neurosci.* **10**, 931–944 (2019).

26. Martin, L., Latypova, X. & Terro, F. Post-translational modifications of tau protein: Implications for Alzheimer's disease. *Neurochem. Int.* **58**, 458–471 (2011).

27. Dixit, R., Ross, J. L., Goldman, Y. E. & Holzbaur, E. L. F. Differential Regulation of Dynein and Kinesin Motor Proteins by Tau. *Science* **319**, 1086–1089 (2008).

28. Violet, M., Delattre, L., Tardivel, M., Sultan, A., Chauderlier, A., Caillierez, R., Talahari, S., Nesslany, F., Lefebvre, B., Bonnefoy, E., BuÃ©e, L. & Galas, M.-C. A major role for Tau in neuronal DNA and RNA protection in vivo under physiological and hyperthermic conditions. *Front. Cell. Neurosci.* **8**, 1–11 (2014).

29. Sultan, A., Nesslany, F., Violet, M., Bégard, S., Loyens, A., Talahari, S., Mansuroglu, Z., Marzin, D., Sergeant, N., Humez, S., Colin, M., Bonnefoy, E., Buée, L. & Galas, M. C. Nuclear Tau, a key player in neuronal DNA protection. *J. Biol. Chem.* **286**, 4566–4575 (2011).

30. Shammas, S. L., Garcia, G. A., Kumar, S., Kjaergaard, M., Horrocks, M. H., Shivji, N., Mandelkow, E., Knowles, T. P. J., Mandelkow, E. & Klenerman, D. A mechanistic model of tau amyloid aggregation based on direct observation of oligomers. *Nat. Commun.* **6**, 1–10 (2015).

31. Melki, R. How the shapes of seeds can influence pathology. *Neurobiol. Dis.* **109**, 201–208 (2018).

32. Harper, J. D. & Lansbury, P. T. Models of Amyloid Seeding in Alzheimer's disease and scrapie: Mechanistic Truths and Physiological Consequences of the Time-Dependent Solubility of Amyloid Proteins. *Annu. Rev. Biochem.* **66**, 385–407 (1997).

33. Jarrett, J. T. & Lansbury Jr., P. T. Seeding 'one-dimensional crystallization' of amyloid: A pathogenic mechanism in Alzheimer's disease and scrapie? *Cell* **73**, 1055–8 (1993).

34. Soto, C., Estrada, L. & Castilla, J. Amyloids, prions and the inherent infectious nature of

misfolded protein aggregates. *Trends Biochem. Sci.* **31**, 150–155 (2006).

35. Nelson, P. T., Jicha, G. A., Alafuzoff, I., Bigio, E. H., Bouras, C., Kövari, E., Braak, H., Tredici, K. Del, Thal, D. R., Cairns, N. J., Morris, J. C., Castellani, R. J., Crain, B. J., Troncoso, J. C., Davies, P., Duyckaerts, C., Frosch, M. P., Hyman, B. T., Haroutunian, V., *et al.* Correlation of alzheimer disease neuropathologic changes with cognitive status: A review of the literature. *J. Neuropathol. Exp. Neurol.* **71**, 362–381 (2012).

36. Morsch, R., Simon, W. & Coleman, P. D. Neurons May Live for Decades with Neurofibrillary Tangles. *J. Neuropathol. Exp. Neurol.* **58**, 188–197 (1999).

37. Morales, R., Callegari, K. & Soto, C. Prion-like features of misfolded Aβ and tau aggregates. *Virus Res.* **207**, 106–112 (2015).

38. Hall, G. F. & Patuto, B. A. Is tau ready for admission to the prion club? *Prion* **6**, 223–233 (2012).

39. Fernández-Borges, N., Eraña, H., Venegas, V., Elezgarai, S. R., Harrathi, C. & Castilla, J. Animal models for prion-like diseases. *Virus Res.* **207**, 5–24 (2015).

40. Walker, L. C., Diamond, M. I., Duff, K. E. & Hyman, B. T. Mechanisms of protein seeding in neurodegenerative diseases. *JAMA Neurol.* **70**, 304–310 (2013).

41. Hoover, B. R., Reed, M. N., Su, J., Penrod, R. D., Kotilinek, L. A., Grant, M. K., Pitstick, R., Carlson, G. A., Lanier, L. M., Yuan, L. L., Ashe, K. H. & Liao, D. Tau Mislocalization to Dendritic Spines Mediates Synaptic Dysfunction Independently of Neurodegeneration. *Neuron* **68**, 1067–1081 (2010).

42. Frandemiche, M. L., De Seranno, S., Rush, T., Borel, E., Elie, A., Arnal, I., Lante, F. & Buisson, A. Activity-Dependent Tau Protein Translocation to Excitatory Synapse Is

Disrupted by Exposure to Amyloid-Beta Oligomers. *J. Neurosci.* **34**, 6084–6097 (2014).

43. Clavaguera, F., Akatsu, H., Fraser, G., Crowther, R. A., Frank, S., Hench, J., Probst, A., Winkler, D. T., Reichwald, J., Staufenbiel, M., Ghetti, B., Goedert, M. & Tolnay, M. Brain homogenates from human tauopathies induce tau inclusions in mouse brain. *Proc. Natl. Acad. Sci.* **110**, 9535–9540 (2013).

44. Clavaguera, F., Bolmont, T., Crowther, R. A., Abramowski, D., Frank, S., Probst, A., Fraser, G., Stalder, A. K., Beibel, M., Staufenbiel, M., Jucker, M., Goedert, M. & Tolnay, M. Transmission and spreading of tauopathy in transgenic mouse brain. *Nat. Cell Biol.* **11**, 909–913 (2009).

45. Holmes, B. B., Furman, J. L., Mahan, T. E., Yamasaki, T. R., Mirbaha, H., Eades, W. C., Belaygorod, L., Cairns, N. J., Holtzman, D. M. & Diamond, M. I. Proteopathic tau seeding predicts tauopathy in vivo. *Proc. Natl. Acad. Sci.* **111**, E4376–E4385 (2014).

46. Iba, M., Guo, J. L., McBride, J. D., Zhang, B., Trojanowski, J. Q. & Lee, V. M.-Y. Synthetic Tau Fibrils Mediate Transmission of Neurofibrillary Tangles in a Transgenic Mouse Model of Alzheimer's-Like Tauopathy. *J. Neurosci.* **33**, 1024–1037 (2013).

47. Lasagna-Reeves, C. A., Castillo-Carranza, D. L., Sengupta, U., Guerrero-Munoz, M. J., Kiritoshi, T., Neugebauer, V., Jackson, G. R. & Kayed, R. Alzheimer brain-derived tau oligomers propagate pathology from endogenous tau. *Sci. Rep.* **2**, (2012).

48. Peeraer, E., Bottelbergs, A., Van Kolen, K., Stancu, I. C., Vasconcelos, B., Mahieu, M., Duytschaever, H., Ver Donck, L., Torremans, A., Sluydts, E., Van Acker, N., Kemp, J. A., Mercken, M., Brunden, K. R., Trojanowski, J. Q., Dewachter, I., Lee, V. M. Y. & Moechars, D. Intracerebral injection of preformed synthetic tau fibrils initiates widespread tauopathy and neuronal loss in the brains of tau transgenic mice. *Neurobiol.*

Dis. **73**, 83–95 (2015).

49. Stancu, I. C., Vasconcelos, B., Ris, L., Wang, P., Villers, A., Peeraer, E., Buist, A., Terwel, D., Baatsen, P., Oyelami, T., Pierrot, N., Casteels, C., Bormans, G., Kienlen-Campard, P., Octave, J. N., Moechars, D. & Dewachter, I. Templated misfolding of Tau by prion-like seeding along neuronal connections impairs neuronal network function and associated behavioral outcomes in Tau transgenic mice. *Acta Neuropathol.* **129**, 875–894 (2015).

50. Wang, Y., Balaji, V., Kaniyappan, S., Krüger, L., Irsen, S., Tepper, K., Chandupatla, R., Maetzler, W., Schneider, A., Mandelkow, E. & Mandelkow, E. M. The release and trans-synaptic transmission of Tau via exosomes. *Mol. Neurodegener.* **12**, 1–25 (2017).

51. Guo, J. L. & Lee, V. M. Y. Seeding of normal tau by pathological tau conformers drives pathogenesis of Alzheimer-like tangles. *J. Biol. Chem.* **286**, 15317–15331 (2011).

52. Frost, B., Jacks, R. L. & Diamond, M. I. Propagation of Tau misfolding from the outside to the inside of a cell. *J. Biol. Chem.* **284**, 12845–12852 (2009).

53. Falcon, B., Cavallini, A., Angers, R., Glover, S., Murray, T. K., Barnham, L., Jackson, S., O'Neill, M. J., Isaacs, A. M., Hutton, M. L., Szekeres, P. G., Goedert, M. & Bose, S. Conformation determines the seeding potencies of native and recombinant Tau aggregates. *J. Biol. Chem.* **290**, 1049–1065 (2015).

54. Cope, T. E., Rittman, T., Borchert, R. J., Jones, P. S., Vatansever, D., Allinson, K., Passamonti, L., Vazquez Rodriguez, P., Bevan-Jones, W. R., O'Brien, J. T. & Rowe, J. B. Tau burden and the functional connectome in Alzheimer's disease and progressive supranuclear palsy. *Brain* **141**, 550–567 (2018).

55. Zhou, J., Gennatas, E. D., Kramer, J. H., Miller, B. L. & Seeley, W. W. Predicting Regional Neurodegeneration from the Healthy Brain Functional Connectome. *Neuron* **73**, 1216–1227 (2012).

56. Raj, A., Kuceyeski, A. & Weiner, M. A Network Diffusion Model of Disease Progression in Dementia. *Neuron* **73**, 1204–1215 (2012).

57. De Calignon, A., Polydoro, M., Suárez-Calvet, M., William, C., Adamowicz, D. H., Kopeikina, K. J., Pitstick, R., Sahara, N., Ashe, K. H., Carlson, G. A., Spires-Jones, T. L. & Hyman, B. T. Propagation of Tau Pathology in a Model of Early Alzheimer's Disease. *Neuron* **73**, 685–697 (2012).

58. Soto, C. In Vivo Spreading of Tau Pathology. *Neuron* **73**, 621–623 (2012).

59. Liu, L., Drouet, V., Wu, J. W., Witter, M. P., Small, S. A., Clelland, C. & Duff, K. Trans-synaptic spread of tau pathology in vivo. *PLoS One* **7**, 1–9 (2012).

60. Braak H.; Braak E. Neuropathological staging of Alzheimer-related changes. *Acta Neuropathol* **82**, 239–259 (1991).

61. Braak, H. & Del Tredici, K. Where, when, and in what form does sporadic Alzheimer's disease begin? *Curr. Opin. Neurol.* **25**, 708–714 (2012).

62. Moreno-Gonzalez, I. & Soto, C. Misfolded protein aggregates: Mechanisms, structures and potential for disease transmission. *Semin. Cell Dev. Biol.* **22**, 482–487 (2011).

63. Edwards III, G., Moreno-Gonzalez, I. & Soto, C. Amyloid-beta and tau pathology following repetitive mild traumatic brain injury. *Biochem. Biophys. Res. Commun.* **483**, 1137–1142 (2017).

64. Masel, B. E. & DeWitt, D. S. Traumatic Brain Injury: A Disease Process, Not an Event.

J. Neurotrauma **27**, 1529–1540 (2010).

65. Sundman M.H., Hall E.E., C. N. Examining the Relationship between Head Trauma and Neurodegenerative Disease: A Review of Epidemiology, Pathology and Neuroimaging Techniques. *J. Alzheimer's Dis. Park.* **04**, (2014).

66. Edwards III, G. A., Gamez, N., Escobedo Jr., G., Calderon, O. & Moreno-Gonzalez, I. Modifiable Risk Factors for Alzheimer's Disease. *Front. Aging Neurosci.* **11**, 1–18 (2019).

67. Graves AB, White E, Koepsell TD, Reifler BV, van Belle G, Larson EB, Raskind M. The association between head trauma and Alzheimer's disease. *AM J Epidemiol* **131**, 491–501 (1990).

68. Guo, Z., Cupples, L. A., Kurz, A., Auerbach, S. H., Volicer, L., Chui, H., Green, R. C., Sadovnick, D., Duara, R., Decarli, C., Johnson, K., Go, R. C., Growdon, J. H., Jonathan, L., Kukull, W. A. & Farrer, L. A. Head injury and the risk of AD in the MIRAGE study. *Neurology* (2007).

69. Mortimer JA, French LR, Hutton JT, Schuman LM. Head injury as a risk factor for Alzheimer's disease. *Neurology* **35**, 264–267 (1985).

70. Plassman, B. L., Havlik, R. J., Steffens, D. C., Helms, M. J., Newman, T. N., Drosdick, D., Phillips, C., Gau, B. A., Welsh-Bohmer, K. A., Burke, J. R., Guralnik, J. M. & Breitner, J. C. S. Documented head injury in early adulthood and risk of Alzheimer's disease and other dementias. *Neurology* **55**, 1158–1166 (2000).

71. Nordström, A. & Nordström, P. Traumatic brain injury and the risk of dementia diagnosis: A nationwide cohort study. *PLoS Med.* **15**, 1–13 (2018).

72. Ribe, A. R., Vestergaard, M., Christensen, J., Fenger-Grøn, M., Pedersen, H. S., Fann, J. R. & Benros, M. E. Long-term risk of dementia among people with traumatic brain injury in Denmark: a population-based observational cohort study. *The Lancet Psychiatry* **5**, 424–431 (2018).

73. Johnson, V. E., Stewart, W. & Smith, D. H. Widespread tau and amyloid-beta pathology many years after a single traumatic brain injury in humans. *Brain Pathol.* **22**, 142–149 (2012).

74. Johnson, V. E., Stewart, W. & Smith, D. H. Traumatic brain injury and amyloid-beta pathology: a link to Alzheimer's disease? *Nat Rev Neurol.* **11**, 361–370 (2014).

75. Breunig, J. J., Guillot-Sestier, M. V. & Town, T. Brain injury, neuroinflammation and Alzheimer's disease. *Front. Aging Neurosci.* **5**, 1–10 (2013).

76. Blennow, K., Hardy, J. & Zetterberg, H. The Neuropathology and Neurobiology of Traumatic Brain Injury. *Neuron* **76**, 886–899 (2012).

77. Blennow, K., Brody, D. L., Kochanek, P. M., Levin, H., McKee, A., Ribbers, G. M., Yaffe, K. & Zetterberg, H. Traumatic brain injuries. *Nat. Rev. Dis. Prim.* **2**, 1–19 (2016).

78. Walker, K. R. & Tesco, G. Molecular mechanisms of cognitive dysfunction following traumatic brain injury. *Front. Aging Neurosci.* **5**, 1–25 (2013).

79. Mez, J., Daneshvar, D. H., Kiernan, P. T., Abdolmohammadi, B., Alvarez, V. E., Huber, B. R., Alosco, M. L., Solomon, T. M., Nowinski, C. J., McHale, L., Cormier, K. A., Kubilus, C. A., Martin, B. M., Murphy, L., Baugh, C. M., Montenigro, P. H., Chaisson, C. E., Tripodis, Y., Kowall, N. W., *et al.* Clinicopathological evaluation of chronic traumatic encephalopathy in players of American football. *JAMA - J. Am. Med. Assoc.*

318, 360–370 (2017).

80. Saulle, M. & Greenwald, B. D. Chronic Traumatic Encephalopathy: A Review. *Rehabil. Res. Pract.* **2012**, 1–9 (2012).

81. Shenton, M. E., Baugh, C. M., Gavett, B. E., Riley, D. O., Stern, R. A., McKee, A. C., Stamm, J. M., Cantu, R. C., Lin, A. & Nowinski, C. J. Chronic traumatic encephalopathy: neurodegeneration following repetitive concussive and subconcussive brain trauma. *Brain Imaging Behav.* **6**, 244–254 (2012).

82. Smith, C., Graham, D. I., Murray, L. S. & Nicoll, J. A. R. Tau immunohistochemistry in acute brain injury. *Neuropathol. Appl. Neurobiol.* **29**, 496–502 (2003).

83. Zemlan, F. P., Rosenberg, W. S., Luebbe, P. A., Campbell, T. A., Dean, G. E., Weiner, N. E., Cohen, J. A., Rudick, R. A. & Woo, D. Quantification of axonal damage in traumatic brain injury: Affinity purification and characterization of cerebrospinal fluid tau proteins. *J. Neurochem.* **72**, 741–750 (1999).

84. McKee, A. C., Gavett, B. E., Budson, A. E., Santini, V. E., Lee, H.-S., Kubilus, C. A., Stern, R. A., Cantu, R. C., Nowinski, C. J. & Hedley-Whyte, E. T. Chronic traumatic encephalopathy in athletes: Progressive tauopathy after repetitive head injury. *J. Neuropathol. Exp. Neurol.* **68**, 709–735 (2009).

85. Roberts, G. W., Lynch, A., Gentleman, S. M., Landon, M., Graham, D. I. & Murray, L. Beta amyloid protein deposition in the brain after severe head injury: implications for the pathogenesis of Alzheimer's disease. *J. Neurol. Neurosurg. Psychiatry* **57**, 419–425 (1994).

86. Roberts, G. W., Gentleman, S. M., Lynch, A. & Graham, D. I. βA4 amyloid protein

deposition in brain after head trauma. *Lancet* **338**, 1422–1423 (1991).

87. Stein, T. D., Montenigro, P. H., Alvarez, V. E., Xia, W., Crary, J. F., Tripodis, Y., Daneshvar, D. H., Mez, J., Solomon, T., Meng, G., Kubilus, C. A., Cormier, K. A., Meng, S., Babcock, K., Kiernan, P., Murphy, L., Nowinski, C. J., Martin, B., Dixon, D., *et al.* Beta-amyloid deposition in chronic traumatic encephalopathy. *Acta Neuropathol.* **130**, 21–34 (2015).

88. Tokuda, T., Ikeda, S., Yanagisawa, N., Ihara, Y. & Glenner, G. G. Re-examination of ex-boxers' brains using immunohistochemistry with antibodies to amyloid β-protein and tau protein. *Acta Neuropathol.* **82**, 280–285 (1991).

89. McKee, A. C., Stein, T. D., Nowinski, C. J., Stern, R. A., Daneshvar, D. H., Alvarez, V. E., Lee, H. S., Hall, G., Wojtowicz, S. M., Baugh, C. M., Riley, D. O., Kubilus, C. A., Cormier, K. A., Jacobs, M. A., Martin, B. R., Abraham, C. R., Ikezu, T., Reichard, R. R., Wolozin, B. L., *et al.* The spectrum of disease in chronic traumatic encephalopathy. *Brain* **136**, 43–64 (2013).

90. Center for Disease Control and Prevention. MMWR Morb. Mortal. Wkly. Rep. *Sports-related recurrent brain injuries*. (1997).

91. Sports Legacy Institute. "Hit Count™" White Paper. *Sports Legacy Institute* (2012).

92. Pellman, E. I., Powell, J. W., Viano, D. C., Casson, I. R., Tucker, A. M., Feuer, H., Lovell, M., Waeckerle, J. F., Robertson, D. W., Kelly, D. F., Maroon, J. C., Valadka, A. B., Ozgur, B., Levy, M. L. & Bailes, J. E. Concussion in Professional Football: Epidemiological Features of Game Injuries and Review of the Literature - Part 3. *Neurosurgery* **54**, 81–96 (2004).

93. Lehman, E. J. Epidemiology of neurodegeneration in American-style professional football players. *Alzheimer's Res. Ther.* **5**, (2013).

94. Stern, R. A., Riley, D. O., Daneshvar, D. H., Nowinski, C. J., Cantu, R. C. & McKee, A. C. Long-term Consequences of Repetitive Brain Trauma: Chronic Traumatic Encephalopathy. *PM R* **3**, S460–S467 (2011).

95. Breedlove, E. L., Robinson, M., Talavage, T. M., Morigaki, K. E., Yoruk, U., O'Keefe, K., King, J., Leverenz, L. J., Gilger, J. W. & Nauman, E. A. Biomechanical correlates of symptomatic and asymptomatic neurophysiological impairment in high school football. *J. Biomech.* **45**, 1265–1272 (2012).

96. Kriegel, Joshua Papadopoulos, Zachary McKee, A. C. Chronic Traumatic Encephalopathy: Is Latency in Symptom Onset Explained by Tau Propagation? *Cold Spring Harb. Perspect. Med.* **8**, (2018).

97. Lin, G. G. & Scott, J. G. Prion-like Mechanisms in Neurodegenerative Diseases. *Nat Rev Neurosci* **11**, 155–159 (2012).

98. Holmes, B. B. & Diamond, M. I. Prion-like properties of Tau protein the importance of extracellular tau as therapeutic target. *J. Biol. Chem.* **289**, 19855–19861 (2014).

99. Frost, B. & Diamond, M. I. The expanding realm of prion phenomena in neurodegenerative disease. *Prion* **3**, 74–77 (2009).

100. Iba, M., McBride, J. D., Guo, J. L., Zhang, B., Trojanowski, J. Q. & Lee, V. M. Y. Tau pathology spread in PS19 tau transgenic mice following locus coeruleus (LC) injections of synthetic tau fibrils is determined by the LC's afferent and efferent connections. *Acta Neuropathol.* **130**, 349–362 (2015).

101. Ahmed, Z., Cooper, J., Murray, T. K., Garn, K., McNaughton, E., Clarke, H., Parhizkar, S., Ward, M. A., Cavallini, A., Jackson, S., Bose, S., Clavaguera, F., Tolnay, M., Lavenir, I., Goedert, M., Hutton, M. L. & O'Neill, M. J. A novel in vivo model of tau propagation with rapid and progressive neurofibrillary tangle pathology: The pattern of spread is determined by connectivity, not proximity. *Acta Neuropathol.* **127**, 667–683 (2014).

102. Smith, D. H., Uryu, K., Saatman, K. E., Trojanowski, J. Q. & McIntosh, T. K. Protein Accumulation in Traumatic Brain Injury. *NeuroMolecular Med.* **4**, 59–72 (2003).

103. Tran, H. T., Sanchez, L., Esparza, T. J. & Brody, D. L. Distinct temporal and anatomical distributions of amyloid-β and tau abnormalities following controlled cortical impact in transgenic mice. *PLoS One* **6**, (2011).

104. Hoshino, S., Tamaoka, A., Takahashi, M., Kobayashi, S., Furukawa, T., Oaki, Y., Mori, O., Matsuno, S., Shoji, S., Inomata, M. & Teramoto, A. Emergence of immunoreactivities for phosphorylated tau and amyloid-β protein in chronic stage of fluid percussion injury in rat brain. *Neuroreport* **9**, 1879–1883 (1998).

105. Lv, Q., Lan, W., Sun, W., Ye, R., Fan, X., Ma, M., Yin, Q., Jiang, Y., Xu, G., Dai, J., Guo, R. & Liu, X. Intranasal nerve growth factor attenuates tau phosphorylation in brain after traumatic brain injury in rats. *J. Neurol. Sci.* **345**, 48–55 (2014).

106. Goldstein, L., Fisher, A., Tagge, C., Zhang, X.-L., Velisek, L., Sullivan, J., Upreti, C., Kracht, J., Ericsson, M., Wojnarowicz, M., Goletiani, C., Maglakelidze, G., Casey, N., Moncaster, J., Minaeva, O., Cormier, K., Kubilus, C., Moir, R., Nowinski, C., *et al.* Chronic traumatic encephalopathy (CTE) in blast-exposed U.S. military veterans and a new blast neurotrauma mouse model. *Alzheimer's Dement.* **8**, P212–P213 (2012).

107. Sawmiller, D., Li, S., Shahaduzzaman, M., Smith, A., Obregon, D., Giunta, B.,

Borlongan, C., Sanberg, P. & Tan, J. Luteolin Reduces Alzheimer's Disease Pathologies Induced by Traumatic Brain Injury. *Int. J. Mol. Sci.* **15**, 895–904 (2014).

108. Tran, H. T., LaFerla, F. M., Holtzman, D. M. & Brody, D. L. Controlled Cortical Impact Traumatic Brain Injury in 3xTg-AD Mice Causes Acute Intra-Axonal Amyloid- Accumulation and Independently Accelerates the Development of Tau Abnormalities. *J. Neurosci.* **31**, 9513–9525 (2011).

109. Jankowsky, J. L. & Zheng, H. Practical considerations for choosing a mouse model of Alzheimer's disease. *Mol. Neurodegener.* **12**, 1–22 (2017).

110. Yoshiyama, Y., Higuchi, M., Zhang, B., Huang, S. M., Iwata, N., Saido, T. C. C., Maeda, J., Suhara, T., Trojanowski, J. Q. & Lee, V. M. Y. Synapse Loss and Microglial Activation Precede Tangles in a P301S Tauopathy Mouse Model. *Neuron* **53**, 337–351 (2007).

111. Furman, J. L., Vaquer-Alicea, J., White, C. L., Cairns, N. J., Nelson, P. T. & Diamond, M. I. Widespread tau seeding activity at early Braak stages. *Acta Neuropathol.* **133**, 91–100 (2017).

112. Brendel, M., Jaworska, A., Probst, F., Overhoff, F., Korzhova, V., Lindner, S., Carlsen, J., Bartenstein, P., Harada, R., Kudo, Y., Haass, C., Van Leuven, F., Okamura, N., Herms, J. & Rominger, A. Small-Animal PET Imaging of Tau Pathology with 18F-THK5117 in 2 Transgenic Mouse Models. *J. Nucl. Med.* **57**, 792–798 (2016).

113. Soto, C. Transmissible proteins: Expanding the prion heresy. *Cell* **149**, 968–977 (2012).

114. Walker, L. C. Proteopathic Strains and the Heterogeneity of Neurodegenerative Diseases. *Annu. Rev. Genet.* **50**, 329–346 (2016).

115. Kaufman, S. K., Sanders, D. W., Thomas, T. L., Ruchinskas, A. J., Vaquer-Alicea, J., Sharma, A. M., Miller, T. M. & Diamond, M. I. Tau Prion Strains Dictate Patterns of Cell Pathology, Progression Rate, and Regional Vulnerability In Vivo. *Neuron* **92**, 796–812 (2016).

116. Daneshvar, D. H., Nowinski, C. J., Mckee, A. C. & Cantu, R. C. The Epidemiology of Sport-Related Concussion. *Clin. Sports Med.* **30**, 1–17 (2011).

117. Stewart, G. W., Mcqueen-borden, E., Bell, R. A., Barr, T. & Juengling, J. Clinical Commentary Comprehensive Assessment and Management of Athletes With Sport Concussion Corresponding Author. *Int. J. Sports Phys. Ther.* **7**, 433–447 (2012).

118. Morales, R., Bravo-Alegria, J., Duran-Aniotz, C. & Soto, C. Titration of biologically active amyloid-β seeds in a transgenic mouse model of Alzheimer's disease. *Sci. Rep.* **5**, 1–8 (2015).

119. Chabrier, M. A., Cheng, D., Castello, N. A., Green, K. N. & LaFerla, F. M. Synergistic effects of amyloid-beta and wild-type human tau on dendritic spine loss in a floxed double transgenic model of Alzheimer's disease. *Neurobiol. Dis.* **64**, 107–117 (2014).

120. Braak, H. & Tredici, K. Del. Spreading of tau pathology in sporadic Alzheimer's disease along cortico-cortical top-down connections. *Cereb. Cortex* **28**, 3372–3384 (2018).

121. Milenkovic, I. & Kovacs, G. G. Incidental corticobasal degeneration in a 76-year old woman. *Clin. Neuropathol.* **32**, 69–72 (2013).

122. Ferrer, I., López-González, I., Carmona, M., Arregui, L., Dalfó, E., Torrejón-Escribano, B., Diehl, R. & Kovacs, G. G. Glial and neuronal tau pathology in tauopathies: Characterization of disease-specific phenotypes and tau pathology progression. *J.*

Neuropathol. Exp. Neurol. **73**, 81–97 (2014).

123. Chin, S.-M. & Goldman, J. Glial Inclusions in CNS Degenerative Diseases. *J. Neuropathol. Exp. Neurol.* **55**, 499–508 (1996).

124. Dickson, D. W., Bergeron, C., Chin, S. S., Duyckaerts, C., Horoupian, D., Ikeda, K., Jellinger, K., Lantos, P. L., Lippa, C. F., Mirra, S. S., Tabaton, M., Vonsattel, J. P., Wakabayashi, K. & Litvan, I. Office of rare diseases neuropathologic criteria for corticobasal degeneration. *J. Neuropathol. Exp. Neurol.* **61**, 935–946 (2002).

125. Higuchi, M., Ishihara, T., Zhang, B., Hong, M., Andreadis, A., Trojanowski, J. Q. & Lee, V. M. Y. Transgenic mouse model of tauopathies with glial pathology and nervous system degeneration. *Neuron* **35**, 433–446 (2002).

126. Viano, D. C., Hamberger, A., Bolouri, H. & Säljö, A. Concussion in professional football: Animal model of brain injury - Part 15. *Neurosurgery* **64**, 1162–1173 (2009).

127. Cantu, R. C. Head injuries in sport. *Br. J. Sports Med.* **30**, 289–296 (1996).

128. Guthkelch, A. N. Post-traumatic amnesia, post-concussional symptoms, and accident neurosis. *Acta Neurochir Suppl* **28**, 120–123 (1979).

129. Lovell, M. R., Collins, M. W., Iverson, G. L., Field, M., Maroon, J. C., Cantu, R., Podell, K., Powell, J. W., Belza, M. & Fu, F. H. Recovery from mild concussion in high school athletes. *J Neurosurg* **98**, 296–301 (2003).

130. Aguzzi, A., Sigurdson, C. & M., H. Molecular mechanisms of prion pathogenesis. *Annu. Rev. Pathol. Mech.* **3**, 11–40 (2008).

131. Privat, N., Levavasseur, E., Yildirim, S., Hannaoui, S., Brandel, J. P., Laplanche, J. L., Béringue, V., Seilhean, D. & Haïk, S. Region-specific protein misfolding cyclic

amplification reproduces brain tropism of prion strains. *J. Biol. Chem.* **292**, 16688–16696 (2017).

132. Hu, P. P., Morales, R., Duran-Aniotz, C., Moreno-Gonzalez, I., Khan, U. & Soto, C. Role of prion replication in the strain-dependent brain regional distribution of prions. *J. Biol. Chem.* **291**, 12880–12887 (2016).

133. Vidal, E., Márquez, M., Tortosa, R., Costa, C., Serafín, A. & Pumarola, M. Immunohistochemical approach to the pathogenesis of bovine spongiform encephalopathy in its early stages. *J. Virol. Methods* **134**, 15–29 (2006).

134. Kovacs, G. G., Makarava, N., Savtchenko, R. & Baskakov, I. V. Atypical and classical forms of the disease-associated state of the prion protein exhibit distinct neuronal tropism, deposition patterns, and lesion profiles. *Am. J. Pathol.* **183**, 1539–1547 (2013).

135. Hladky S.B.; Barrand M.A. Mechanisms of fluid movement into, through and out of the brain: evaluation of the evidence. *Fluids Barriers CNS* **11**, 26 (2014).

136. Hansson, O., Zetterberg, H., Buchhave, P., Londos, E., Blennow, K. & Minthon, L. Association between CSF biomarkers and incipient Alzheimer's disease in patients with mild cognitive impairment: A follow-up study. *Lancet Neurol.* **5**, 228–234 (2006).

137. Counts, S. E., Ikonomovic, M. D., Mercado, N., Vega, I. E. & Mufson, E. J. Biomarkers for the Early Detection and Progression of Alzheimer's Disease. *Neurotherapeutics* **14**, 35–53 (2017).

138. Fagan, A. M., Roe, C. M., Xiong, C., Mintun, M. A., Morris, J. C. & Holtzman, D. M. Cerebrospinal fluid tau/β-amyloid42 ratio as a prediction of cognitive decline in nondemented older adults. *Arch. Neurol.* **64**, 343–349 (2007).

139. Li, G., Sokal, I., Quinn, J. F., Leverenz, J. B., Brodey, M., Schellenberg, G. D., Kaye, J. A., Raskind, M. A., Zhang, J., Peskind, E. R. & Montine, T. J. CSF tau/Abeta42 ratio for increased risk of mild cognitive impairment. *Neurology* **69**, 631–639 (2007).

140. Dubois, B., Feldman, H. H., Jacova, C., Hampel, H., Molinuevo, J. L., Blennow, K., Dekosky, S. T., Gauthier, S., Selkoe, D., Bateman, R., Cappa, S., Crutch, S., Engelborghs, S., Frisoni, G. B., Fox, N. C., Galasko, D., Habert, M. O., Jicha, G. A., Nordberg, A., *et al.* Advancing research diagnostic criteria for Alzheimer's disease: The IWG-2 criteria. *Lancet Neurol.* **13**, 614–629 (2014).

141. McKhann, G. M., Knopman, D. S., Chertkow, H., Hyman, B. T., Jack, C. R., Kawas, C. H., Klunk, W. E., Koroshetz, W. J., Manly, J. J., Mayeux, R., Mohs, R. C., Morris, J. C., Rossor, M. N., Scheltens, P., Carrillo, M. C., Thies, B., Weintraub, S. & Phelps, C. H. The diagnosis of dementia due to Alzheimer's disease: Recommendations from the National Institute on Aging-Alzheimer's Association workgroups on diagnostic guidelines for Alzheimer's disease. *Alzheimer's Dement.* **7**, 263–269 (2011).

142. Molinuevo, J. L., Ayton, S., Batrla, R., Bednar, M. M., Bittner, T., Cummings, J., Fagan, A. M., Hampel, H., Mielke, M. M., Mikulskis, A., O'Bryant, S., Scheltens, P., Sevigny, J., Shaw, L. M., Soares, H. D., Tong, G., Trojanowski, J. Q., Zetterberg, H. & Blennow, K. *Current state of Alzheimer's fluid biomarkers*. *Acta Neuropathologica* **136**, (Springer Berlin Heidelberg, 2018).

143. Mattsson, N., Ewers, M., Rich, K., Kaiser, E., Mulugeta, E. & Rose, E. CSF Biomarkers and Incipient Alzheimer Disease. *JAMA* **302**, 385–393 (2009).

144. Goedert, M., Falcon, B., Clavaguera, F. & Tolnay, M. Prion-like mechanisms in the pathogenesis of tauopathies and synucleinopathies. *Curr. Neurol. Neurosci. Rep.* **14**, 1–

11 (2014).

145. Kwon, S., Moreno-Gonzalez, Ines Taylor-Presse, Kathleen Edwards III, George Gamez, N., Calderon, O., Zhu, B., Velasquez, Fred Christian Soto, C. & Sevick-Muraca, E. M. Impaired Peripheral Lymphatic Function and Cerebrospinal Fluid Outflow in a Mouse Model of Alzheimer's disease. *J. Alzheimer's Dis.* **69**, 585–595 (2019).

146. Iliff, J. J., Wang, M., Liao, Y., Plogg, B. A., Peng, W., Gundersen, G. A., Benveniste, H., Vates, G. E., Deane, R., Goldman, S. A., Nagelhus, E. A. & Nedergaard, M. A paravascular pathway facilitates CSF flow through the brain parenchyma and the clearance of interstitial solutes, including amyloid β. *Sci. Transl. Med.* **4**, 1–13 (2012).

147. Tarasoff-Conway, J. M., Carare, R. O., Osorio, R. S., Glodzik, L., Butler, T., Fieremans, E., Axel, L., Rusinek, H., Nicholson, C., Zlokovic, B. V., Frangione, B., Blennow, K., Ménard, J., Zetterberg, H., Wisniewski, T. & De Leon, M. J. Clearance systems in the brain - Implications for Alzheimer disease. *Nat. Rev. Neurol.* **11**, 457–470 (2015).

148. Iliff, J. J., Chen, M. J., Plog, B. A., Zeppenfeld, D. M., Soltero, M., Yang, L., Singh, I., Deane, R. & Nedergaard, M. Impairment of glymphatic pathway function promotes tau pathology after traumatic brain injury. *J. Neurosci.* **34**, 16180–16193 (2014).

149. Turner, R. C., Naser, Z. J., Bailes, J. E., Smith, D. W., Fischer, J. A. & Rosen, C. L. Effect of slosh mitigation on histologic markers of traumatic brain injury. *J. Neurosurg.* **117**, 1110–1118 (2012).

150. Farah, G., Siwek, D. & Cummings, P. Tau accumulations in the brains of woodpeckers. *PLoS One* **13**, 1–11 (2018).

151. May, P. R., Fuster, J. M., Newman, P. & A., H. Woodpeckers and head injury. *Lancet* **1**,

1347–8 (1976).

152. Holth, J. K., Fritschi, S. K., Wang, C., Pedersen, N. P., Cirrito, J. R., Mahan, T. E., Finn, M. B., Manis, M., Geerling, J. C., Fuller, P. M., Lucey, B. P. & Holtzman, D. M. The sleep-wake cycle regulates brain interstitial fluid tau in mice and CSF tau in humans. *Science (80-.).* **363**, 880–884 (2019).

153. Monti, G., Tondelli, M., Giovannini, G., Bedin, R., Nichelli, P. F., Trenti, T., Meletti, S. & Chiari, A. Cerebrospinal fluid tau proteins in status epilepticus. *Epilepsy Behav.* **49**, 150–154 (2015).

154. Uryu, K., Chen, X. H., Martinez, D., Browne, K. D., Johnson, V. E., Graham, D. I., Lee, V. M. Y., Trojanowski, J. Q. & Smith, D. H. Multiple proteins implicated in neurodegenerative diseases accumulate in axons after brain trauma in humans. *Exp. Neurol.* **208**, 185–192 (2007).

155. Grady, S. M., McLaughlin, M. R., Christman, C. W., Valadka, A. B., Fligner, C. L. & Povlishock, J. T. The Use of Antibodies Targeted Against the Neurofilament Subunits for the Detection of Diffuse Axonal Injury in Humans. *J. Neuropathol. Exp. Neurol.* **52**, 143–152 (1993).

156. Christman, C. W., Grady, S. M., Walker, S. A., Holloway, K. L. & Povlishock, J. T. Ultrastructural Studies of Diffuse Axonal Injury in Humans. *J. Neurotrauma* **11**, 173–186 (1994).

157. Tang-Schomer, M. D., Johnson, V. E., Baas, P. W., Stewart, W. & Smith, D. H. Partial interruption of axonal transport due to microtubule breakage accounts for the formation of periodic varicosities after traumatic axonal injury. *Exp. Neurol.* **233**, 364–372 (2012).

158. Gorrie, C., Oakes, S., Duflou, J., Blumbergs, P. & Waite, P. M. E. Axonal injury in children after motor vehicle crashes: Extent, distribution, and size of axonal swellings using β-APP immunohistochemistry. *J. Neurotrauma* **19**, 1171–1182 (2002).

159. Iwata, A., Chen, X. H., McIntosh, T. K., Browne, K. D. & Smith, D. H. Long-term accumulation of amyloid-β in axons following brain trauma without persistent upregulation of amyloid precursor protein genes. *J. Neuropathol. Exp. Neurol.* **61**, 1056–1068 (2002).

160. Ikonomovic, M. D., Uryu, K., Abrahamson, E. E., Ciallella, J. R., Trojanowski, J. Q., Lee, V. M. Y., Clark, R. S., Marion, D. W., Wisniewski, S. R. & DeKosky, S. T. Alzheimer's pathology in human temporal cortex surgically excised after severe brain injury. *Exp. Neurol.* **190**, 192–203 (2004).

161. Smith, D. H., Nonaka, M., Miller, R., Leoni, M., Chen, X. H., Alsop, D. & Meaney, D. F. Immediate coma following inertial brain injury dependent on axonal damage in the brainstem. *J. Neurosurg.* **93**, 315–322 (2000).

162. Gennarelli, T., Thibault, L., Adams, J., Graham, D., Thompson, C. & Marcincin, R. Diffuse axonal injury and traumatic coma in the primate. *Ann. Neurol.* **12**, 564–74 (1982).

163. Montgomery, K. S., Simmons, R. K., Edwards, G., Nicolle, M. M., Gluck, M. A., Myers, C. E. & Bizon, J. L. Novel age-dependent learning deficits in a mouse model of Alzheimer's disease: Implications for translational research. *Neurobiol. Aging* **32**, 1273–1285 (2011).

164. Montgomery, K. S., Edwards, G., Levites, Y., Kumar, A., Myers, C. E., Gluck, M. A., Setlow, B. & Bizon, J. L. Deficits in hippocampal-dependent transfer generalization

learning accompany synaptic dysfunction in a mouse model of amyloidosis. *Hippocampus* **26**, 455–471 (2016).

165. Barnes, C. Memory deficits associated with senescence: a neurophysiological and behavioral study in the rat. *J Comp Physiol Psychol.* **93**, 74–104 (1979).

166. Squire, L. R. & Zola-Morgan, S. The medial temporal lobe memory system. *Science (80-.).* **253**, 1380–1386 (1991).

167. Eichenbaum, H. What H.M. taught us. *J Cogn Neurosci.* **25**, 14–21 (2013).

168. Izquierdo, A., Brigman, J. L., Radke, A. K., Rudebeck, P. H. & Holmes, A. The neural basis of reversal learning: An updated perspective. *Neuroscience* **345**, 12–26 (2017).

169. Gómez-Isla, T., Hollister, R., West, H., Mui, S., Growdon, J. H., Petersen, R. C., Parisi, J. E. & Hyman, B. T. Neuronal loss correlates with but exceeds neurofibrillary tangles in Alzheimer's disease. *Ann Neurol.* **41**, 17–24 (1997).

170. Giacobini, E. & Gold, G. Alzheimer disease therapy - Moving from amyloid-β to tau. *Nat. Rev. Neurol.* **9**, 677–686 (2013).

171. Wagner, J., Krauss, S., Shi, S., Ryazanov, S., Steffen, J., Miklitz, C., Leonov, A., Kleinknecht, A., Göricke, B., Weishaupt, J. H., Weckbecker, D., Reiner, A. M., Zinth, W., Levin, J., Ehninger, D., Remy, S., Kretzschmar, H. A., Griesinger, C., Giese, A., *et al.* Reducing tau aggregates with anle138b delays disease progression in a mouse model of tauopathies. *Acta Neuropathol.* **130**, 619–631 (2015).

172. DeVos, S. L., Miller, R. L., Schoch, K. M., Holmes, B. B., Kebodeaux, C. S., Wegener, A. J., Chen, G., Shen, T., Tran, H., Nichols, B., Zanardi, T. A., Kordasiewicz, H. B., Swayze, E. E., Bennett, C. F., Diamond, M. I. & Miller, T. M. Tau reduction prevents

neuronal loss and reverses pathological tau deposition and seeding in mice with tauopathy. *Sci. Transl. Med.* **9**, (2017).

173. Cheng, J. S., Craft, R., Yu, G. Q., Ho, K., Wang, X., Mohan, G., Mangnitsky, S., Ponnusamy, R. & Mucke, L. Tau reduction diminishes spatial learning and memory deficits after mild repetitive traumatic brain injury in mice. *PLoS One* **9**, 1–17 (2014).

174. Menkes-Caspi, N., Yamin, H. G., Kellner, V., Spires-Jones, T. L., Cohen, D. & Stern, E. A. Pathological tau disrupts ongoing network activity. *Neuron* **85**, 959–966 (2015).

175. Wu, J. W., Hussaini, S. A., Bastille, I. M., Rodriguez, Gustavo A Mrejeru, A., Rilett, K., Sanders, D. W., Cook, C., Fu, H., Boonen, R. A. C. M., Herman, Mathieu Nahmani, E., Emrani, S., Figueroa, Y Helen Diamond, M. I., Clelland, Catherine L Wray, S. & Duff, K. E. Neuronal activity enhances tau propagation and tau pathology in vivo. *Nat. Neurosci.* **19**, 1085–1092 (2016).

176. Khan, U. A., Liu, L., Provenzano, F. A., Berman, D. E., Profaci, C. P., Sloan, R., Mayeux, R., Duff, K. E. & Small, S. A. Molecular drivers and cortical spread of lateral entorhinal cortex dysfunction in preclinical Alzheimer's disease. *Nat. Neurosci.* **17**, 304–311 (2013).

177. Roberson, E. D., Halabisky, B., Yoo, J. W., Yao, J., Chin, J., Yan, F., Wu, T., Hamto, P., Devidze, N., Yu, G.-Q., Palop, J. J., Noebels, J. L. & Mucke, L. Amyloid- /Fyn-Induced Synaptic, Network, and Cognitive Impairments Depend on Tau Levels in Multiple Mouse Models of Alzheimer's Disease. *J. Neurosci.* **31**, 700–711 (2011).

178. Mucke, L. & Selkoe, D. J. Neurotoxicity of amyloid β-protein: Synaptic and network dysfunction. *Cold Spring Harb. Perspect. Med.* **2**, 1–17 (2012).

179. Shipton, O. A., Leitz, J. R., Dworzak, J., Acton, C. E. J., Tunbridge, E. M., Denk, F., Dawson, H. N., Vitek, M. P., Wade-Martins, R., Paulsen, O. & Vargas-Caballero, M. Tau Protein Is Required for Amyloid -Induced Impairment of Hippocampal Long-Term Potentiation. *J. Neurosci.* **31**, 1688–1692 (2011).

180. Yan, X. X., Cai, Y., Shelton, J., Deng, S. H., Luo, X. G., Oddo, S., LaFerla, F. M., Cai, H., Rose, G. M. & Patrylo, P. R. Chronic Temporal Lobe Epilepsy Is Associated with Enhanced Alzheimer-Like Neuropathology in 3×Tg-AD Mice. *PLoS One* **7**, 1–13 (2012).

181. Das, M., Maeda, S., Hu, B., Yu, G. Q., Guo, W., Lopez, I., Yu, X., Tai, C., Wang, X. & Mucke, L. Neuronal levels and sequence of tau modulate the power of brain rhythms. *Neurobiol. Dis.* **117**, 181–188 (2018).

182. Walsh, D. M. & Selkoe, D. J. A critical appraisal of the pathogenic protein spread hypothesis of neurodegeneration. *Nat. Rev. Neurosci.* **17**, 251–260 (2016).

183. Surmeier, D. J., Obeso, J. A. & Halliday, G. M. Selective neuronal vulnerability in Parkinson's disease. *Nat Rev Neurosci* **18**, 101–113 (2017).

184. Cuanalo-Contreras, K., Park, K. W., Mukherjee, A., Millán-Pérez Peña, L. & Soto, C. Delaying aging in Caenorhabditis elegans with protein aggregation inhibitors. *Biochem. Biophys. Res. Commun.* **482**, 62–67 (2017).

185. David, D. C., Ollikainen, N., Trinidad, J. C., Cary, M. P., Burlingame, A. L. & Kenyon, C. Widespread protein aggregation as an inherent part of aging in C. elegans. *PLoS Biol.* **8**, 47–48 (2010).

186. Wegmann, S., Bennett, R. E., Delorme, L., Robbins, A. B., Hu, M., McKenzie, D., Kirk, M. J., Schiantarelli, J., Tunio, N., Amaral, A. C., Fan, Z., Nicholls, S., Hudry, E. &

Hyman, B. T. Experimental evidence for the age dependence of tau protein spread in the brain. *Sci. Adv.* **5**, (2019).

187. Falcon, B., Zivanov, J., Zhang, W., Murzin, A. G., Garringer, H. J., Vidal, R., Crowther, R. A., Newell, K. L., Ghetti, B., Goedert, M. & Scheres, S. H. W. Novel tau filament fold in chronic traumatic encephalopathy encloses hydrophobic molecules. *Nature* **568**, 420–423 (2019).

188. Falcon, B., Zhang, W., Murzin, A. G., Murshudov, G., Garringer, H. J., Vidal, R., Crowther, R. A., Ghetti, B., Scheres, S. H. W. & Goedert, M. Structures of filaments from Pick's disease reveal a novel tau protein fold. *Nature* **561**, 137–140 (2018).

189. Goedert, M., Falcon, B., Zhang, W., Ghetti, B. & Scheres, S. H. W. Distinct Conformers of Assembled Tau in Alzheimer's and Pick's Diseases. *Cold Spring Harb. Symp. Quant. Biol.* **LXXXIII**, 037580 (2019).

190. Baker, H. F., Ridley, R. M., Duchen, L. W., Crow, T. J. & Bruton, C. J. Induction of beta (A4)-amyloid in primates by injection of Alzheimer's disease brain homogenate. Comparison with transmission of spongiform encephalopathy. *Mol Neurobiol.* **8**, 25–39 (1994).

191. Meyer-Luehmann, M., Coomaraswamy, J., Bolmont, T., Kaeser, S., Schaefer, C., Kilger, E., Neuenschwander, A., Abramowski, D., Frey, P., Jaton, A. L., Vigouret, J. M., Paganetti, P., Walsh, D. M., Mathews, P. M., Ghiso, J., Staufenbiel, M., Walker, L. C. & Jucker, M. Exogenous induction of cerebral β-amyloidogenesis is governed by agent and host. *Science (80-.).* **313**, 1781–1784 (2006).

192. Braak, H. & Del Tredici, K. Spreading of Tau Pathology in Sporadic Alzheimer's Disease Along Cortico-cortical Top-Down Connections. *Cereb. Cortex2* **28**, 3372–3384

(2018).

193. Necula, M., Kayed, R., Milton, S. & Glabe, C. G. Small molecule inhibitors of aggregation indicate that amyloid beta oligomerization and fibrillization pathways are independent and distinct. *J. Biol. Chem.* **282**, 10311–10324 (2007).

194. Cowan, C. M., Quraishe, S., Hands, S., Sealey, M., Mahajan, S., Allan, D. W. & Mudher, A. Rescue from tau-induced neuronal dysfunction produces insoluble tau oligomers. *Sci. Rep.* **5**, doi: 10.1038/srep17191. (2015).

195. Chiti, F., Webster, P., Taddei, N., Clark, A., Stefani, M., Ramponi, G. & Dobson, C. M. Designing conditions for in vitro formation of amyloid protofilaments and fibrils. *Proc Natl Acad Sci U S A.* **96**, 3590–3594 (1999).

196. Chin, S.-M. & Goldman, J. E. Glial Inclusions in CNS Degenerative Diseases. *J. Neuropathol. Exp. Neurol.* **55**, 499–508 (1996).

197. Ferrer, I., Santpere, G. & van Leeuwen, F. W. Argyrophilic grain disease. *Brain* **131**, 1416–1432 (2008).

198. Wakabayashi, K., Oyanagi, K., Makifuchi, T., Ikuta, F., Homma, A., Homma, Y., Horikawa, Y. & Tokiguchi, S. Corticobasal degeneration: etiopathological significance of the cytoskeletal alterations. *Acta Neuropathol.* **87**, 545–553 (1994).

199. Abe, H., Yagishita, S., Amano, N., Iwabuchi, K., Hasegawa, K. & Kowa, K. Argyrophilic glial intracytoplasmic inclusions in multiple system atrophy: immunocytochemical and ultrastructural study. *Acta Neuropathol.* **84**, 273–277 (1992).

200. Ikeda, K., Akiyama, H., Kondo, H. & Haga, C. A study of dementia with argyrophilic grains. Possible cytoskeletal abnormality in dendrospinal portion of neurons and

oligodendroglia. *Acta Neuropathol.* **89**, 409–414 (1995).

201. Yamada, T. & McGeer, P. L. Oligodendroglial microtubular masses: an abnormality observed in some human neurodegenerative diseases. *Neurosci. Lett.* **120**, 163–166 (1990).

202. Narasimhan, S., Guo, J. L., Changolkar, L., Stieber, A., McBride, J. D., Silva, L. V., He, Z., Zhang, B., Gathagan, R. J., Trojanowski, J. Q. & Lee, V. M. Y. Pathological Tau Strains from Human Brains Recapitulate the Diversity of Tauopathies in Nontransgenic Mouse Brain. *J. Neurosci.* **37**, 11406–11423 (2017).

203. Tolnay, M., Spillantini, M. G., Goedert, M., Ulrich, J., Langui, D. & Probst, A. Argyrophilic grain disease: widespread hyperphosphorylation of tau protein in limbic neurons. *Acta Neuropathol.* **93**, 477–484 (1997).

204. Shitaka Y, Tran HT, Bennett RE, Sanchez L, Levy MA, Dikranian K, B. D. Repetitive Closed-Skull Traumatic Brain Injury in Mice Causes Persistent Multifocal Axonal Injury and Microglial Reactivity. *J Neuropathol Exp Neurol* **70**, 551–567 (2011).

205. Ramlackhansingh AF, Brooks DJ, Greenwood RJ, Bose SK, Turkheimer FE, Kinnunen KM, Gentleman S, Heckemann RA, Gunanayagam K, Gelosa G, Sharp DJ. Inflammation after trauma: Microglial activation and traumatic brain injury. *Ann. Neurol.* **70**, 374–383 (2011).

206. Gentleman, S. M., Leclercq, P. D., Moyes, L., Graham, D. I., Smith, C., Griffin, W. S. T. & Nicoll, J. A. R. Long-term intracerebral inflammatory response after traumatic brain injury. *Forensic Sci. Int.* **146**, 97–104 (2004).

207. Asai, H., Ikezu, S., Tsunoda, S., Medalla, M., Luebke, J., Haydar, T., Wolozin, B.,

Butovsky, O., Kügler, S. & Ikezu, T. Depletion of microglia and inhibition of exosome synthesis halt tau propagation. *Nat. Neurosci.* **18**, 1584–1593 (2015).

208. Piacentini, R., Li Puma, D. D., Mainardi, M., Lazzarino, G., Tavazzi, B., Arancio, O. & Grassi, C. Reduced gliotransmitter release from astrocytes mediates tau-induced synaptic dysfunction in cultured hippocampal neurons. *Glia* **65**, 1302–1316 (2017).

209. Ferrer, I., García, M. A., Carmona, M., Andrés-Benito, P., Torrejón-Escribano, B., Garcia-Esparcia, P. & Del Rio, J. A. Involvement of oligodendrocytes in tau seeding and spreading in tauopathies. *Front. Aging Neurosci.* **11**, 1–16 (2019).

210. Sauerbeck, A. D., Fanizzi, C., Kim, J. H., Gangolli, M., Bayly, P. V., Wellington, C. L., Brody, D. L. & Kummer, T. T. ModCHIMERA: A novel murine closed-head model of moderate traumatic brain injury. *Sci. Rep.* **8**, 1–17 (2018).

211. Kane, M. J., Angoa-Pérez, M., Briggs, D. I., Viano, D. C., Kreipke, C. W. & Kuhn, D. M. A mouse model of human repetitive mild traumatic brain injury. *J. Neurosci. Methods* **203**, 41–49 (2012).

212. Xiong, Y., Mahmood, A. & Chopp, M. Animal models of traumatic brain injury. *Nat. Neurosci. Rev.* **14**, 128–142 (2013).

213. Kalish, B. T. & Whalen, M. J. Weight Drop Models in Traumatic Brain Injury. in *Injury Models of the Central Nervous System* **1462**, 193–209 (2016).

214. Angoa-Perez, M., Kane, M. J., Briggs, D. I., Herrera-mundo, N., Viano, D. C. & Kuhn, D. M. Animal models of sports-related head injury: bridging the gap between pre-clinical research and clinical reality. *J Neurochem* **129**, 916–931 (2014).

215. Ohhashi, G., Tani, S., Murakami, S., Kamio, M., Abe, T. & Ohtuki, J. Problems in health

management of professional boxers in Japan. *Br. J. Sports Med.* **36**, 346–352 (2002).

216. Gibbons, G. S., Banks, R. A., Kim, B., Xu, H., Changolkar, L., Leight, S. N., Riddle, D. M., Li, C., Gathagan, R. J., Brown, H. J., Zhang, B., Trojanowski, J. Q. & Lee, V. M. Y. GFP-mutant human tau transgenic mice develop tauopathy following CNS injections of Alzheimer's brain-derived pathological tau or synthetic mutant human tau fibrils. *J. Neurosci.* **37**, 11485–11494 (2017).

217. Spittaels, K., Van Den Haute, C., Van Dorpe, J., Bruynseels, K., Vandezande, K., Laenen, I., Geerts, H., Mercken, M., Sciot, R., Van Lommel, A., Loos, R. & Van Leuven, F. Prominent axonopathy in the brain and spinal cord of transgenic mice overexpressing four-repeat human tau protein. *Am. J. Pathol.* **155**, 2153–2165 (1999).

218. Götz, J., Probst, A., Spillantini, M. G., Schäfer, T., Jakes, R., Bürki, K. & Goedert, M. Somatodendritic localization and hyperphosphorylation of tau protein in transgenic mice expressing the longest human brain tau isoform. *EMBO J.* **14**, 1304–1313 (1995).

219. Gilley, J., Seereeram, A., Ando, K., Mosely, S., Andrews, S., Kerschensteiner, M., Misgeld, T., Brion, J. P., Anderton, B., Hanger, D. P. & Coleman, M. P. Age-dependent axonal transport and locomotor changes and tau hypophosphorylation in a 'P301L' tau knockin mouse. *Neurobiol. Aging* **33**, 621.e1-621.e15 (2012).

220. McMillan, P., Korvatska, E., Poorkaj, P., Evstafjeva, Z., Robinson, L., Greenup, L., Leverenz, J., Schellenberg, G. D. & D'Souza, I. Tau isoform regulation is region- and cell-specific in mouse brain. *J. Comp. Neurol.* **511**, 788–803 (2008).

221. Andorfer, C., Kress, Y., Espinoza, M., De Silva, R., Tucker, K. L., Barde, Y. A., Duff, K. & Davies, P. Hyperphosphorylation and aggregation of tau in mice expressing normal human tau isoforms. *J. Neurochem.* **86**, 582–590 (2003).

222. Zhou, J., Burns, M. P., Huynh, L., Villapol, S., Taub, D. D., Saavedra, J. M. & Blackman, M. R. Temporal Changes in Cortical and Hippocampal Expression of Genes Important for Brain Glucose Metabolism Following Controlled Cortical Impact Injury in Mice. *Front Endocrinol* **8**, doi: 10.3389/fendo.2017.00231. eCollection 2017. (2017).

223. Correia, S. C., Santos, R. X., Perry, G., Zhu, X., IMoreira, P. I. & Smith, M. A. Insulin-resistant brain state: The culprit in sporadic Alzheimer's disease? *Ageing Res. Rev.* **10**, 264–273 (2011).

224. Gilmer, L. K., Scheff, S. W., Sullivan, P. G., Roberts, K. N. & Joy, K. Early Mitochondrial Dysfunction after Cortical Contusion Injury. *J. Neurotrauma* **26**, 1271–1280 (2009).

225. Xiong Y, Gu Q, Peterson PL, Muizelaar JP, L. C. Mitochondrial Dysfunction and Calcium Perturbation Induced by Traumatic Brain Injury. *J. Neurotrauma* **14**, (1997).

226. Lloyd, E., Somera-Molina, K., Van Eldik, L. J., Watterson, D. M. & Wainwright, M. S. Suppression of acute proinflammatory cytokine and chemokine upregulation by post-injury administration of a novel small molecule improves long-term neurologic outcome in a mouse model of traumatic brain injury. *J. Neuroinflammation* **5**, 1–14 (2008).

227. Seo, J. S., Lee, S., Shin, J. Y., Hwang, Y. J., Cho, H., Yoo, S. K., Kim, Y., Lim, S., Kim, Y. K., Hwang, E. M., Kim, S. H., Kim, C. H., Hyeon, S. J., Yun, J. Y., Kim, J., Kim, Y., Alvarez, V. E., Stein, T. D., Lee, J., *et al.* Transcriptome analyses of chronic traumatic encephalopathy show alterations in protein phosphatase expression associated with tauopathy. *Exp. Mol. Med.* **49**, e333-12 (2017).

228. Chen, L. J., Wang, Y. J. & Tseng, G. F. Compression alters kinase and phosphatase activity and tau and MAP2 phosphorylation transiently while inducing the fast adaptive

dendritic remodeling of underlying cortical neurons. *J. Neurotrauma* **27**, 1657–1669 (2010).

229. Ferrer, I., Gomez-Isla, T., Puig, B., Freixes, M., Ribe, E., Dalfo, E., Avila, J., Ribé, E., Dalfó, E. & Avila, J. Current advances on different kinases involved in tau phosphorylation, and implications in Alzheimer's disease and tauopathies. *Curr Alzheimer Res* **2**, 3–18 (2005).

230. Shahim, P., Gren, M., Liman, V., Andreasson, U., Norgren, N., Tegner, Y., Mattsson, N., Andreasen, N., Öst, M., Zetterberg, H., Nellgård, B. & Blennow, K. Serum neurofilament light protein predicts clinical outcome in traumatic brain injury. *Sci. Rep.* **6**, 1–9 (2016).

231. Palmqvist, S., Janelidze, S., Stomrud, E., Zetterberg, H., Karl, J., Zink, K., Bittner, T., Mattsson, N., Eichenlaub, U., Blennow, K. & Hansson, O. Performance of Fully Automated Plasma Assays as Screening Tests for Alzheimer Disease-Related β-Amyloid Status. *JAMA Neurol.* 1–10 (2019). doi:10.1001/jamaneurol.2019.1632

232. Bacioglu, M., Maia, L. F., Preische, O., Schelle, J., Apel, A., Kaeser, S. A., Schweighauser, M., Eninger, T., Lambert, M., Pilotto, A., Shimshek, D. R., Neumann, U., Kahle, P. J., Staufenbiel, M., Neumann, M., Maetzler, W., Kuhle, J. & Jucker, M. Neurofilament Light Chain in Blood and CSF as Marker of Disease Progression in Mouse Models and in Neurodegenerative Diseases. *Neuron* **91**, 56–66 (2016).

233. Pierce, J. E. S., Trojanowski, J. Q., Graham, D. I., Smith, D. H. & McIntosh, T. K. Immunohistochemical characterization of alterations in the distribution of amyloid precursor proteins and β-amyloid peptide after experimental brain injury in the rat. *J. Neurosci.* **16**, 1083–1090 (1996).

234. Neselius, S., Brisby, H., Theodorsson, A., Blennow, K., Zetterberg, H. & Marcusson, J.

Csf-biomarkers in olympic boxing: Diagnosis and effects of repetitive head trauma. *PLoS One* **7**, 1–8 (2012).

235. Washington, P. M., Villapol, S. & Burns, M. P. Polypathology and dementia after brain trauma: Does brain injury trigger distinct neurodegenerative diseases, or should they be classified together as traumatic encephalopathy? *Exp. Neurol.* **275**, 381–388 (2016).

236. Gardner, R. C., Byers, A. L., Barnes, D. E., Li, Y., Boscardin, J. & Yaffe, K. Mild TBI and risk of Parkinson disease: A Chronic Effects of Neurotrauma Consortium Study. *Neurology* **90**, e1771–e1779 (2018).

237. Furman, J. L., Holmes, B. B. & Diamond, M. I. Sensitive detection of proteopathic seeding activity with FRET flow cytometry. *J. Vis. Exp.* **2015**, 1–10 (2015).

238. Kaufman, S. K., Thomas, T. L., Del Tredici, K., Braak, H. & Diamond, M. I. Characterization of tau prion seeding activity and strains from formaldehyde-fixed tissue. *Acta Neuropathol. Commun.* **5**, 41 (2017).

239. Mirbaha, H., Holmes, B. B., Sanders, D. W., Bieschke, J. & Diamond, M. I. Tau trimers are the minimal propagation unit spontaneously internalized to seed intracellular aggregation. *J. Biol. Chem.* **290**, 14893–14903 (2015).

240. Kotecha, N., Krutzik, P. O. & Irish, J. M. Web-based analysis and publication of flow cytometry experiments. *Curr Protoc Cytom* **10**, p.Unit10.17 (2010).

241. Shahnawaz M.; Tokuda T.; Waragai M.; Mendez N.; Ishii R.; Trenkwalder C.; Mollenhauer B.; Soto C. Development of a Biochemical Diagnosis of Parkinson Disease by Detection of α-Synuclein Misfolded Aggregates in Cerebrospinal Fluid. *JAMA Neurol.* **74**, 163–172 (2017).

242. Salvadores N.; Shahnawaz M.; Scarpini E.; Tagliavini F.; Soto C. Detection of misfolded Aβ oligomers for sensitive biochemical diagnosis of Alzheimer's disease. *Cell Rep.* **7**, 261–268 (2014).

243. Edwards III, G. & Moreno-Gonzalez, I. Early Diagnostic Approaches for Alzheimer's Disease. in *Recent Research in Alzheimer's Disease* **1**, 17–29 (2019).

244. Liu, L. & Duff, K. A Technique for Serial Collection of Cerebrospinal Fluid from the Cisterna Magna in Mouse. *JoVE* **21**, (2008).

245. Zhao, J., Hylin, M. J., Kobori, N., Hood, K. N., Moore, A. N. & Dash, P. K. Post-Injury Administration of Galantamine Reduces Traumatic Brain Injury Pathology and Improves Outcome. *J. Neurotrauma* **35**, 362–374 (2017).

246. Osier, N. D. & Dixon, C. E. The controlled cortical impact model: Applications, considerations for researchers, and future directions. *Front. Neurol.* **7**, 1–14 (2016).

247. Edward Dixon, C., Clifton, G. L., Lighthall, J. W., Yaghmai, A. A. & Hayes, R. L. A controlled cortical impact model of traumatic brain injury in the rat. *J. Neurosci. Methods* **39**, 253–262 (1991).

248. Faul, F., Erdfelder, E., Lang, A. G. & Buchner, A. G*Power 3: A flexible statistical power analysis program for the social, behavioral, and biomedical sciences. *Behav. Res. Methods* **39**, 175–191 (2007).

249. Erdfelder, E., FAul, F., Buchner, A. & Lang, A. G. Statistical power analyses using G*Power 3.1: Tests for correlation and regression analyses. *Behav. Res. Methods* **41**, 1149–1160 (2009).

250. Surget, A., Saxe, M., Leman, S., Ibarguen-Vargas, Y., Chalon, S., Griebel, G., Hen, R. &

Belzung, C. Drug-Dependent Requirement of Hippocampal Neurogenesis in a Model of Depression and of Antidepressant Reversal. *Biol. Psychiatry* **64**, 293–301 (2008).

251. Deacon, R. M. J. Assessing nest building in mice. *Nat. Protoc.* **1**, 1117–1119 (2006).

252. Brooks, S. P. & Dunnett, S. B. Tests to assess motor phenotype in mice: A user's guide. *Nat. Rev. Neurosci.* **10**, 519–529 (2009).

253. Gallyas, F. & Wolff, J. R. Metal-catalyzed oxidation renders silver intensification selective. Applications for the histochemistry of diaminobenzidine and neurofibrillary changes. *J. Histochem. Cytochem.* **34**, 1667–1672 (1986).

254. Uchihara, T. Silver diagnosis in neuropathology: Principles, practice and revised interpretation. *Acta Neuropathol.* **113**, 483–499 (2007).

255. Hurtado, D. E., Molina-Porcel, L., Iba, M., Aboagye, A. K., Paul, S. M., Trojanowski, J. Q. & Lee, V. M. Y. Aβ accelerates the spatiotemporal progression of tau pathology and augments tau amyloidosis in an Alzheimer mouse model. *Am. J. Pathol.* **177**, 1977–1988 (2010).

VITA

George Edwards III received his Associates in Science from Blinn College in Brenham. He obtained his Bachelors of Biology from Texas A&M University in College Station, TX. George worked in Dr. Jennifer Bizon and Dr. Barry Setlow's laboratory at Texas A&M Psychology Department and the University of Florida McKnight Brain Institute for 3 years. George obtained his M.S. in Neuroscience in 2013 at The University of Texas Health Science Center at Houston Graduate School of Biomedical Sciences for his working studying the "Molecular interaction between type II diabetes and Alzheimer's disease through cross-seeding of protein misfolding" which was published in *Molecular Psychiatry*. He continued his research path as a Ph.D. graduate student in Dr. Claudio Soto's research laboratory in 2013. George has accrued many awards and honors – most notable being funded by a National Institute of Health F31 Kirschstein-NRSA pre-doctoral fellowship award for his Ph.D. dissertation work – as well as having nine peer-reviewed publications (six as a first author) and over 37 conference presentations. George plans to continue his pursuit in research of neurodegenerative diseases, in particular Alzheimer's disease, and age-related neurodegeneration as a Postdoctoral Associate.